THE VALORIZATION OF VARIOUS WASTEWATER FOR HYDROGEN PRODUCTION BY PHOTOCATALYTIC OXIDATION

A Thesis Submitted to
the Graduate School of
İzmir Institute of Technology
in Partial Fulfilments of the Requirements for the Degree of

DOCTOR OF PHILOSPHY

in Chemical Engineering

by

Ceren ORAK

July 2021

İZMİR

AKNOWLEDGEMENTS

I would like to express my thankfulness to my supervisor Assoc. Prof. Dr. Aslı YÜKSEL ÖZŞEN for her guidance during my thesis study. Additionally, I appreciate for her endless support and encouragement throughout my thesis study.

Iwould like to thank Prof. Dr. Erol ŞEKER and Assoc. Dr. Gülin ERSÖZ for their guidance throughout my thesis study.

I would like to thank you İzmir Institute of Technology (IZTECH) Integrated Research Centers (Center for Materials Research and Environmental Research and Development Center), Ege University Central Research Test and Analysis Laboratory Application and Research Center, Dokuz Eylül University Electronic Materials Production and Application Center for analyses. Additionally, this thesis was supported by TUBITAK (project number: 217M272).

I am very grateful to my friends Işıl İLTER, Esin KOYUNCU, Merve DİKMEN, Canan TAŞ and Cemal GÜNER for their endless support, guidance and friendship during my whole study.

Lastly, and most importantly, my deepest thanks to my brother, Alperen ORAK, my parents, Gülsüm ORAK and Özcan ORAK, and my aunt, Şengül ŞAHİN, for their support, motivation and encouragement during my lifetime.

ABSTRACT

THE VALORIZATION OF VARIOUS WASTEWATER FOR HYDROGEN PRODUCTION BY PHOTOCATALYTIC OXIDATION

Hydrogen is a clean, green and sustainable energy and photocatalysis a better approach for hydrogen production from various wastewaters.

It was aimed to evolve new hybrid solar-driven catalysts for photocatalytic hydrogen production from various wastewaters. Firstly, catalysts were synthesized. Their characterization study were performed and PL results show that the most promising catalyst was GLFO.

The impacts of pH, catalyst loading and light over hydrogen production from SMS were investigated using all synthesized catalysts. The hybrid catalysts show higher efficiency. FFD was created to elucidate the impacts of reaction parameters and graphene content of catalyst had a major impact. To optimize the reaction parameters for all hybrid catalysts, an experimental matrix was created using BBD. The higher hydrogen amounts were observed using GLFO.

The same experimental matrix was used to search the effects of reaction parameters over produced hydrogen amounts from sugar beet wastewater using all hybrid catalysts and the highest hydrogen production was observed using GLFO. The observed reaction followed first order reaction model based on TOC removal. Therefore, the degradation of organic pollutants in wastewater streams and hydrogen evolution could simultaneously be achieved.

Same experimental matrix was also used for hydrogen evolution from DBU using all hybrid catalysts. Relatively lower hydrogen amounts were obtained so that it was also treated under subcritical conditions. FFD was created to search the impacts of reaction parameters and NaOH concentration and current density had an impact over DBU removal. Based on GC-MS results, the hazardous intermediates did not form during hydrothermal electrolysis.

ÖZET

FOTOKATALİTİK OKSİDASYON YÖNTEMİ İLE HİDROJEN ÜRETİMİ İÇİN ÇEŞİTLİ ATIK SULARIN DEĞERLENDİRİLMESİ

Hidrojen temiz, yeşil ve sürdürülebilir bir enerjidir ve fotokataliz, çeşitli atık sulardan hidrojen üretimi için iyi bir yaklaşımdır.

Çeşitli atık sulardan fotokatalitik hidrojen üretimi için yeni hibrit gün ışığına duyarlı katalizörlerin geliştirilmesi amaçlanmıştır. İlk olarak, katalizörler sentezlenmiştir. Karakterizasyon çalışmaları yapılmıştır ve PL sonuçları, en umut verici katalizörün GLFO olduğunu göstermiştir.

Sentezlenen tüm katalizörler kullanılarak pH, katalizör yüklemesi ve ışığın sukroz model çözeltisinden hidrojen üretimi üzerindeki etkileri araştırılmıştır. Hibrit katalizörler daha yüksek verimlilik göstermiştir. FFD ile reaksiyon parametrelerinin etkilerini açıklamak için obir deney deseni oluşturulmuştur ve katalizörün grafen içeriğinin büyük bir etkisi olduğu belirlenmiştir. Tüm hibrit katalizörler için reaksiyon parametrelerini optimize etmek için BBD kullanılarak bir deneysel matris oluşturulmuştur. GLFO varlığında daha yüksek hidrojen miktarları gözlemlenmiştir.

Tüm hibrit katalizörler kullanılarak şeker pancarı atık suyundan üretilen hidrojen miktarları üzerinde reaksiyon parametrelerinin etkilerini araştırmak için aynı deney matrisi kullanılmış ve en yüksek hidrojen üretimi GLFO varlığında gözlemlenmiştir. Gözlenen reaksiyon, KOİ giderimine dayalı birinci dereceden reaksiyon modelini takip etmiştir. Sonuç olarak, atık su akımlarındaki organik kirleticilerin bozunması ve hidrojen üretimi eş anlı gerçekleştirilebilir.

Aynı deneysel matris, tüm hibrit katalizörler varlığında DBU'dan hidrojen üretimi için de kullanılmıştır. Nispeten daha düşük hidrojen miktarları elde edilmiştir. Bu sebeple, kritik altı koşullar altında da arıtılmıştır. Reaksiyon parametrelerinin etkilerini araştırmak için FFD ile bir deney deseni oluşturulmuştur ve NaOH konsantrasyonu ve akım yoğunluğu, DBU'nun giderimi üzerinde bir etkiye sahip olduğu görülmüştür. GK-KS sonuçlarına göre, hidrotermal elektroliz sırasında tehlikeli ara ürünlerin oluşmadığı belirlenmiştir.

TABLE OF CONTENTS

LIST OF FIGURES

Figure **Page**

Figure **Page**

Figure **Page**

LIST OF TABLES

Table **Page**

Table **Page**

LIST OF ABBREVIATIONS

In Full Factorial (FFD) and Box Behnken Design (BBD) for photocatalytic hydrogen production from sucrose model solution, real sugar beet wastewater and DBU model solution:

A: pH

B: Catalyst loading

C: Initial hydrogen peroxide oxidation

D: Graphene content

In FFD for treatment of DBU via hydrothermal and hydrothermal electrolysis:

A: NaOH concentration

B: Current density

C: Reaction duration

Other abbreviations:

BFO: $BiFeO_3$

DBU: 1,8-Diazabicyclo[5.4.0]undec-7-ene

GBFO: Graphene supported $BiFeO_3$

GLFO: Graphene supported $LaFeO_3$

GLRO: Graphene supported $LaRuO_3$

HCW: Hot-compressed-water

LFO: $LaFeO_3$

LRO: $LaRuO_3$

SMS: Sucrose model solution

CHAPTER 1

INTRODUCTION

Hydrogen is a clean, sustainable and greener energy source and it could be used as a fuel so that it could be give a contribution to energy demand of humanity. It could be used in hybrid engines of vehicles and air transportation so that the hazardous effects of greenhouse gases (i.e. CO_2) originated from fossil fuels could be diminished. It is also considering as an ideal fuel since its combustion productions (water) are not hazardous for human and environmental health. During its combustion process, the chemical energy stored in H-H bonds release and its energy yield per mass is relatively higher compared to other fuels. For instance, while energy yield per mass of gasoline is 40 kJ/g, this value for hydrogen is 122 kJ/g. Therefore, hydrogen provides a carbon-free, environmentally benign and sustainable solution for current energy demand (Liao et al., 2012; Acar et al., 2014; Acar and Dincer, 2015).

Although hydrogen is the most common element, it is generally found in some compounds such as water, biomass and hydrocarbon so that the gas form of hydrogen is produced from various sources. Natural gas, methanol, coal, heavy oil, naphtha as well as biomass and wastes could be used as a hydrogen source to produce hydrogen via different processes. Moreover, sustainable and renewable sources such as water, organic compound containing wastewater and sulfurous aqueous waters wasted by industry could be utilized for hydrogen evolution (Navarro et al., 2009; Iervolino et al., 2017).

Hydrogen production processes can be divided into two main groups which are renewable and conventional based on the used material in hydrogen production. Hydrogen is commonly produced by conventional processes. In this context, it is widely produced from fossil fuels (i.e. oil and natural gas) via steam reforming. The usage of fossil fuels cause CO and CO_2 formation as by-products and CO_2 –is a greenhouse gas- cause climate change. Additionally, high temperature requirement for the hydrogen production with these processes cause a high energy consumption. The formation of hazardous products originated from usage of these non-renewable sources and high energy need has triggered to search for new, sustainable, renewable and environmentally

friendly hydrogen production methods. Alternative to conventional processes, hydrogen could be produced from renewable sources (biomass, wastes, organic acids etc.) using heterogeneous photocatalysts via photocatalytic oxidation (Iervolino et al., 2017; Tahir et al., 2019b; Acar and Dincer, 2015).

Photocatalytic oxidation could be used for many purposes such as environmental improvement and solar energy conversion. Thus, degradation of organic compounds, wastewater treatment, reduction of carbon dioxide and hydrogen production are some of the usage purposes of photocatalytic oxidation. There is a need for electron donor to produce hydrogen by photocatalytic oxidation so that this process becomes a costly method to produce hydrogen. In order to diminish cost of electron donor, any wastewater containing organic compound(s) could be used. Thus, wastewater treatment and hydrogen production can be achieved as concomitant. Moreover, it can occur under visible light illumination depending on the photocatalytic properties of used catalyst (Riaz et al.; 2019; Iervolino et al., 2017; Bahari et al., 2019; Hosseini and Wahid et al., 2020). Consequently, to solve energy problem and produce hydrogen, photocatalytic oxidation could be one of the most promising hydrogen production method.

Hydrogen production via photocatalytic oxidation could be performed using semiconductor catalysts under UV and Vis-light illumination. However, recently, developing of visible-light driven semiconductor catalysts for hydrogen production has gained a great attention and it is reported that plenty of metal oxides were used to produce hydrogen (Chen et al., 2016a; Badawy et al., 2015; Tahir et al., 2018). For instance; ZnS and Cu-ZnS were used to produce hydrogen from an aqueous solution contains Na_2S and Na_2SO_3 (as electron donors) via photocatalysis (Dong et al., 2017). Chang et al. used ZnS-graphene and Ni doped ZnS-graphene catalysts for hydrogen production from an aqueous solution of NaCl, Na_2S and Na_2SO_3 as electron donors via photocatalytic oxidation (Chang et al., 2015). Graphene is a catalyst supporting material with outstanding properties (i.e., high chemical stability and extensive surface area). Additionally, it may act as an electron transfer channel and accelerates the catalytic adsorption (Hu et al., 2014). Besides these catalysts, Pd/TiO_2, Pt/TiO_2 and Au/TiO_2 were used for hydrogen evolution from various alcohol solutions (Al-Azri et al., 2015). For instance, Badawy et al. produced hydrogen from olive mill wastewater using TiO_2 and hence, the cost of electron could be reduced (Badawy et al., 2011). Kalyani and Gurunathan was also used Polythiophene-rGO-TiO2 as catalyst to produce hydrogen from a dye solution (methyl

viologen) and hence, hydrogen production and degradation of organic compound could be achieved simultaneously (Kalyani and Gurunathan 2013).

Besides aforementioned catalysts, perovskite type catalysts were also used to produce hydrogen via photocatalytic oxidation. Perovskite type catalysts show high catalytic activity even at low catalyst dosages. Moreover, they are thermally stable and environmentally friendly. They could be easily deported from the reaction media by filtration and they cause very low metal leaching into the reaction media. Furthermore, the reusability of these catalysts with minor loses in their photocatalytic activities is possible (Taherian et al., 2013; Gao et al., 2013; Khan et al., 2020; Sanaeishoar et al., 2014). Therefore, they were widely used in photocatalytic hydrogen evolution due to their outstanding properties. The hydrogen production from different electron donors (i.e. methanol, 2-propanol, acetic acid, glucose, and formaldehyde etc.) using various perovskite type catalysts -$LaFeO_3$, $NaTaO_3$, $LaCoO_3$ etc.- (Iervolino et al., 2017; Jana et al., 2014; Wang et al., 2015). For instance, Acharya et al. performed a study over hydrogen evolution using a composite material ($LaFeO_3$/reduced graphene oxide (rGO)) under vis-light illumination via water splitting. Due to the incorporation of rGO, the chance of electron-hole recombination fell and the efficiency of photocatalytic activity of $LaFeO_3$ enhanced. Moreover, the charge transfer was triggered by rGO and rGO enlarged the active sites on the surface of composite material so that the efficiency of photocatalytic activity of $LaFeO_3$/rGO enhanced (Acharya et al., 2017). Also, Tahir et al. used reduced graphene oxide in $BiVO_4$ to evolve hydrogen from methylene blue solution (Tahir et al., 2019a). As a result, hydrogen can be evolved from different sources (i.e. wastewater) using various type of photocatalysts (TiO_2-based, perovskite type etc.) under UV and/or Vis-light illumination.

Sugar beet wastewater, which contains high amount of sucrose, was chosen as electron donor for photocatalytic hydrogen evolution since Turkey is one of the greatest sugar beet producer countries across the world so that 33 of sugar factories exists in Turkey to produce sugar from sugar beet (www.sekerkurumu.gov.tr). These factories produce wastewater in large scales originated from the washing and floating step. The release of this wastewater could cause reverse impact over the environmental health so that usage of this wastewater as electron donor for photocatalytic hydrogen evolution could help to prevent the environmental health. Moreover, the treatment of this wastewater could be achieved simultaneously. Additionally, sucrose was selected as a model solution to stand for this wastewater due to its high content of sucrose.

1,8-Diazabicyclo[5.4.0]undec-7-ene (DBU) which is found in various industrial wastewaters (textile, pharmaceutical etc.) is a nitrogen containing heterocyclic compound. Due to the wide spread usage of DBU, it was chosen as another wastewater to produce hydrogen via photocatalytic oxidation in the context of this study. The degradation of DBU was investigated in a TiO_2-coated monolithic reactor, however, very low TOC removal % was achieved since it is a chemically stable and non-biodegradable compound (Ochuma et al., 2007a). DBU was also treated via supercritical water oxidation (SCWO) in some studies (Al-Duri et al., 2008; Al-Duri et al., 2016; Al-Duri et al., 2017). However, SCWO requires high reaction temperature and pressure as well as high cost. Therefore, the treatment of DBU in subcritical water or Hot-Compressed-Water (HCW) was also investigated in the scope of this study. The ion value of HCW is 10^{-11} at 250 °C whereas water has 10^{-14} of ion value at the room temperature. Additionally, HCW also has distinct properties as per the ambient water. For example, HCW has lower dynamic viscosity and relative dielectric constant as per the ambient water (Ochuma et al., 2007a). The wastewater treatment in HCW provides a greener and environmentally friendly solution.

In this thesis, it was aimed to synthesize perovskite type catalysts, namely, $LaFeO_3$, $BiFeO_3$, and $LaRuO_3$ (abbreviations of them are LFO, BFO and LRO, respectively) and hybrid catalysts, namely, graphene supported $LaFeO_3$, graphene supported $BiFeO_3$, and graphene supported $LaRuO_3$ (abbreviations of them are GLFO, GBFO and GLRO, respectively) to produce hydrogen from various wastewaters (sucrose model solution, sugar beet wastewater and DBU model solution) via photocatalytic oxidation. Firstly, the perovskite and hybrid catalysts were prepared and then, their characterization study comprises the analysis of SEM-EDX, TEM, BET, FT-IR, XRD and PL.

After that, the impact of reaction parameters (pH, catalyst loading and solar light) over production of hydrogen from SMS which was chosen to represent the real sugar beet wastewater were investigated in the presence of all synthesized catalyst and then, the impact of initial hydrogen peroxide concentration and catalyst calcination temperature were also search using best promising catalyst.

A general full factorial design was created via Minitab 2018 statistical analysis program to investigate the effects of reaction parameters which are catalyst loading, pH of SMS, graphene content of catalysts and initial hydrogen peroxide concertation and the experimental results were analysed by statistically. In this part, LFO and GLFO were used

since it was expected that they show better photocatalytic efficiency based on the results of catalyst characterization study. After that, the optimization of reaction parameters was achieved in the presence of GLFO. In this context, Box Behnken model was used and the experimental results were analysed by statistically. In addition, the photocatalytic hydrogen production efficiency of other hybrid catalysts (GBFO and GLRO) was also searched using the same experimental matrix. Besides, a kinetic study was also performed using GLFO to comprehend the reaction kinetic model for hydrogen production from SMS.

After completion of SMS experiments, the production of hydrogen from sugar beet wastewater using hybrid catalysts (GLFO, GBFO and GLRO) was investigated using the same experimental matrix. Additionally, the reaction kinetic model for hydrogen production from sugar beet wastewater was searched in the presence of GLFO.

DBU model solution was also used to produce hydrogen using GLFO, GBFO and GLRO via photocatalytic oxidation. The same experimental matrix was also used for each of these catalysts. Additionally, DBU was also treated in HCW. In this context, a full factorial design was created via Minitab to investigate the main and interaction effects of reaction parameters (NaOH concentration, reaction duration, current density). In addition, the impact of initial DBU concentration and reaction temperature was also investigated.

CHAPTER 2

HYDROGEN AS A SOURCE OF ENERGY

Energy is a fundamental requirement for the continuity of agriculture as well as industry. Firstly, in the 1970s, an energy crisis lived because of the oil embargo. Therefore, the research for alternative energies gained great attention. However, the decrease and stabilization in cost of fossil fuels due to the end of the embargo caused a decrease in the search for alternative energies. After that, in the 1990s, the world faced fossil fuel shortages (Holladay et al., 2009; Midilli et al., 2005). The energy demand increased due to the population increase and industrialization. Additionally, the cost of fossil fuels increased continuously in the past years. Beside the high price of fossil fuels, the usage of petroleum causes serious environmental hazardous such as CO_2, volatile organic compound (VOC) and nitrogen oxides (NOx) emissions (Holladay et al., 2009). For instance, CO_2 is one of greenhouse gases and it causes global warming.

Therefore, the search for alternative energies has become a great concern again to diminish the environmental hazardous of usage of fossil fuels and to use sustainable and renewable energies for the stability of the future world. Hydrogen is an attractive energy source with regard to environmental compatibility and sustainability so that it could be good alternative energy instead of usage of fossil fuels because hydrogen has zero or near-zero emissions of end-products (Dincer and Acar, 2015). The properties of hydrogen are given in Table 2.1.

Table 2.1.Properties of hydrogen

Property	**Value**
Symbol, number	H, 1
Atomic weight	1.008
Color, odor	Colorless, odorless
Density	Liquid: 0.07 g/cm^3 and Gas: 0.089 gL^{-1}
Melting point	−259.14 °C
Boiling point	−252.87 °C

Hydrogen has some advantageous compared to fossil fuels. For instance, it is abundant and it has high-energy conversion efficiency. Moreover, it could be produced from water without emissions and it could convert other forms of energy easily. It could be stored at various forms and it is appropriate for long distance transportation. Furthermore, hydrogen has higher (HHV) and lower (LHV) heating values as per conventional fossil fuels and HHV and LHV values of them is given in Table 2.2 (Dincer and Acar 2015, Mazloomi and Gomes 2012). Hydrogen has higher HHV and LHV as per all known fuels and it gives a carbon-free solution for energy utilization and thus, it gives a better solution in terms of environmental concerns for energy demand.

Table 2.2.Higher and lower heating values (P:1 atm, T:25°C)

Fuels	**HHV, [kJ/g]**	**LHV, [kJ/g]**
Hydrogen	141.9	119.9
Methane	55.5	50.0
Gasoline	47.5	44.5
Diesel	44.8	42.5

2.1. Hydrogen Production Methods

On the basis of the raw materials employed, hydrogen production processes can be split into two categories: conventional and renewable. For instance, while fossil fuels are used in conventional processes, biomass or water could be used in renewable processes (Holladay et al., 2009; Nikolaidis and Poullikkas, 2007).

2.1.1. Hydrogen Production Methods from Fossil Fuels

Hydrogen production processes based on fossil fuels are shown in Figure 2.1. Hydrogen evolution from fossil fuels could be carried out via two pathways which are hydrocarbon pyrolysis and hydrocarbon reforming. The used fossil fuels in these

processes are coal, natural gas, heavy oils and naphtha and the used amounts of them for hydrogen production is given in Figure 2. 2. Among them, natural gas has the highest ratio (48%) and then, heavy oils and naphtha are commonly used for hydrogen evolution (Holladay et al., 2009; Nikolaidis and Poullikkas, 2007).

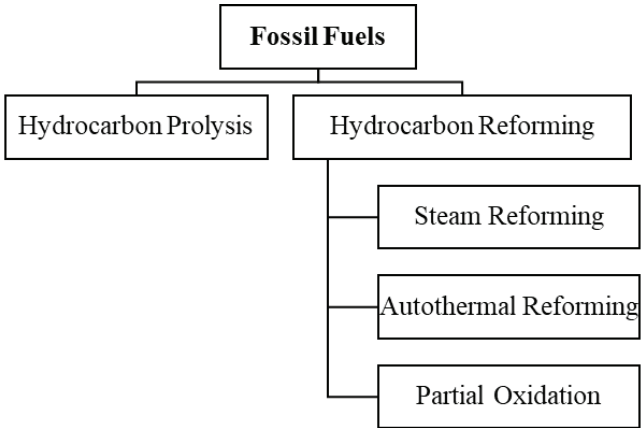

Figure 2.1. Hydrogen production methods based on fossil fuels

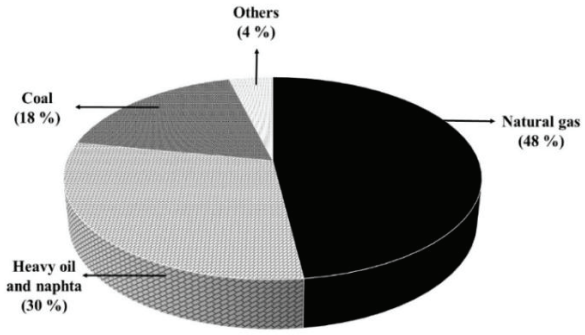

Figure 2.2. Distribution of fossil fuels for hydrogen production

2.1.1.1. Hydrocarbon Reforming Processes

In hydrocarbon reforming processes, hydrocarbons convert to hydrogen via three different techniques that are steam reforming (SR), partial oxidation (POX) and autothermal reforming (ATR). While SR is an endothermic reaction, POX is an exothermic reaction. The combination of SR and POX consists the autothermal reforming

process. In all processes, one or more water-gas-shift (WGS) reactors are used to produce hydrogen and large amounts of CO is produced as well as H_2 (Holladay et al., 2009; Nikolaidis and Poullikkas, 2007).

- **Steam Reforming:** In this process, hydrocarbons (i.e., methane, natural gas, ethane, and heavy naphtha etc.) and steam are used to obtain hydrogen and carbon oxides by catalytic conversion. If feedstock contains sulfur containing organic compounds, then desulphurization step is required to prevent the catalyst (i.e., nickel and nickel-based catalysts) from poisoning. In order to produce hydrogen in large scale, most commonly, steam methane reforming process is used and the conversion efficiency of this process varied between 74–85%. There is no requirement to usage of oxygen and the obtained H_2/CO ratio is almost 3. In addition, this process could be operated at lower temperatures (850-900 °C) compared to POX and ATR.
- **Partial Oxidation (POX):** In this process, hydrocarbons are partially oxidizing at higher temperatures using pure oxygen by controlled combustion. Due to the usage of pure oxygen, this process become an expensive technique to produce hydrogen. It is the most suitable approach to produce hydrogen from heavy oil residues and coal. The catalyst usage is not necessary in this process; however, it could be used. Whereas the process temperature is 950 °C using catalysts, it is varied between 1150–1315 °C in the absence of a catalyst. While this process has higher sulfur tolerance and has lower methane slip compared to others. H_2/CO ratio is 1:1 to 2:1 in this process.
- **Autothermal reforming:** In this process, partial oxidation is used to obtain heat and steam reforming is used to enhance the H_2/CO ratio. POX and steam reforming occurs simultaneously. This process takes places at lower pressures compared to POX. No heat required for this process since POX is an exothermic reaction.

2.2.1.2. Hydrocarbon Pyrolysis

Hydrogen could be produced by thermal decomposition of hydrocarbons in the absence of water or oxygen. In this process, a significant reduction in emissions, no

formation of CO and CO_2, requirement for secondary reactors could be obtained due to the absence of water or oxygen. Moreover, fuel flexibility, clean carbon by-product as well as relative simplicity and compactness are the advantages of hydrocarbon pyrolysis. However, carbon formation could cause fouling in this process. To prevent the fouling, appropriate design could be done to overcome this challenge (Holladay et al., 2009; Nikolaidis and Poullikkas, 2007). The general reaction of hydrocarbon pyrolysis is given below:

$$C_nH_m \rightarrow nC + {}^{1}/_{2}\, mH_2 \qquad \textbf{Eq. 1}$$

Whereas the formation of elemental carbon and hydrogen is observed throughout the thermocatalytic decomposition of light hydrocarbons whose boiling points varied between 50-200 °C, hydrogen could be produced in two steps (gasification and cracking of methane) using heavy hydrocarbons which has higher boiling points (above 350 °C) (Holladay et al., 2009; Nikolaidis and Poullikkas, 2007). The gasification, the cracking of methane and overall reaction is given below:

$Hydrogasification$: $$CH_{1.6} + 1.2H_2 \rightarrow CH_4 \qquad \textbf{Eq. 2}$$

$Cracking\ of\ methane$: $$CH_4 \rightarrow C + 2H_2 \qquad \textbf{Eq. 3}$$

$Overall\ reaction$: $$CH_{1.6} \rightarrow C + 0.8H_2 \qquad \textbf{Eq. 4}$$

In steam reforming process, there is a need for 63.3 kJ/mol of energy to produce hydrogen. However, in hydrocarbon pyrolysis process, the energy demand for hydrogen production is 37.6 kJ/mol. Therefore, hydrocarbons pyrolysis is a better option to produce hydrogen from hydrocarbons. Moreover, hydrocarbons pyrolysis process does not contain CO_2 capture and storage and water-gas-shift steps while steam methane reforming (SRM) process have these steps. Therefore, the hydrogen production price reduces 25-30% in hydrocarbon pyrolysis process compared to SRM process. The challenge in this process is that the partial pressure of hydrogen is low in the reaction mixture so that the separation efficiency of hydrogen is low. To increase the separation of hydrogen, membranes could be used (Holladay et al., 2009; Nikolaidis and Poullikkas, 2007).

2.1.2. Hydrogen Production Methods from Renewable Source

The schema of hydrogen production methods based on renewable sources and detailed information about these processes are given in Figure 2. 3.

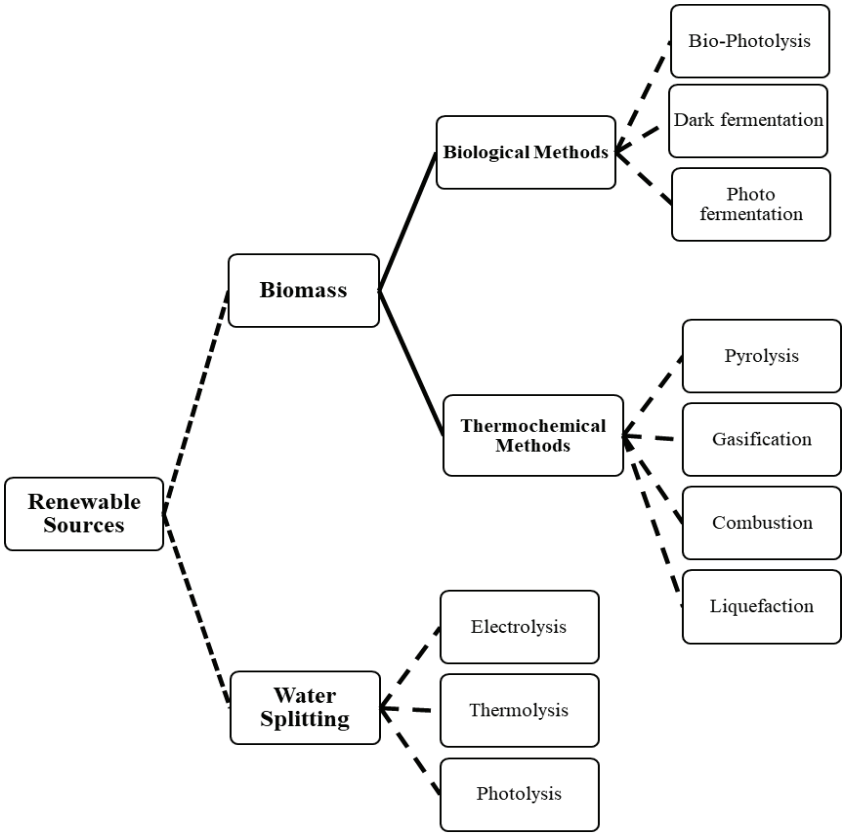

Figure 2.3. Hydrogen production methods based on renewable sources

Due to the depletion of fossil fuels and the greenhouse productions and effects with respect to the usage of fossil fuels, the search for renewable sources for hydrogen becomes unavoidable. Therefore, hydrogen could also be evolved from renewable sources such as water and biomass (i.e., animal wastes, crop residues, agricultural wastes, sawdust, aquatic plants, municipal solid wastes, etc.) via different production techniques. While biological and thermochemical methods are used to evolve hydrogen from various biomasses, water-splitting is used to produce hydrogen from water (Holladay et al., 2009; Nikolaidis and Poullikkas, 2007).

2.1.2.1. Hydrogen Production from Biomass

Hydrogen production methods based on biomass usage are divided into the two main groups that are biological and thermochemical methods with various subgroups (Dincer and Acar, 2015; Holladay et al., 2009; Nikolaidis and Poullikkas, 2007).

2.1.2.1.1. Biological Methods

Biological methods are divided into three subgroups which are bio-photolysis, dark and photo fermentation processes. They are environmentally friendly and can be carried out at milder conditions. Additionally, they are less energy intensive. Yet, the yield of produced hydrogen is low with respect to the content of used biomass compared to the thermochemical processes (Dincer and Acar, 2015; Holladay et al., 2009; Nikolaidis and Poullikkas, 2007).

- **Bio-photolysis:** Plants and some organisms use the solar energy to turn into H_2O and CO_2 to carbohydrates and O_2 and thus, it is called as photosynthesis. Whereas green plants could convert only CO_2 to oxygen, some algae and bacteria has enzymes to produce hydrogen. Thus, excess solar energy is used to direct photolysis of water to evolve hydrogen under certain conditions by some organisms such as algae and bacteria. Hydrogen can be produced via direct and indirect bio-photolysis. In direct bio-photolysis, hydrogen ions and oxygen form by hydrogenase enzymes of green algea throughout the photosynthesis. However, hydrogenase enzyme is sensitive to oxygen so that the oxygen in the media must be below 0.1%. Additionally, the 90% of photons in sunlight is used by chlorophyll and other pigments during photosynthesis. To overcome these challenges, some mutant algaes are derived and they have less pigment to use sun light for photosynthesis and they are less sensitive to oxygen. Therefore, higher yields of hydrogen could be obtained. Cyanobacteria or blue-green algae can produce hydrogen from water via in indirect photolysis using hydrogenase and nitrogenase enzymes. However, indirect photolysis is still in conceptual stage. Low hydrogen production yields are one of the drawbacks of bio-photolysis.

Additionally, to provide considerable surface area to collect sufficient sun light to produce hydrogen and no waste utilization are other disadvantages.

- **Dark fermentation:** In this process, anaerobic bacteria use in a carbohydrate rich substrate media (generally, glucose and cellulose) under anoxic and dark conditions. In this process, generally, glucose and cellulose are used since the agricultural wastes and starch containing materials have high content of glucose and cellulose. It is a pH depended process, so that pH value of reaction must be optimized and it is found as between 5 and 6 of pH. Moreover, produced hydrogen must be evacuated from the reaction media since as the pressure of reaction increases depending on the produced hydrogen amount as the production yield of hydrogen decreases. In this process, no light source is required and hence, hydrogen could be produced during all day.
- **Photo fermentation:** Some photo-synthetic bacteria can convert organic acids to H_2 and CO_2 using solar light in the presence of nitrogenase enzyme. The mostly used organic acids in this process are acetic, lactic and butyric acids. If light intensity increases, then the produced hydrogen amount and production rate increase. On the other hand, the yield of light conversion reduces. In this process, real industrial wastewaters could be used to produce hydrogen. However, the colour of wastewater affects the penetration of light. Additionally, heavy metals in wastewater streams could affect the produced amount of hydrogen so that there is a need for pre-treatment for heavy metals to remove them from the reaction media. Therefore, usage of real wastewater in this process has some challenges. Compared to the dark fermentation, the presence of light causes an increase in the hydrogen yields. However, elaborate and complicated bioreactors are necessary for this process and large areas are required to install them. In addition to this drawback, the limited availability of organic acids and low efficiency of solar energy conversion are other drawbacks.

2.1.2.1.2. Thermochemical Methods

Thermochemical methods (pyrolysis, gasification, liquefaction and combustion) are used to produce hydrogen from various biomasses and they offer higher yields of

produced hydrogen by gasification compared to biological methods so that they could be considered as more economical and environmentally friendly way to produce hydrogen. In addition, they are carried out much faster than biological methods (Dincer and Acar, 2015; Holladay et al., 2009; Nikolaidis and Poullikkas, 2007).

- **Pyrolysis:** In this process, biomasses are heated up to 650–800 K at 0.1–0.5 MPa and hence, liquid oils, solid charcoal and gaseous compounds form. In order to achieve higher yields of H_2, water-gas-shift reactions are applied during this process. Some reaction parameters that are type of biomass and used catalyst, the reaction duration and temperature affect the yield of hydrogen.
- **Gasification:** This process is generally used for coal and biomass and it is a variation of pyrolysis process and biomass converted into the syngas in an air, oxygen and/or steam media. The reaction temperature and pressure vary between 500-1400 °C and 1-33 atm, respectively. Biomass type, reaction temperature, ratio of steam and biomass, particle size and type of used catalyst have an effect over the hydrogen yield.
- **Combustion and Liquefaction:** They are less used methods for hydrogen evolution from biomass compared to pyrolysis and gasification since these methods require high pressure (5-20 MPa). Additionally, these processes must be performed in the absence of air and by-products that have hazardous effects over the environment form at the end of reaction. Moreover, low hydrogen yields could be achieved by these processes so that they do not preferred to produce hydrogen from biomass.

2.1.2.2. Hydrogen Production by Water-splitting

Hydrogen can be evolved from water, which is endless and abundant source in the Earth via water-splitting processes that are thermolysis, electrolysis and photo-electrolysis.

- **Electrolysis:** To convert water into H_2 and O_2 is highly endothermic reaction so that in this process electricity is used to comprise the required energy to split water to H_2. In this process, an anode, a cathode and an electrolyte are necessary. Generally, solid oxide electrolysis cells (SOEC), alkaline and proton exchange

membrane (PEM) are used for this process. In PEM electrolyzer, water is splitted into protons (H^+) in the anode side, then they passed through membrane. After that, they form hydrogen in the cathode side. However, in alkaline and SOEC, water is introduced to the cathode side to form hydrogen by the help of an external separation unit. The anode and cathode side reactions for PEM and SOEC are given in Table 2. 3. Although pure hydrogen can be produced via electrolysis, usage of electricity causes high cost. If the usage of electricity could replace by solar, wind and any other renewable energy sources, a cleanest energy carrier could be produced.

Table 2.3. Anode and cathode reactions of PEM and SOEC

	Anode Reactions	**Cathode Reactions**
PEM	$2H_2O \rightarrow O_2 + 4H^+ + 4e^-$	$4H^+ + 4e^- \rightarrow 2H_2$
SOEC	$4OH^- \rightarrow O_2 + 2H_2O + 4e^-$	$2H_2O + 2e^- \rightarrow 2OH^- + H_2$

- **Thermolysis:** In this process, water is splitted into hydrogen and oxygen by heating over 2500 °C because Gibbs free energy is zero for these high temperatures and hence, the separation of hydrogen from the obtained mixture becomes feasible. Various thermochemical cycles are purposed to reduce the required reaction temperature, however, the required temperature for these cycles is still high.
- **Photo-electrolysis:** Water is splitted into H_2 and O_2 using a semiconducting material (i.e., photocatalysts) using the energy of visible light. If a photon whose energy is equal or higher than the band gap energy of semiconducting material strikes the anode surface of semiconducting material, it generates an electron-hole pair and thus, semiconducting material and electrolyte are separated by an electric field. Water is splitted into H^+ ions at holes in the anode side, H^+ ions are passed through the electrolyte to the cathode side and electrons flow through an external circuit to the cathode side. Therefore, hydrogen form in the cathode side. The required free energy for water-splitting is 1.23 eV. However, high bandgap energy is required to separate electron from hole without applying any external bias potential. Therefore, it causes low efficiency.

2.2. Usage Areas of Hydrogen

The mixture of hydrogen and petroleum-derived fuels can be used in internal engines and thus, the formed harmful exhaust gases amount could be reduced. Additionally, some researches show that usage of fuels by enriching with hydrogen in hybrid engines enhanced the performance of hybrid engine and reduce the emission values. Besides the hydrogen-enriched petroleum derived fuels, some companies make researches over the fuel cells for direct usage of hydrogen. Therefore, hydrogen can be used as a direct or secondary fuel in vehicles. The usage of hydrogen can reduce the amount of greenhouse gases and air pollution which are originated from petroleum-derived fuels since the combustion product of hydrogen is only H_2O and thus, it does not contain any hazardous materials such as CO, CO_2 and HC for environment. The green factor of hydrogen based on 1 kg is calculated as 1 and it means that the energy source is greener due to the amount of hydrogen in fuel. Consequently, the usage of hydrogen in the engine of vehicles provides many benefits regarding environmental concerns (Akal et al., 2020; Midilli et al., 2005).

Air transportation comprises 2.5%-5% of the world total energy consumption and the consumed energy of transportation increased almost 4.8% per years. Additionally, 12 % of CO_2 emissions from all transports vehicles originated from aviation sector. For instance, 770 million tons of CO_2 form because of the all around the world flights in 2015. Moreover, kerosene formation due to these flights could cause acid rains and it is another hazard of usage of conventional fuels in aviation sector. To prevent these hazardous effects, many researches were conducted to replace conventional fuels with alternative fuels. Air vehicle fuels must have some properties which are high specific energy, low viscosity, good atomization, high heat capacity, rapid evaporation, high energy density and good burning properties etc. Hydrogen as a fuel to use in air vehicles met these properties. Furthermore, hydrogen has 2.5 times more energy based on weight than a jet fuel so that the usage of hydrogen in aircrafts and transportation sector provides economic advantages. Additionally, the CO_2 emissions, greenhouse gases effects and global warming effects could be reduced by replacing conventional fuels with hydrogen in air vehicles (Akal et al., 2020; Sürer and Arat, 2018; Yılmaz et al., 2018). Additionally, hydrogen can be used in many application areas and they were listed and summarized in Figure 2. 4. (Midilli et al., 2005).

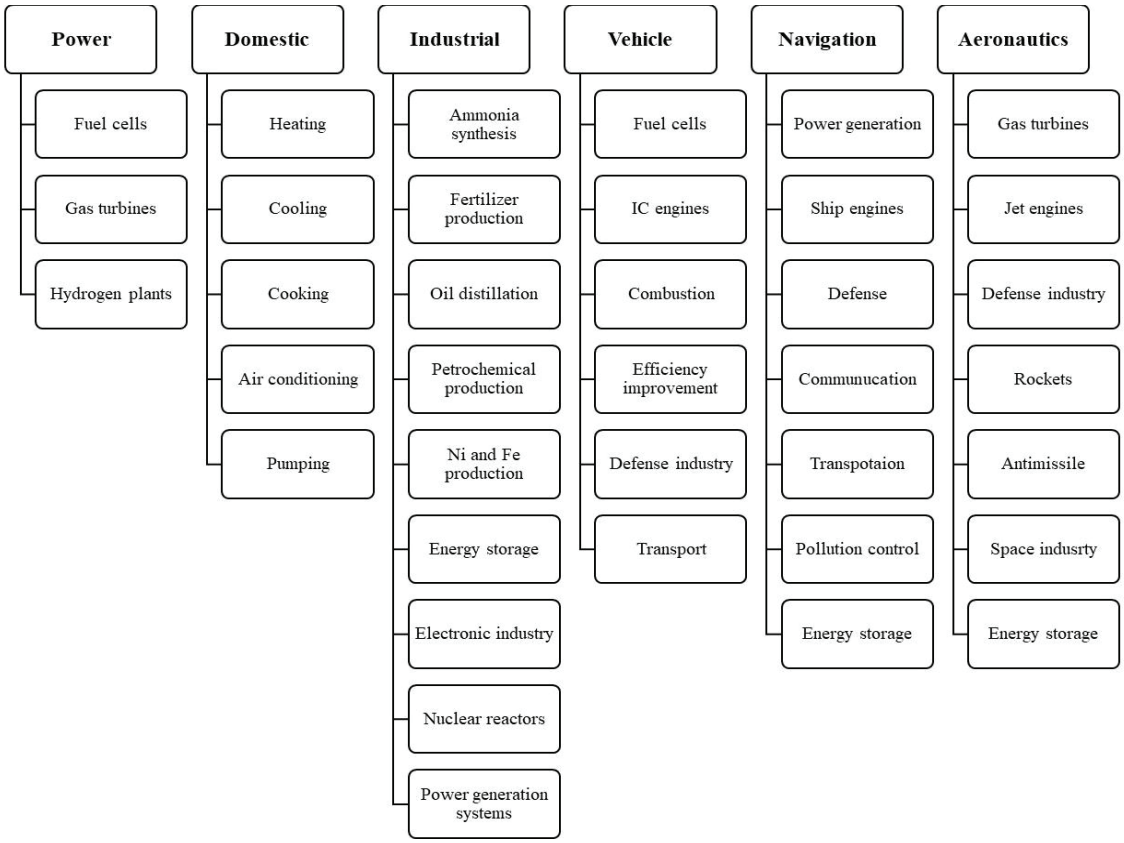

Figure 2.4. Application areas of hydrogen

CHAPTER 3

PHOTOCATALYSIS FOR HYDROGEN PRODUCTION

In this chapter, general information about photocatalytic oxidation and hydrogen production via photocatalytic oxidation will be given. Then, the types of photocatalysts used for photocatalytic hydrogen production and particularly, the studies related to hydrogen production via photocatalytic oxidation using TiO_2-based and perovskite type catalysts will be summarized. Consequently, a brief literature survey will be completed for the hydrogen evolution via photocatalytic oxidation using various catalysts.

3.1. Photocatalytic Oxidation

Advanced Oxidation Processes (i.e. photocatalytic oxidation, wet air oxidation etc.) are promising methods for wastewater treatment since degradation and complete mineralization of different organic pollutants in various wastewaters could be achieved. These processes could be divided into two groups as homogeneous and heterogeneous processes (Levchuk and Sillanpää, 2018; Ameta and Ameta, 2017).

In homogeneous photocatalytic oxidation, transition metals complexes are generally used as catalysts and hydroxyl radicals form because of the higher oxidation state of metal ion complexes so that the organic compounds can be degraded. Among the heterogeneous processes, photocatalytic oxidation has recently gained a great attention to degrade organic compounds and to treat wastewater using various photocatalysts or semiconductor materials such as TiO_2 based and perovskite type catalysts under UV and solar light illumination. It was invented by two Japan scientists, Fujishima and Honda, in 1972. They were used TiO_2 to split water under UV light irradiation and after that, various photocatalysts have been developed to use in wastewater treatment via photocatalytic oxidation. Therefore, a photocatalyst and an energy source to provide required photon energy to carry the chemical reactions are required. In this process, highly reactive oxidizing species (i.e. HO·) can degraded organic compounds which have resistance to

decompose with conventional oxidizing species (i.e. oxygen, chlorine etc.) and the end products could be CO_2 and H_2O as well as inorganic ions. Heterogeneous photocatalytic oxidation offers some advantages compared to other processes (Levchuk and Sillanpää, 2018; Ameta and Ameta, 2017; Saravanan et al., 2017).

- Complete mineralization
- No waste extermination issue
- Low cost
- Milder operating conditions (room temperature and atmospheric pressure)

Photocatalytic oxidation occurs depending on the photon energy and catalyst type. In this process, semiconductor materials are generally used as catalysts due to their superior electrical properties since they possess a filled valence band (VB) and a vacant conduction band (CB). Thanks to this property, the redox reactions (oxidation and reduction) could occur in the presence of a light source. As a summary, if a semiconductor material is exposed to light irradiation with a proper wavelength, an electron is excited to CB by leaving a positive hole in VB. Thus, any organic compounds could be degraded using the electron in CB while some compounds are oxidized by the hole in VB (Ameta and Ameta, 2017; Saravanan et al., 2017).

Oxidation Mechanism:

Firstly, water molecules absorb on the surface of photocatalyst or semiconductor material by the positive holes in VB and they formed by electron shift to CB due to the light irradiation. So, hydroxyl radicals form to degrade the organic molecules and CO_2 and H_2O form as end products (Saravanan et al., 2017). The oxidation mechanism is illustrated in Figure 3. 1.

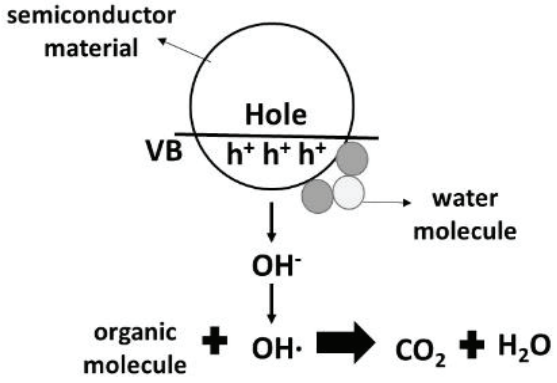

Figure 3.1. Oxidation mechanism

Reduction Mechanism:

The electrons in CB reacts with dissolved oxygen molecules and hence superoxide anions form to react with intermediate products of oxidation step. So, firstly, hydrogen peroxide form and then, it turns into water. The reduction step takes place easier than oxidation step. Additionally, the amount of organic compound affects the number of holes. As the concentration of organic compounds rises in wastewater, the number of formed holes increases and hence, it causes an enhancement in the effectiveness of photocatalytic activity (Saravanan et al., 2017). The reduction mechanism is illustrated in Figure 3. 2.

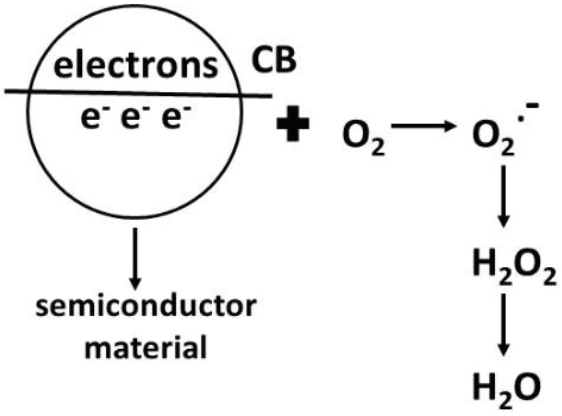

Figure 3.2. Reduction mechanism

3.1.1. Hydrogen Production via Photocatalytic Oxidation

Water and sunlight are renewable, ample and clean sources to produce hydrogen energy so that the problems related to exhaustion of fossil fuels and environmental pollution originated from fossil fuels. Photocatalytic water splitting of water into H_2 and O_2 in the presence of a semiconductor photocatalyst is an efficient process. In this process, the sunlight or solar energy converts to green, sustainable and renewable hydrogen fuel (Ahmad et al., 2015). In addition to the aforementioned processes in previous chapter, it is the most promising method to evolve hydrogen. Thanks to solar energy, the oxidative and reductive reactions occur concurrently in photocatalytic water splitting reaction (PWSR). The principle of PWSR is illustrated in Figure 3. 3.

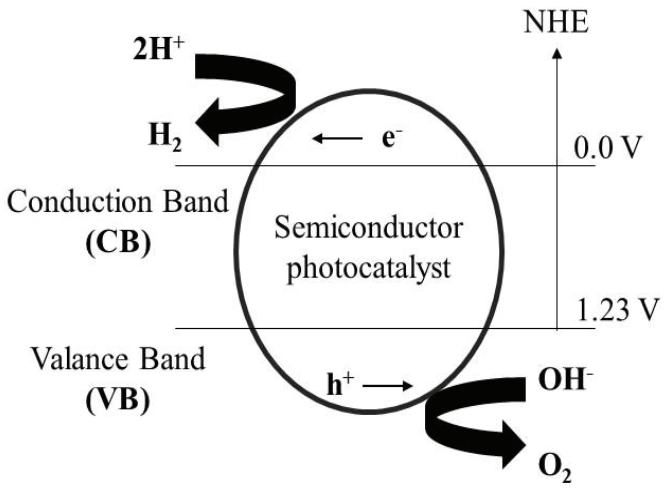

Figure 3.3. Mechanism of photocatalytic water splitting reaction

Production of hydrogen via PWSR occurs in three main steps. Firstly, semiconductor photocatalysts are excited by a light source and then, electrons and holes form. Then, photogenerated electrons and holes are separated and transferred to the surface of the photocatalysts. Finally, reduction and oxidation reaction sites capture them to split the water into hydrogen and oxygen (Chen and Mao, 2007; Chen et al., 2010; Li and Li, 2017).

The band gap energies of semiconductor photocatalysts are generally varied between 0.2 eV to 4 eV. If the photon energy of light is equal and/or the band gap energy of semiconductor photocatalyst, the electrons in VB are excited to CB whereas the holes are left in VB. Then, while the photoexcited electrons are transported to the surface of semiconductor photocatalyst for reduction reaction, the holes are transported to the surface of semiconductor photocatalyst for oxidation reaction. While holes oxidize the water molecules to form protons and oxygen, electrons reduce the released protons to the hydrogen. Whereas the nether level of VB must be more positive than chemical redox potential of O_2/H_2O, the bottom level of CB must be more negative than redox potential of H^+/H_2. Therefore, it means that 1.23 eV is the lower limit of required Gibbs free energy to split water so that the band gap energies of semiconductor photocatalysts must be at least 1.23 eV or higher than 1.23 for particularly water splitting (Li and Li, 2017).

Semiconductor photocatalysts must have appropriate band gap energy, CB and VB levels for redox reactions to convert solar energy efficiently. Additionally, the band gap energies of them have to be efficient light absorption. Furthermore, the charge

separation and recombination are competitive so that they must be efficient for transfer and separation of photogenerated charges. Recombination of photoexcited charges happens in a short time interval and thus, the redox reactions on the surface of semiconductor photocatalyst should proceed within the lifespans of photoexcited charges. Therefore, the charge separation should be considered to develop a highly effective photocatalyst. The surface-active sites of photocatalyst must capture the holes and electrons quickly and a reaction with adsorbed species takes place. The surface reaction occurs in a long-time interval relative to the generation and separation processes and hence, to develop an efficient photocatalyst, the surface reactions should also be considered. Co-catalysts should be loaded on the surface of photocatalyst since active sites on the surface of photocatalyst enhanced so that the catalytic reaction and overall effectiveness of water splitting augment. Furthermore, the charge separation and surface reactions are synergistically involved to each other. If the surface reaction occurs fast, then the charge separation is more efficient. Addition to them, enhance the reaction efficiency, sacrificial agents such as methanol and lactic acid could be used (Hisatomi et al., 2014; Li and Li, 2017).

3.2. Types of Photocatalysts

A photocatalyst for hydrogen production via PWSR should be environmentally benign, stable, recyclable and inexpensive. In literature, various semiconductors are tested for PWSR under UV or Vis-light illumination. For instance, oxides and sulphides are commonly used in PWSR. Besides, nitrides of d0 or d10 transition metal cations are also commonly used in PWSR. Some of these photocatalysts are CdS, Ta_3N_5, Fe_2O_3, C_3N_4, $BiVO_4$, Cu_2O, and WO_3. Among them, metal oxide photocatalysts (i.e. Fe_2O_3, WO_3) show low efficiency because they have high charge recombination rates. Even though Cu_2O show higher efficiency for solar to hydrogen conversion, it is prone to self-reduction in aqueous solutions. On the other hand, CdS show similar properties with Cu_2O, yet it is prone to self-oxidation. Band gap energies of some photocatalysts are listed in Table 3. 1. (Li et al., 2015; Tentu and Basu, 2017; Zhao et al., 2016; Zhang et al., 2015, Xu et al., 2016; Ameta and Ameta, 2017).

Table 3.1. Band gap energies

Photocatalyst	Band gap (eV)
CdS	2.40
CuO	1.90
WO_3	2.50-2.80
$BiVO_4$	2.40
ZnO	3.20
$SrTiO_3$	3.40
$BaTiO_3$	3.00
TiO_2	3.02-3.20

Consequently, some studies reported in literature related to the mainly used photocatalysts for PWSR is summarized in the following paragraphs.

Sprick et al. used polymer P7 (25 mg) and the mixture of water, trimethylamine (TEoA) and methanol as photocatalyst and sacrificial agent, respectively. Additionally, Pt was used as co-catalyst and the experiments were carried out using a 300 W Xe lamp. In this study, the highest hydrogen production was reported as 116 μmol h^{-1} g^{-1} (Sprick et al., 2015). Stegbauer et al. studied with 1,3,5-tris-(4-formyl-phenyl) triazine (TFPT, 5 mg), a covalent organic framework, and Pt as a photocatalyst and co-catalyst. Besides, the mixture of water and TEoA was used to produce hydrogen using 300 W Xe lamp. The highest hydrogen yield was found as 1970 μmol h^{-1} g^{-1} (Stegbauer et al., 2014). Despite the usage of Pt as co-catalyst and lower catalyst amount of TFPT compared to P7, TFPT shows higher hydrogen production efficiency.

Zhang et al. produce hydrogen from the mixture of water, Na_2S and Na_2SO_3 using NiS/$Zn_{0.5}Cd_{0.5}S$/RGO composite (50 mg) under 300 W Xe lamp irradiation. The highest hydrogen amount was achieved as 375.7 μmol h^{-1} (Zhang et al., 2014). Zheng et al. studied over the hydrogen evolution from TEoA solution using hollow C_3N_4 nanospheres (20 mg) and Pt as co-catalyst under 300 W Xe lamp irradiation. The obtained hydrogen amount was 275 μmol h^{-1} (Zheng et al., 2015). Wen et al. used 50 mg of g-C_3N_4/carbon black/NiS (NiS:co-catalyst) as photocatalyst and hydrogen was produced from TEoA solution under 300 W Xe lamp illumination. The highest hydrogen evolution was found as 992 μmol h^{-1} g^{-1} (Wen et al., 2015). Compared to NiS/$Zn_{0.5}Cd_{0.5}S$/RGO and hollow C_3N_4 nanospheres (Pt: co-catalyst), C_3N_4/carbon black/NiS (NiS:co-catalyst) show lower

catalytic efficiency to produce hydrogen. Among them, NiS/$Zn_{0.5}Cd_{0.5}S$/RGO has the highest catalytic activity.

Lu et al. studied over the hydrogen production from Na_2SO_3 solution using hydrogenated ZnO nanorods arrays (1.64 mg) under 300 W Xe lamp irradiation and the highest hydrogen yield was reported as 122,500 μmol h^{-1} g^{-1} (Lu et al., 2012). Chen et al. used $Cu_{1.94}S$–$Zn_xCd_{1-x}S$ and Pt (20 mg) as photocatalyst and co-catalyst, respectively. Na_2S and Na_2SO_3 were used as sacrificial agents and the highest hydrogen production was 13,533 μmol h^{-1} g^{-1} under 300 W Xe lamp irradiation (Chen et al., 2016b). Jiang et al. produced hydrogen without using a sacrificial agent in the presence of CdS/ZnS core-shell (1 mg) under 300 W Xe lamp irradiation and the highest obtained hydrogen amount was 239 μmol h^{-1} g^{-1} (Jiang et al., 2016). Therefore, the usage of sacrificial agents causes an increase in the evolved hydrogen amount.

3.2.1. TiO_2-based Catalysts

TiO_2-based photocatalysts were used for different purposes. For instance, NO_x removal, degradation volatile organic compounds (VOC), wastewater treatment could be accomplished using TiO_2-based catalysts. Thanks to degradation of NO_x to N_2 and other nitrogen containing compounds, less hazardous compounds form as well as global atmospheric pollution could be reduced. In addition, various organic compounds (i.e. phenolic compounds, Methylene Blue, Congo Red etc.) in wastewater are degraded in the presence of TiO_2-based catalysts (Gnaser et al., 2004). Additionally, TiO_2-based photocatalysts are extensively used in PWSR and the mechanism of PWSR for hydrogen production in the presence of TiO_2 is illustrated in Figure 3. 4.

While electrons move to the surface of TiO_2 for reduction reaction, holes migrate the surface of TiO_2 for oxidation reaction. To produce hydrogen using a semiconductor (i.e. TiO_2), CB level of this semiconductor should be lower than hydrogen production level and VB level of this semiconductor should be higher than the oxidation level for an effective oxygen formation from water via photocatalytic oxidation. Additionally, the efficiency of adsorption and photocatalytic reactions (reduction and oxidation) can be enhanced using nano-sized semiconductors since these semiconductors have more reactive surface (Ni et al., 2007).

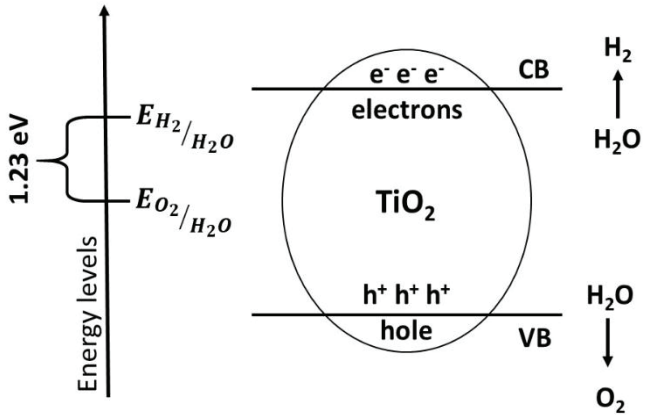

Figure 3.4. The mechanism of photocatalytic hydrogen production using TiO_2

Some related studies are summarized. Badawy et al. studied the hydrogen evolution from Remazole dye (sacrificial agent) using TiO_2 and Simonkolleite-TiO_2 and 150 W of a medium pressure mercury lamp was used as a light source. The dye removal and hydrogen production occur simultaneously and hence, the cost of sacrificial agent could be reduced using a dye as a sacrificial agent. After 240 minutes of reaction duration, whereas 3.3 mmol of H_2 was produced in the presence of Simonkolleite-TiO_2, 2.1 mmol of H_2 was evolved using TiO_2 (Badawy et al., 2015). Zou et al. used rutile TiO_2 loaded with Cu to produce hydrogen from methanol solution under UV light and almost 22.1 mmol g^{-1} h^{-1} of H_2 was evolved during the first five hours of reaction duration (Zou et al., 2014). Sadanandam et al. used cobalt doped TiO_2 catalyst for photocatalytic H_2 evolution from H_2O and glycerol under solar light irradiation. Whereas the highest produced hydrogen amount (220 μmol h^{-1} g^{-1}) from water was observed using 2 w% cobalt doped TiO_2, the highest evolved hydrogen amount from 5 % of glycerol solution was 11,021 μmol h^{-1} g^{-1} and it was accomplished using 1 w% cobalt doped TiO_2 (Sadanandam et al., 2013).

Moreover, various elements (Au, Pt, Ag, N etc.) and metal oxides (WO_3, CuO, ZnO etc.) were used to prepare TiO_2-based photocatalysts and they were tested for photocatalytic hydrogen production from various sacrificial agents (El-Bery et al., 2017; Fan et al., 2014; Wang et al., 2014; Gao et al., 2017; Chen et al., 2013; Perez-Larios et al., 2012). For instance, El-Bery et al. performed a study about the photocatalytic H_2 evolution from methanol solution using Au or Pt doped TiO_2/RGO under solar light irradiation and results show that the maximum hydrogen production (670 μmol h^{-1}) was observed using 3 wt% Pt doped catalyst (El-Bery et al., 2017). Perez-Larios et al. used

TiO_2-ZnO to produce hydrogen from ethanol solution. While 10 μmol h^{-1} of H_2 produced using TiO_2, 1300 μmol h^{-1} of H_2 produced using TiO_2-ZnO catalyst and thus, incorporation of ZnO cause significant increase in the produced hydrogen amount.

In order to overcome low catalytic effective of TiO_2 in photocatalytic hydrogen production, TiO_2 is synthesized via flame spray pyrolysis. Also, Au modified TiO_2 synthesized by flame spray pyrolysis was also tested for photocatalytic hydrogen production. Much better results are obtained using Au modified TiO_2 as per bare TiO_2 (Chiarello et al., 2018). Consequently, drawbacks of TiO_2 led to search new semiconductor materials for photocatalytic hydrogen production.

3.2.2. Perovskite Type Catalysts

Perovskite type catalysts that have a general formula as ABO_3 where A and B could be large and small alkali, alkaline earth or transition metal cations, respectively. General structure of perovskite type catalysts is given in Figure 3. 5.

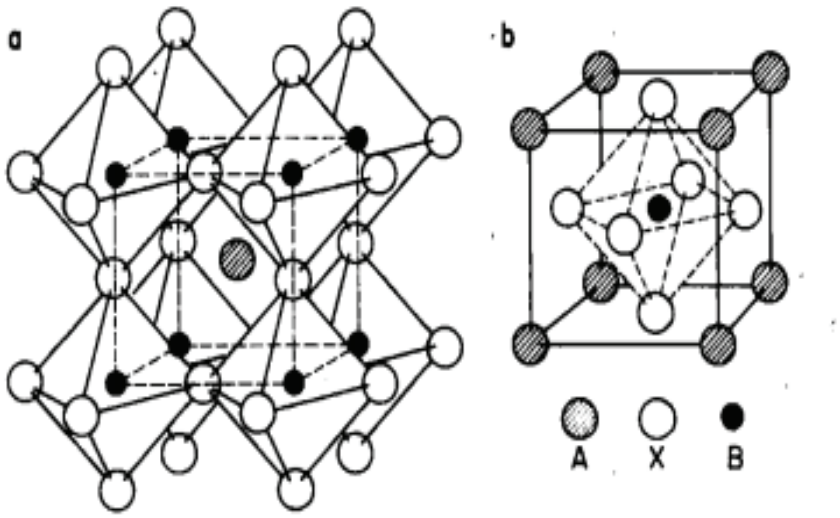

Figure 3.5. ABX_3 ideal perovskite structure: (a), cation A, or (b). cation B, at the center of the unit cell (Source: Tejuca et al., 1989)

They are promising semiconductor photocatalysts for photocatalytic hydrogen production since they have resistance to photocorrosion and high stability and they are environmentally friendly. Furthermore, they have high photocatalytic activity and they can show high catalytic activity even at low catalyst amounts. They may easily be

separated from the reaction media via filtration. Moreover, the metal leaching (i.e. iron leaching) into the reaction medium is low and they can be used repeatedly without any considerable loss of photocatalytic efficiency of them (Taherian et al. 2013, Gao et al., 2013; Sanaeishoar et al., 2014; Nguyen et al., 2020).

In the literature, there have been studies on the production of hydrogen by photocatalytic oxidation using perovskite type catalysts (i.e., $LaFeO_3$, $NaTaO_3$, and $LaCoO_3$ etc.) from a plenty of electron donors (i.e., glucose, methanol and acetic acid etc.). Some of these studies were summarized in this section.

Iervolino et al. produced hydrogen from the glucose model solution by photocatalytic oxidation using $LaFeO_3$ and Ru-doped $LaFeO_3$. Two different reactor systems and different amounts of Ru-loaded catalysts were tested. In this study, in the reactor system where the highest efficiency was obtained, beer wastewater was used as the actual wastewater for the evolution of hydrogen via photocatalytic oxidation using the catalyst with the best activity. In this study, in the second reactor system, in the presence of $LaFeO_3$ containing 0.47 Ru of 4% glucose in the 1000 mg/L glucose model solution exposed to UV light for 4 hours, 70% glucose degradation was observed, while 3474 μmol/L hydrogen was produced. In this reactor system, 2128 $\mu mol/g_{cat}$ of hydrogen was produced from the actual wastewater (Iervolino et al., 2017). Iervolino et al. performed another study over the hydrogen evolution by photocatalytic oxidation from glucose model solution in the presence of $LaFeO_3$ catalysts which are prepared by using different amounts of citric acid. Based on the results, the highest hydrogen amount (1.6 $mmol/g_{cat}$) was obtained using $LaFeO_3$ which is prepared using 1.86 g citric acid. In addition, 73% glucose degradation was obtained (Iervolino et al., 2016).

Acharya et al. examined water decomposition reaction using $LaFeO_3$ nanotubes/graphene oxide (GO) composite via photocatalytic oxidation and methanol as sacrificial agent. The illustration of hydrogen production with this catalyst is given in Figure 3. 6. Maximum hydrogen production (611.3 $mmol h^{-1} g^{-1}$) was performed in the presence of $LaFeO_3$ nanotubes/(1% by mass)GO. Furthermore, it has been found that the reduced GO addition to $LaFeO_3$ reduces band gap and it was found that the reduced GO provided a more active surface for adsorption and photocatalytic reaction because of the wide surface area and the reduced GO layer could efficaciously collect and transport electron, which reduced the probability of electron-hole recombination and increased efficiency of separation (Acharya et al., 2017).

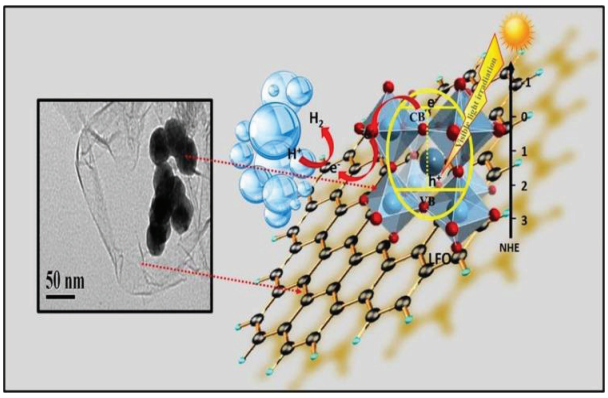

Figure 3.6. Hydrogen production with $LaFeO_3$ nanotubes/graphene oxide composite (Source: Acharya et al., 2017)

Chen et al. carried out a study about the impact of modification of the magnesium nanolayer interface (MIN) to Pt/Ta_3N_5 for photocatalytic hydrogen evolution under visible light illumination. In this study, methanol-water model solution containing 20 % methanol by volume was used as the model solution. Magnesium nanolayer interface modification was performed by in situ and ex situ methods. The illustration of pristine and modified Pt/Ta_3N_5 were illustrated in Figure 3. 7. The highest hydrogen production (22.4 $\mu molh^{-1}$) was obtained in the presence of $Pt/MgO_{(in)}$-Ta_3N_5 photocatalyst was prepared using in situ method whereas the lowest hydrogen production (1.3 $\mu molh^{-1}$) was achieved in the presence of pristine Pt/Ta_3N_5 (Chen et al. 2016a).

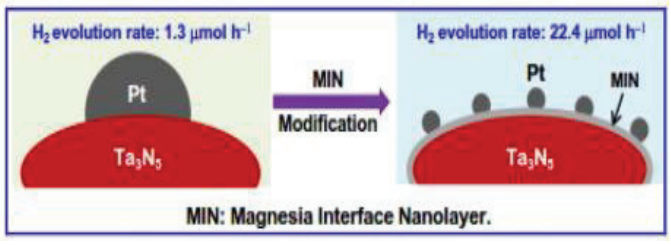

Figure 3.7. Illustriation of pristine and modified Pt/Ta_3N_5 catalysts (Source: Chen et al., 2016a)

Jana et al. performed a study over the hydrogen e by photocatalytic oxidation from water/methanol solution using Pt/RE: $NaTaO_3$ (RE: Y, La, Ce, Yb) catalysts. In this study, photocatalysts of perovskite-type RE-doped $NaTaO_3$ (RE: Y, La, Ce, Yb) are synthesized by solid-state synthesis and photocatalytic hydrogen production

performances were investigated using 10% methanol-containing methanol-water model solution. Y: $NaTaO_3$ with and without Pt showed the best photocatalytic hydrogen production efficiency. As the end of 400 minutes of reaction, while approximately 300 $\mu mol/g_{cat}$ hydrogen was produced in the presence of Y: $NaTaO_3$; approximately 450 $\mu mol/g_{cat}$ hydrogen was produced in the presence of Pt/Y: $NaTaO_3$ (Jana et al. 2014). Lee et al. investigated the synthesis, characterization of Zn_xTi_yS and its photocatalytic activity for hydrogen production from methanol-water model solution. Zn_xTi_yS was prepared to be x=1, 0.95, 0.9, 0.85, 0.8 mol and y=0, 0.05, 0.1, 0.15, 0.2 mol. Using these catalysts, hydrogen production from the methanol-water (1:1) model solution showed a dramatic increase compared to the pure ZnS catalyst. In particular, when 1.0 g of $Zn_{0.9}Ti_{0.1}S$ was used, 4.0 mmol of hydrogen was produced in 10 hours. The performance of this catalyst was enhanced with the addition of KOH solutions and 8.0 mmol of hydrogen was produced using KOH solution within 10 hours (Lee et al., 2013). Martha and Parida studied over the hydrogen production under visible light from a methanol-water model solution containing 10% methanol by volume using N-doped $In_2Ga_2ZnO_7$ catalyst in nanoparticle. It was found that the most effective photocatalyst for hydrogen production was N-GaInZn-500 (containing 1% N by mass and calcined at 500 °C). In the presence of this catalyst, 263 mmol/h hydrogen was produced under visible light irradiation. The hydrogen production with this catalyst were depicted in Figure 3. 8. (Martha and Parida, 2012).

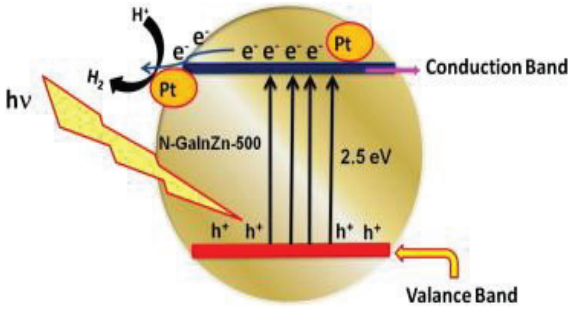

Figure 3.8. Hydrogen production with N-doped $In_2Ga_2ZnO_7$
(Source: Martha and Parida, 2012)

Jang et al. synthesized $CaTi_{1-x}Fe_xO_3$ photocatalysts by solid-state reaction method. It was found that Fe doping plays an important role in inducing visible light

absorption in $CaTiO_3$ and photocatalytic activity of $CaTiO_3$ was investigated for hydrogen production using methanol-water model solution containing 30% methanol in volume under visible light. $CaTi_{0.9}Fe_{0.1}O_3$ containing 25% Pt by mass was found to be the most effective catalyst in hydrogen production and 83 mmol/g of hydrogen production was achieved (Jang et al. 2011). Xie et al. studied over the synthesize of LaOF catalyst by an easy hydrothermal method and then a heat treatment was applied and this catalyst was used for the first time for photocatalytic hydrogen production under UV light. In addition, Pt was used as the auxiliary catalyst and it was observed that it increased the efficiency of photocatalytic hydrogen production. The highest efficency (190 µmol hydrogen) for the photocatalytic hydrogen production from the methanol-water model solution containing 3% methanol was obtained in the presence of LaOF containing 1% Pt by mass for 10 hours under UV light (Xie et al., 2012). The illustration of hydrogen evolution with LaOF is given in Figure 3. 9.

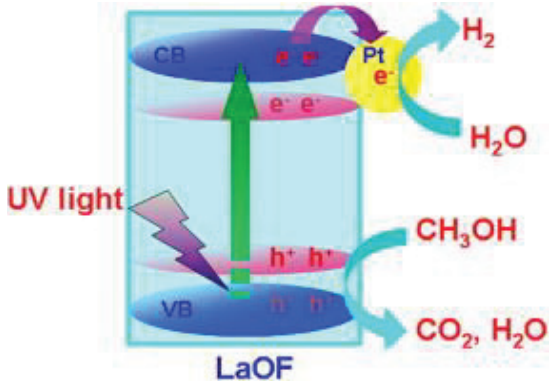

Figure 3.9. Hydrogen evolution with LaOF
(Source: Xie et al., 2012)

Wang et al. investigated the catalytic performance of $LaCoO_3$, $LaCo_{0.8}Cu_{0.2}O_3$, $LaCo_{0.7}Cu_{0.3}O_3$, $LaCo_{0.6}Cu_{0.4}O_3$ perovskite type catalysts to produce hydrogen using the formaldehyde model solution under solar light radiation. In this study, the catalyst which is showed the highest catalytic performance was also prepared by microbial method and the effect of preparation method was investigated. For this study, it was determined that the optimum catalyst was $LaCo_{0.7}Cu_{0.3}O_3$ and the maximum amount of produced hydrogen was 0.31 $mmolh^{-1}g^{-1}$. This catalyst was also prepared by microbial method, namely M- $LaCo_{0.7}Cu_{0.3}O_3$ catalyst (proposed synthesis mechanism is

given in Figure 3. 10. In this study, 1.13 $mmolh^{-1}g^{-1}$ hydrogen was produced in the presence of this catalyst after 60 minutes of radiation. After 270 minutes, this value was 2.20 $mmolh^{-1}g^{-1}$. In line with this result, it has been found that biomass can help to adjust the crystal structure and surface structure of the catalyst and that some organic functional groups in the biomass residue that act as photosensitizer may increase the light absorption capacity (Wang et al., 2015).

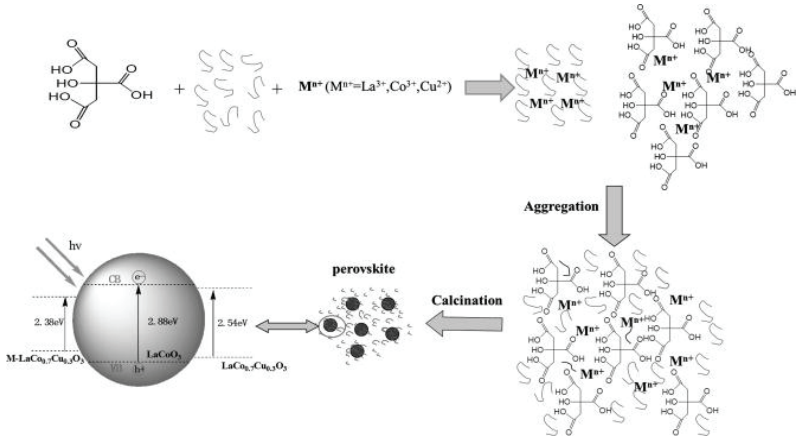

Figure 3.10. Proposed mechanism of M-$LaCo_{0.7}Cu_{0.3}O_3$ synthesis
(Source: Wang et al., 2015)

Zieliñska et al., studied hydrogen production from different model organic electron donor solutions which were formic acid, acetic acid, methanol, 2-propanol and formaldehyde in the presence of $CaTiO_3$:TiO_2, $SrTiO_3$:TiO_2, $BaTiO_3$:TiO_2 (TiO_2 used as cocatalyst) via photocatalytic oxidation and also the catalytic performance of commercial titanium dioxide (TiO_2-A11) was tested. All catalysts were tested in the solution using 2-propanol as the model organic electron donor (3 mol/dm^3) and after 5 hours of UV irradiation, the highest hydrogen production (30 μmol/h) was performed in the presence of $SrTiO_3$:TiO_2 catalyst. Then, all model organic electron donors were tested in the presence of this catalyst and the highest hydrogen production was performed using 4 mol/dm^3 formic acid model solution and found to be 43.78 μmol/h. The optimum value of the amount of catalyst was determined as 0.1 g and 56 μmol/h hydrogen was obtained when this amount of catalyst was used (Zieliñska et al., 2008). Puangpetch et al. studied over the hydrogen production by photocatalytic decomposition of water in the presence of $SrTiO_3$ nanocrystalline structure. In this study, various hole scavengers, which are

methanol, ethanol, 2-propanol, d-glucose and Na_2SO_3, were used. It was found that the highest hydrogen production photocatalytically was produced using the cation scavenger as methanol. In the experiments which are carried out using methanol, it was concluded that the prepared catalyst was much more effective than commercial $SrTiO_3$ and commercial TiO_2, and $SrTiO_3$ containing 0.5% by mass Pt showed the highest catalytic activity to produce hydrogen by photocatalytic oxidation. While 276 µmol $h^{-1}gcat^{-1}$ hydrogen production was performed under UV light in the presence of $SrTiO_3$ catalyst containing 0.5% Pt, 188 µmol $h^{-1}gcat^{-1}$ hydrogen was produced under visible light (Puangpetch et al. 2009). Zhu et al., prepared Si/$MgTiO_3$ heterostructures were synthesized from SiO_2/TiO_2 composites by HF-treatment and thermal reduction of Mg and direct synthesis of them is illustrated in Figure 3. 11. Si and $MgTiO_3$ have non-ideal band structure for photocatalytic water splitting, however, thanks to the combination of these two materials, the hydrogen production from pure water was achieved without using any electron donors (sacrificial agents) in the presence of Si/$MgTiO_3$ hetero-structures. This catalyst showed excellent stability under visible light and yielded 159.33 H_2/$umolh^{-1}g^{-1}$ (Zhu et al., 2016).

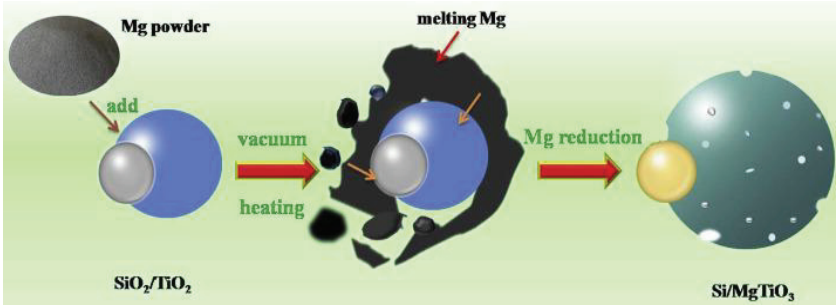

Figure 3.11. The porposed synthesis mechanism of Si/$MgTiO_3$ composite nanoparticles (Source: Zhu et al., 2016)

Tijare et al., studied over the hydrogen production by photocatalytic oxidation from ethanol (electron donor) under visible light in the presence of $LaFeO_3$ catalyst. In this study, Pt was used as cocatalyst. The optimum reaction conditions were determined as follows: 0.1 mg catalyst, 400 W visible light irradiation and 4 hours reaction time. Under these conditions, 3315 µmol $g^{-1}h^{-1}$ hydrogen was produced (Tijare et al., 2012). Puangpetch et al. In a study published in 2010, they examined some factors affecting the

amount of hydrogen production. These factors are type of mesoporous perovskite titanate nanocrystalline photocatalysts ($MgTiO_3$, $CaTiO_3$ and $SrTiO_3$), Pt loading amount, calcination temperature of photocatalyst, type and concentration of electron donor (diethanolamine, DEA and triethanolamine, TEA), sensitizer concentration (Eosin Y, E.Y. is the loading amount of the photocatalyst and the starting pH of the model solution. The results of the experiment revealed that the highest amount of photocatalytic hydrogen was obtained from the aqueous solution containing 15% DEA with 0.5% Pt loaded mesoporous $SrTiO_3$ nanocrystalline which was synthesized by a single-stage sol-gel method with 0.5 mM E.Y. and calcined at 650 °C. In addition, it was found that the optimum amount of photocatalyst loading for the maximum photocatalytic hydrogen production activity was 6 g/L and the initial pH of the solution was 11.6. The hydrogen content obtained under these conditions is approximately 1.4 cm^3/h (Puangpetch et al., 2010). Zhang et al., studied over the photocatalytic hydrogen production from KI solution using $(CuAg)_{0.15}In_{0.3}Zn_{1.4}S_2$ which was synthesized by precipitation and calcination. The photocatalytic activities of this catalyst depending on the calcination temperature is depicted in Figure 3. 12. The characterization results of the synthesized catalyst show that the calcination temperature and time significantly affect the crystallinity of the photocatalysts, the specific surface area and the apparent light absorption capacity. The photocatalyst activity was studied with an electron donor (KI) under visible light illumination. Consequently, it was concluded that the photocatalyst which was calcined at 600 °C for 5 hours showed the highest photocatalytic activity (hydrogen production rate 1750 $umolg^{-1}h^{-1}$) (Zhang et al., 2013).

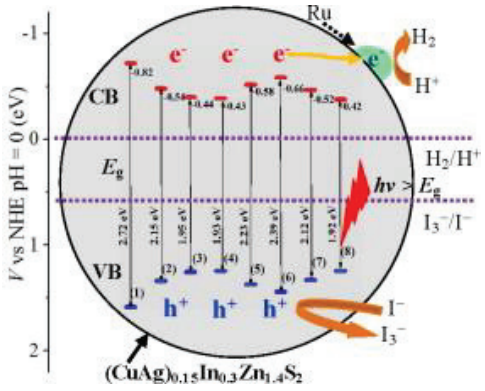

Figure 3.12. Photocatalytic activity of catalyst depending on calcination temperature (Source: Zhang et al., 2013)

CHAPTER 4

WASTEWATER AS A SOURCE OF HYDROGEN

In this chapter, particularly, the studies related to hydrogen production from real wastewater (a sustainable and renewable source) via various processes such as dark fermentation, electrocoagulation, photocatalytic and photoelectrocatalytic oxidation. In addition, particularly, hydrogen evolution from sugar beet and sugar beet wastewater by different processes will be summarized. Besides, the studies about DBU removal with different methods will be summarized.

4.1. Studies over Hydrogen Production from Wastewaters via Various Processes

Hydrogen can be produced from different sources via various processes. For instance, Lin et al. produced hydrogen from ethanol in the presence of $LaNiO_3$ via catalytic steam reforming (CSR). This reaction took place in a fix bed reactor and total ethanol conversion was accomplished at 300 °C. Also, the hydrogen selectivity was obtained over 70 % at 300 °C and less than 1% of CO formed. $LaNiO_3$ showed high catalytic activity since Ni particles were well dispersed on the surface of $LaNiO_3$. It prevented its catalytic activity for 80 h at 350 °C and total ethanol conversion and 70% of hydrogen selectivity were obtained at these conditions (Lin et al., 2013). Liu et al. used solid oxide electrolysis cells (SOECs) with $Sr_2Fe_{1.5}Mo_{0.5}O_{6-\delta}$ (SFM) which is a perovskite type electrode material to produce hydrogen. In this study, single cells with symmetrical configuration (SFM|$La_{0.9}Sr_{0.1}Ga_{0.8}Mg_{0.2}O_3$ (LSGM)|SFM) were used. The hydrogen evolution rate as high as 380 $mLcm^{-2}h$ was obtained applying 60 % of absolute humidity and electrolysis voltage of 1.3 V at 900 °C. (Liu et al., 2010). This electrolysis cell showed better results compared to some electrode materials reported in the literature and it could be better option for hydrogen production. However, these processes require severe reaction conditions such as high reaction temperature and duration. Therefore, to produce

hydrogen, more appropriate processes could be used in terms of reaction conditions. In this context, electrocoagulation, microbial fuel cells, dark fermentation etc. could be used for hydrogen production. In literature, many researches about treatment of various real wastewater and concomitant hydrogen production via these processes were carried out and some of them were summarized to give a brief idea about optimal reaction conditions and obtained hydrogen yields.

Microbial fuel cells (MFCs) are used to produce hydrogen and in literature, there is many researches for hydrogen production in MFCs. Various substrates from different industrial wastewaters were used to produce hydrogen in MFCs. Mainly used substrates in MFCs are milk, starch, and glycerol and they are found in dairy and potato industries (Tang, 2021). For instance, Marone et al. studied with six different wastewaters that are cheese, fruit juice, paper, sugar and fruit processing wastewaters to produce hydrogen in MFCs. While the highest COD removal was achieved as 78.5±5.7%, the overall hydrogen yield was found as 1608.6±266.2 $mLH_2/gCOD_{consumed}$. Moreover, this value is much higher than the obtained hydrogen yield via only fermentation (Marone et al., 2017).

Bouchareb et al. studied over hydrogen production from bulgur processing industry wastewater via dark fermentation. In this study, the effect of anaerobic sludge pre-treatment methods, applying durations for ultrasonic and thermal pre-treatment methods, and the ratio of inoculums and substrate over produced bio-hydrogen were investigated. The highest bio-hydrogen yield (90.83 mL H_2 $g^{-1}VS_{added}$) was obtained using thermally pre-treated inoculums at 1:3 (inoculums to substrate ratio) on day 16 whereas highest bio-hydrogen yield (54.076 mL H_2 $g^{-1}VS_{added}$) for ultrasonic pre-treated inoculums at 1:3 of ratio of inoculums to substrate (Bouchareb et al., 2021).

Sharma et al. studied over the hydrogen production from domestic wastewater via electrocoagulation. In this study, Fe (anode) and Al (cathode) metal plates was used as electrodes and the effects of some parameters that are electrode material, pH, and current density over the amount of produced hydrogen was investigated. The optimum reaction parameters are found as 5-7 of pH, 1.25 mA cm^{-2} of current density and the combination of cathode and anode with a mono-polar electrode connection in parallel. At these conditions, 91.8 % of COD, 94.3 % of BOD and 96.5 % of turbidity removal were achieved after treatment of 30 minutes and 0.107 hydrogen yield was obtained (Sharma et al., 2021).

Sun et al. studied over biohydrogen production from medicine wastewater in an in anaerobic packed bed reactor with some supporting materials (activated carbon,

maifanite and tourmaline). The organic loading of this wastewater varied between 15.2 and 91.3 g COD $L^{-1}d^{-1}$. The reactor system was continuously operated for 165 day. The highest hydrogen evolution rate and yield were determined as 7.92±0.27 $mmolL^{-1}h^{-1}$ and 3.50±0.09 $mmolg^{-1}$ COD in reactor with tourmaline at 6 h of hydraulic retention time (Sun et al., 2021). Therefore, wastewater could be a cost-effective source to produce hydrogen instead of high-cost substrates.

Consequently, hydrogen could successfully be evolved via different processes. Alternative to these processes, hydrogen production via photocatalytic oxidation has several advantages. It could be applied various wastewaters for degradation of organic pollutants and hydrogen production at milder reaction conditions. In addition, minimal secondary waste formation occurs and no hazardous end products form with this process. Thus, a literature survey for hydrogen production from various wastewater streams via photocatalytic oxidation was also performed.

4.2. Studies over Photocatalytic Hydrogen Production from Various Wastewaters

In the photocatalytic hydrogen production, there is a requirement for electron donors to control the fast recombination by quenching the hole and to increase the obtained hydrogen amount (Hipargi et al. 2021). To construct a sustainable and economical route for photocatalytic hydrogen production, wastewater streams -can be defined as the end-product of freshwater used in municipal, agricultural and industrial processes and it could contain various pollutants- could be used since the pollutants in the wastewater and as-generated intermediates act as electron donors. (Sharma et al., 2021; Wu et al., 2021). Therefore, hydrogen production and treatment of wastewater could be achieved simultaneously. In literature, many researches about photocatalytic hydrogen production from different wastewater to reduce electron donor costs and some of these studies are summarized to comprehend the produced amounts of hydrogen and COD removals using different photocatalysts.

Badawy et al. studied over the hydrogen evolution from olive mill wastewater using TiO_2 (nanostructure, mesoporous) under UV light illumination via photocatalytic oxidation. The effect of catalyst (TiO_2) loading, solution pH, reaction time on the

produced hydrogen amount was investigated in this study. Optimum conditions were found as pH 3, 2 g/L TiO_2 loading and 2 hours of reaction time. While 36 mmol hydrogen was produced at these reaction conditions, 87 % of COD removal was achived (Badawy et al., 2011).

Wu et al. performed a study to evolve hydrogen by photocatalytic oxidation from pharmaceutical-contaminated water, which contains enrofloxacin (ENR), ciprofloxacin (CIP), or ibuprofen (IBU). In order to produce hydrogen, Co_3O_4 modified {001}/{101}-TiO_2 nanosheet was synthesized and used as photocatalyst. When the photocatalyst was exposed to light illumination, the electrons accumulated on the {101} facets and holes accumulated on the Co_3O_4 nanoparticles so that the efficiency of degradation of wastewater and produced hydrogen amount enhanced due to the charge separation. The obtained highest hydrogen amount was around 2200 $\mu mol^{-1}g^{-1}$ (Wu et al., 2021).

Hippargi et al. performed a study over a blend fuel (hydrogen and methane) evolution from primary treated wastewater collected from Common Effluent Treatment Plant in India by photocatalysis using Au-Pt/TiO_2 catalyst. This wastewater was enriched with acetic acid. Addition of Au and Pt nanoparticles provide that the photocatalyst could use under UV and Vis light irradiation. 9386 µmol/h of hydrogen was obtained (Hippargi et al., 2021).

Kalyani and Gurunathan was studied about the hydrogen evolution from dye solution (namely, methyl viologen) using PTh-rGO-TiO_2 under visible light irradiation. The optimum PTh-rGO-TiO_2 loading was found as 0.1 %w/v. H_2 production amount and dye removal were 214.08 $\mu molh^{-1}$ and 63 %, respectively (Kalyani and Gurunathan, 2016).

Kuang and Zhang synthesized carbon doped TiO_2 (C-TiO_2) and reduced graphene decorated C-TiO_2 (C-TiO_2/rGO) to produce hydrogen from water using methanol as an electron donor under visible light irradiation. 0.67 ± 0.12 to 1.50 ± 0.2 mmolg-1h-1 of hydrogen was produced using C-TiO_2 and C-TiO_2/rGO, respectively. Graphene has large surface area and also, it provides better electron transfer so that the obtained hydrogen amount enhanced. Additionally, the band gap energies of C-TiO_2 and C-TiO_2/rGO were reported as 2.5 eV and 2.2 eV, respectively. Hence, the introduction of rGO cause a decrease in band gap energy so the utilization of visible light become a fesaible option (Kuang and Zhang, 2016).

Jia et al. synthesized highly carbon-doped TiO_2 to produce hydrogen using an aqueous solution contains a hole capturing agent (TEOA). This catalyst showed 9.7 times

higher photocatalytic efficiency than taw TiO_2 and 33.04 μmol $g^{-1}h^{-1}$ of hydrogen was evolved (Jia et al., 2018).

Zhang et al. prepared chemically bonded TiO_2/graphene sheets to produce hydrogen from an aqueous solution contains Na_2S and Na_2SO_3 under UV-Vis light illumination and this catalyst showed better photocatalytic activity compared to raw TiO_2. Its catalytic efficiency was 1.6 times higher than TiO_2. The highest hydrogen production was observed as 5.4 μmol h^{-1} in the presence of TiO_2/graphene sheets which contains 2.0 wt% of graphene sheets (Zhang et al., 2012).

Cheng et al. synthesized a hybrid catalyst (TiO_2-graphene nanocomposite) via solvothermal reaction to produce hydrogen from the mixture of methanol and water by photocatalytic oxidation. Hybrid catalysts were prepared at different graphene mass ratios. Higher mass ratios of graphene cause a decrease in the evolved hydrogen amount so that the mass ratio of graphene was optimized as 0.5%wt and almost 6000 μmol of H_2 was evolved using this catalyst. Graphene provided as an acceptor of the photogenerated electrons of TiO_2 and transporter to separate the photogenerated electron-hole pairs effectively. The hybrid catalysts had enhanced ability of light absorption and a lower recombination rate of photogenerated electrons-holes pairs, hence showed higher photocatalytic activity toward the hydrogen production from the methanol and water mixture under visible light illumination than raw TiO_2 (Cheng et al., 2012).

Sekar et al. studied over hydrogen production from Bisphenol A which is a endocrine disrupting chemical and have severe toxic effects over the human health using hierarchical bismuth vanadate (h-$BiVO_4$)/reduced graphene oxide (rGO) composite. While 11.5 $\mu molg^{-1}h^{-1}$ of hydrogen was produced in the presence of h-$BiVO_4$/rGO, 0.03 $\mu molg^{-1}h^{-1}$ of hydrogen was obtained using $BiVO_4$. Whereas 57% of Bisphenol A removal was achieved in the presence of $BiVO_4$, 72% Bisphenol A was obtained using h-$BiVO_4$/rGO. Hence, introduction of graphene causes an increase in the produced hydrogen amount and Bisphenol A removal since graphene has outstanding properties. For instance, it behaves as a co-catalyst, charge transfer mediator, photosensitizer and electron trap (Sekar et al., 2021).

Wang et al. studied over production of hydrogen from an azo dye (namely, methylene blue) solution using $(Sr_{0.6}Bi_{0.3}0_5)_2Bi_2O_7/TiO_2$ (SBO/P25) under Vis-light illumination. SBO/P25 show better photocatalytic activity and it could be deduced that SBO/P25 has higher ability to absorb visible light compared to P25 and also, SBO/P25 show better charge separation. The produced hydrogen amount and methylene blue

removal were reported as 3.18 mmol $g^{-1}h^{-1}$ and 3.42×10^{-2} min^{-1}, respectively (Wang et al., 2021).

Vaiano and Iervolino synthesized Ru-modified ZnO for degradation of an azo dye (Methyl Orange) and simultaneous hydrogen production. The effect of Ru amount was investigated and 0.25 mol % of Ru showed the best photocatalytic activity. 78 % of mineralization and 1216 µmol L-1 hydrogen was produced in the presence of 25 mol% Ru containing Ru-modified ZnO catalyst (Vaiano and Iervolino, 2009). This result indicates that the dye removal and hydrogen production can be achieved simultaneously.

Negar et al. produce hydrogen from azo dyes (acid black and acid brown) using a perovskite nanocomposite ($CoFe_2O_4$–$SrTiO_3$) under UV and Vis-light. The perovskite nanocomposite showed better photocatalytic activity compared to pristine $SrTiO_3$ under UV light illumination since incorporation of $CoFe_2O_4$ provided efficient charge separation. Also, N doped $SrTiO_3$ nanoparticles were also used to synthesized another perovskite nanocomposite ($SrTiO_3$:N–$CoFe_2O_4$) and usage of N doped $SrTiO_3$ nanoparticles provided a decrease in the band gap energy so that it became possible to use under visible light irradiation. $SrTiO_3$:N–$CoFe_2O_4$ showed better catalytic efficiency for the degradation of azo dyes compared to $SrTiO_3$ and $SrTiO_3$–$CoFe_2O_4$.

Speltini et al. performed a study over hydrogen evolution from saccharides solutions using perovskite type catalysts $DMASnBr_3$/g-C_3N_4 and PEA_2SnBr_4/g-C_3N_4 under solar light illumination. Effects of co-catalyst (Pt) and sacrificial agent (glucose) were investigated and 0.5 w% and 0.2 M were found optimum conditions for Pt and glucose, respectively. The highest hydrogen production was observed as 925 µmoles g^{-1} h^{-1} using $DMASnBr_3$/g-C_3N_4. This type perovskite type catalysts could be used for hydrogen production from sugar-rich wastewaters (Speltini et al., 2020).

Chen et al. synthesized Z-scheme catalyst (MnIS/g-C_3N_4) which is $MnIn_2S_4$ (MnIS) nanoflakes loaded metal-free graphitic carbon nitride (g-C_3N_4) to produce hydrogen from pharmaceutical wastewater under visible light irradiation. Additionally, the performance of MnIS were also evaluated to compare with MnIS/g-C_3N_4. The results showed that isolation of MnIS with g-C_3N_4 enhanced the transfer and separation of photogenerated charge carriers. Additionally, reusability experiments showed that MnIS/g-C_3N_4 has excellent stability. The produced hydrogen amounts in the presence of MnIS, CN and MnISCN-20 (20 represents the mass ratio of CN) were found as 58.3, 24.5, 200.8 µmoles g^{-1} h^{-1}, respectively. Thus, usage of composite catalyst (MnISCN) caused a

significant increase in the produced hydrogen amount compared to CN and MnIS (Chen et al., 2019).

4.3. Studies over Hydrogen Production from Sugar Beet and Sugar Beet Wastewater

Turkey, is the world's fifth- sugar beet producing country, is also the fourth largest country in Europe. In Turkey, 33 of sugar factories with different capacities produce sugar from sugar beet and corn. These factories can produce sugar almost 3.5 million tons/year (www.sekerkurumu.gov.tr). In these factories, at the end of production step, large amounts of wastewater form. If this wastewater releases to nature without any treatment, it causes critical environmental concerns in our country as well as in the world. The sugar factories use high amounts of water for washing and flotation of sugar beets and the generated wastewater from sugar factories mainly composes of washing and flotation water. This wastewater contains organic substances with high carbohydrate content that mix with water from the surface of sugar beets. Alkaya and Demirer studied over the hydrolysis and acidification of sugar beet processing wastewater and beet pulp for volatile fatty acid production by acidogenic anaerobic metabolism. The sugar industry wastes (wastewater and pressed beet pulp) used in this study were obtained from the sugar factory in Amasya. The characterization study of the wastewater containing high amounts of hydrocarbons taken from the sugar plant (total COD of 6621±113.2 mg/L, soluble COD of 6165±517.1 mg/L) and pressed sugar beet pulp (1.22±0.15) was performed (Alkaya and Demirer, 2011a). The fact that sugar beet wastewater and pulp contain high amounts of hydrocarbons has enabled to carried out studies to produce hydrogen, bioethanol, acetone, butanol, ethanol, methane valuable substances from these wastes. For example, Almohammed et al. studied over the bioethanol production from sugar beet roots by pulsed electric field treatment (Almohammed et al., 2016). Bellido et al., carried out a study to produce acetone, butanol, ethanol with *Clostridium beijerinckii* from sugar beet pulp (Bellido et al., 2015). Demirel and Scherer performed a study over the production of methane from sugar beet silage (Demirel and Scherer, 2008).

Besides, the sugar industry wastewaters can be used to produce hydrogen via different processes and some studies in the literature of hydrogen production from sugar beet wastewater and molasses are summarized briefly.

Dhar et al. studied over the hydrogen production from sugar beet juice using an integrated biological hydrogen process consisting of dark fermentation and microbial electrolysis cells. The total hydrogen production obtained in this study was 25% of initial COD amount. That is, this is equal to six moles of H_2/mol hexose. In addition, 57% energy recovery was achieved from sugar beet juice using combined biological hydrogen production (Dhar et al., 2015).

Kars and Alparslan studied over the production of biological hydrogen and 5-aminolevulinic acid from sugar beet molasses in bio-refinery concept. In this study, *Rhodobacter sphaeroides O.U.001* was used to produce biological hydrogen and 5-aminolevulinic acid (5-ALA) and different culture media with various sugar content were tested. The results obtained indicate that molasses is promising substrate for the production of biological hydrogen and 5-ALA. The highest amounts of biological hydrogen and 5-ALA were observed in media containing 28 g/L sugar (1.01 L H_2 L culture, 23337 µM) (Kars and Alparslan, 2013).

Keskin and Hallenbeck performed a study over the production of hydrogen from two main wastes (beet molasses and last molasses) of the sugar industry by a single-stage photofermentation method. Both wastes contain high amounts of sucrose, making them suitable substrates for the production of biological hydrogen. The amounts of hydrogen obtained from beet molasses (1 g/L sugar), last molasses (1 g/L sugar) and pure sucrose were determined as 10.5 mol H_2/mol sucrose, 8 mol H_2/mol sucrose and 14 mol H_2 mol sucrose, respectively (Keskin and Hallenbeck, 2012).

Özkan et al. studied over the impact of culture type on biological hydrogen evolution from sugar industry waste. In the first part of this work, the enrichment of the acidogenic anaerobic culture and mixed anaerobic culture (MAC) was carried out by acidification of glucose. In the second part of the study, domestic microorganisms, MAC, MAC treated with 2-bromoethanesulfonate, and the heat-treated MAC with acidogenic seed treated in the glucose medium were used. Two different COD levels (4.5 and 30 g/L COD) were investigated for each culture type. The reactors with initial COD concentration of 4.5 g/L gave a higher H_2 yield (20.3-87.7 mL H_2/g COD) than the reactors with an initial COD concentration of 30 g/L (0.9-16.6 mL H_2/g COD) (Özkan et al., 2010).

Hussy et al. studied the evolution of hydrogen by continuous fermentation from sucrose, sugar beet and sugar beet water extract. A non-heat treatment of the sludge and the initial nitrogen scattering yielded a culture producing hydrogen in 5 days, and the stability of this culture was investigated with two experiments and this culture remained stable over the 45 and 32 days. For the processed sucrose and pulverized sugar beet, the hydrogen yield at 14-15 hours of retention time (16 kg of total sugar $m^{-3}d^{-1}$ organic loading rate) was found to be 1.0±0.1 and 0.9±0.2 mol/mol hexose converted, respectively. These values for nitrogen sparging condition were found to be 1.7±0.2 and 1.7±0.2-1.9±0.2 mol/mol hexose converted for water extract of sugar beet and sucrose, respectively (Hussy et al. 2005).

As a result, Turkey and other countries produce sugar beet in large quantities. In these countries, there are many sugar factories so that the high amount of used water for sugar production process cause the formation of wastewater in large quantities for sugar factories. The recovery of this wastewater is an extremely important issue in terms of operating cost, human and environmental health. In order to help to solve this problem, it is aimed to produce hydrogen from sugar beet wastewater by photocatalytic oxidation in the presence of perovskite (LFO, BFO and LRO) and hybrid catalysts (GLFO, GBFO and GLRO) in the context of this thesis. Thus, organic wastes in wastewater will be degraded and hydrogen, an environmentally friendly, sustainable and clean energy source, will be produced.

4.4. DBU Removal Studies

Various pesticides, insecticides, drugs, dyes, and pharmaceuticals could contain nitrogen-containing organic compounds and hence, these compounds can be present in different industrial wastewaters such as textile, coke and pharmaceutical (Klare et al., 2000; Reddy et al., 2004; Li et al., 2001). Different chemical industries produce massive amounts of wastewater that contain non-biodegradable and chemically stable nitrogen-containing heterocyclic organic compounds. In literature, they were decomposed via incineration and highly hazardous by-products (i.e. dioxins) were observed. Moreover, some by-products show higly toxic effect even at low concentrations (Al-Duri et al., 2008; Pinto et al., 2006).

1,8–Diazabicyclo[5.4.0]undec-7-ene (abbreviated as DBU) is one of the nitrogen-containing heterocyclic organic compounds that is used in various industries such as cosmetic, pharmaceutical and dye industries and it has a severe treat over the aquatic life (Ochuma et al., 2007 a; Ochuma et al., 2007 b). It is widely used in many industries and has hazardous effects so that it was chosen as a model solution in this thesis. Although hydrogen production from DBU solution with any processes, in literature, some researches were reported for degradation of DBU with different processes such as photocatalytic oxidation and supercritical water oxidation (SCWO) and these studies are summarized.

Al-Duri et al. studied over DBU decomposition via SCWO in a plug flow reactor. Also, H_2O_2 was utilized as oxidant. In this research, various reaction temperatures and pressures were tested. Additionally, the other reaction parameters which are initial concentration of DBU, oxidant ratio and residence time were also investigated. The residence time varied between 6 and 17 h and it is a very long treatment duration. More than 90% of TOC removal was obtained at 600 °C (Al-Duri et al., 2008). Al-Duri et al. performed another study over DBU removal via SCWO in a plug flow reactor to investigate the effect of isopropyl alcohol (IPA) as a cofuel. The end-products of DBU degradation are hazardous compounds and to prevent their formation, a cofuel was used. IPA provided the conversion of recalcitrant intermediate NH_4^+ to gaseous nitrogen and also, addition of IPA cause an increase in TOC removal % (Al-Duri et al., 2016). TN removal % enhanced due to the addition of IPA and the reaction followed first order reaction kinetic model (Al-Duri et al., 2017). Ochuma et al. performed a study of DBU removal via photocatalytic oxidation in TiO_2-coated monolith reactor. While the highest TOC conversion was accomplised as almost %23 and overall DBU removal was obtained (Ochuma et al., 2007).

Based on the literature survey, DBU is widely used in various industrial fields and does not used to produce hydrogen via any process so that it was decided to use DBU for hydrogen evolution via photocatalytic oxidation using perovskite (LFO, BFO and LRO) and hybrid catalysts (GLFO, GBFO and GLRO) in the context of this thesis.

CHAPTER 5

HYPOTHESIS OF STUDY

The energy originated from fossil fuels is not considered ideal since the main end product of the combustion process of fossil fuels (i.e., coal and petroleum) is CO_2 and it is one of the greenhouse gases so that cause climate change. Another reason is that fossil fuels are not infinite and the global energy consumption is very high compared to the energy supplied from fossil fuels and it implies that they will deplete someday (Liao et al. 2012). To meet global energy demand, it is critical to find a sustainable energy source that is both easy to create and environmentally beneficial. Several alternative energies that are renewable, sustainable, and emit fewer carbon emissions than traditional energy sources have been created to replace or minimize the usage of fossil fuels. Because renewable energies are considered clean energy sources, they are considered viable alternatives to fossil fuels (Acar et al., 2016). Hydrogen (H_2) is a renewable energy source as well as a potential fuel.

Hydrogen is the most common element on the Earth but it does not find much in elemental form. It is mostly present in water; besides it exists in hydrocarbons and biomass. Hydrogen can form from plenty of sources which are biomass, natural gas, methanol, heavy oil, wastes, coal and solar (Navarro et al., 2009).

Hydrogen is considered as a clean and greener energy fuel since it is the amplest element in the universe and it can be obtained from various sustainable sources such as sweet or salty water and biomass. Additionally, it could be produced from the hydrogen sulfide resources such as some oil wells and geothermal wells. Furthermore, when the hydrogen combines with oxygen, only water forms and it is not a hazardous end product so that it is considered as an environmentally friendly and carbon-free solution. No pollutants, greenhouse gases, nor any harmful effect on the environment form in this process. Besides, in this process, the chemical energy stored in hydrogen bond comes out and this energy (122 kJ/g) is relatively higher than the energy obtained from fossil fuels (i.e. gasoline, 40 kJ/g) based on the mass. Therefore, hydrogen is a sustainable,

renewable; greneer and clean energy source so that it was decided to produce hydrogen in this study.

Hydrogen could be produced by several processes that are steam methane reforming, coal gasification, thermochemical and biological processes, and photocatalysis. Brief information about these processes will be given below.

Steam reforming process is widely used for theevolution of hydrogen and methane is generally used as fuel in this process due to its high hydrogen-carbon ratio among the hydrocarbons. Thanks to the high hydrogen-carbon ratio, the formation of by-products could be minimized. Steam methane reforming process takes place in two steps and firstly, the reformation process occurs. In the reformation step, methane and steam were mixed and this mixture at 700-900 °C of temperature and 1.5–3 MPa of pressure is passed over a catalyst bed so that a mixture of H_2 and CO could be obtained. In the second step of this process (shift reaction), obtained CO gives a reaction with excess steam to produce CO_2 and hydrogen (Hou and Hughes, 2001).

Another process for hydrogen production is coal gasification and, in this process; coal gives a reaction with O_2 and steam at high temperature and pressure. As a result of partial oxidation of coal, hydrogen, CO, CO_2, methane and other compounds can form as a mixture. In order to eliminate some by-products, partial oxidation takes place at 1 bar and over 1000 °C so that mostly hydrogen and carbon monoxide remain in the mixture (Nowotny et al.,2005).

Hydrogen can also be produced from biomass (i.e. crops, plants, and animal wastes) via thermochemical and biological processes. Among these processes, pyrolysis and gasification can be considered as feasible thermochemical processes for hydrogen production. Biomass is heated rapidly in the absence of oxygen at a high temperature (400 to 600 °C) and pressure ranging from 0.1 to 0.5 MPa during pyrolysis to produce a mixture of H_2, CH_4, CO, CO_2, carbon, and other compounds and the content of the mixture is depending on the nature of the biomass (Czernik et al., 2007; Ni et al., 2006).

If H_2 is evolved from natural gas, coal, or biomass, then a considerable amount of carbon dioxide will form as a by-product. Additionally, there is a requirement for high temperature and pressure for the production of hydrogen in the mentioned processes, so that a lot of energy is necessary to produce hydrogen with these processes and hence, the production of hydrogen by an environmentally friendly and cost-effective process is a main concern. Therefore, a water-splitting reaction using solar energy is a promising

approach to produce hydrogen without the formation of by-products besides the energy cost of this process is relatively lower than the mentioned processes (Liao et al., 2012).

Hydrogen production via the solar water-splitting process can be categorized into three categories that are thermochemical, photobiological and photocatalytic (Steinfeld 2002). Among them, thermochemical water splitting is a simple way for hydrogen production, however, it has some challenges that are heat management and control and the search for suitable heat-resisting materials. Moreover, there is a high-temperature need for large-scale systems so that the high cost and low efficiency are drawbacks of this method (Akkerman, 2002). Photobiological water splitting consists of organic biophotolysis and water biophotolysis is another process to produce hydrogen. While in organic biophotolysis, organic molecules are degraded into hydrogen, however, carbon dioxide form as a by-product, in water biophotolysis, water is divided into H_2 and O_2 by bacteria or green algae that had special enzymes for splitting reaction and this process takes place under the light. Yet, it has many drawbacks which are the poisoning effect of enzymes due to the presence of oxygen in reaction media, low yield of hydrogen and complexity of the design and scale up the bioreactor (Das and Veziroglu 2008; Guan et al., 2004). Photocatalytic water splitting is promising for hydrogen production using solar energy. It has the potential to use in a small-scale or large-scale application and compared to thermochemical and photobiological water-splitting processes, it has many advantages. In this process, a low-cost catalyst can be used to reduce process cost and solar-to-hydrogen efficiency is high. Small or large reactors could be used and mass production is allowable. Besides, the streams of hydrogen and oxygen could be separated easily. Thanks to this process, hydrogen can be produced in a renewable and sustainable way (Acar et al., 2014).

In the scientific community, the production of hydrogen in an environmentally, sustainable, renewable, and feasible way gained significance because hydrogen is using in fuel cells. Photocatalytic water splitting is a simple chemical reaction to produce hydrogen. In this process, there is a need for photocatalyst and light source. Therefore, it starts with the light irradiation and the energy of irradiated light should be greater than the band gap energy of the photocatalyst. During the process, the light causes an excitation of an electron in the valence band (VB) to the conduction band (CB) so that an electron (e^-) hole (h^+) pair form. Chemical compounds are degraded on the surface of photocatalysts with the help of these electron-hole pairs. During the degradation of chemical compounds, if the number of consumed e^- and h^+ is equal, the structure of the

photocatalyst does not change. The water-splitting reaction is given below: (Liao et al., 2012)

$$H_2O \rightarrow H_2 + {}^1/_2\, O_2 \qquad \Delta G = 237\ kJ/mol \qquad \textbf{Eq. 5}$$

In order to rearrange valance electrons, there is an energy need to meet ΔG in this reaction because it is a multi-electron process so that the formation of H_2 and O_2 can be possible. The required energy to form one molecule of hydrogen is 2.458 eV at the standard conditions and this value represents that the energy is required for rearranging electrons under 1.229 V of potential difference. Two molecules of H_2 form and four valance electrons are displaced in a full reaction so that 4.915 eV of energy is required for a full reaction. Light can be utilized as a potential energy source and especially, the required energy for water-splitting reaction could reduce using solar light irradiation. A schematic of water splitting on semiconductor is given in Figure 5.1 (Acar et al., 2014; Acar et al., 2016).

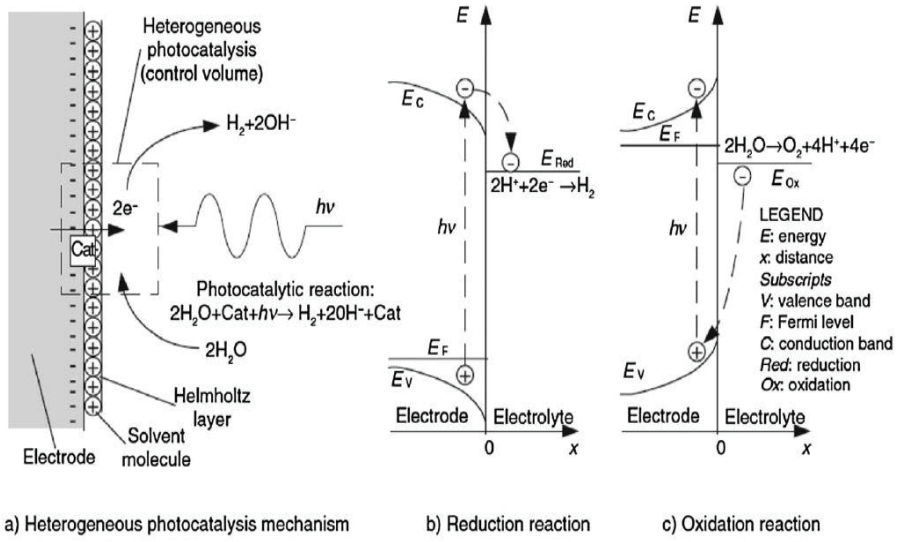

Figure 5.1. Schematic representation of water splitting reaction on a semiconductor photocatalyst (Source: Acar et al., 2014)

In photocatalytic systems, some key compounds that are photosensitizing, charge transfer, electron donation, and acceptance compounds and catalysts are required for

hydrogen production from pure water. The reason of photosensitizer usage is that pure water could not adsorb solar light. Solar light-driven water photo-oxidizing and reduction reactions are given below: (Baniasadi et al., 2012; Zamfirescu et al., 2012)

$$2H_2O_{(l)} \overset{hv}{\rightarrow} 4H^+ + 4e^- \qquad V_{ox} = +0.82\,V, NHE \qquad \textbf{Eq. 6}$$

$$2H_2O_{(l)} + 2e^- \overset{hv}{\rightarrow} 2OH^- + H_2 \qquad V_{red} = -0.41\,V, NHE \qquad \textbf{Eq. 7}$$

The major limitation of solar water splitting reaction is band gap energy of most of photocatalysts and low hydrogen yield because most of photocatalysts are appropriate for UV light and UV light consists of approximately 4% of solar energy (Acar et al., 2014). In order to eliminate this disadvantage, solar-light driven photocatalysts for solar water splitting reaction should be developed. Another challenge is to keep photogenerated electrons and holes separately in this reaction and the separation and electron-hole generation of them affected from the crystallinity and surface properties of photocatalysts. If the photocatalysts have high crystallinity, then their photocatalytic activities will be high. Additionally, while the photocatalyst has fewer surface defects, its crystallinity enhance so that the photocatalytic activity should be high and hence it could prevent electron–hole recombination sites. Moreover, the lifetime and mobility could enhance if the photocatalyst has fewer surface defects and high crystallinity. In order to enhance the photocatalytic activity, the diffusion length for photogenerated electron–hole pairs should be decreased so that the particle size could be reduced to shorten this length. Active sides of photocatalyst is also effected from the surface area of the photocatalyst (Acar et al., 2014; Liao et al., 2012).

According to the literature survey, oxide-based and non-oxide-based (i.e., sulfide-based) semiconductors are widely used as heterogeneous photocatalysts. Whereas they are unstable and they became deactivated rapidly, oxide-based photocatalysts are reported to be stable against the photo-corrosion, but developing of them has some challenges. In order to develop a photocatalyst that has a sufficiently negative CB and its band gap should be lower than 3.0 eV for visible light absorption due to the highly positive VB formed by the O2p orbital. For example, band levels of CdS are appropriate for the reduction and oxidation reactions of water and its narrow band gap gives permission to visible light absorption, however, CdS is not stable to form O_2 throughout the oxidation

reaction because the S^{2-} anion is more delicate to oxidation than water. Therefore, CdS cannot conserve its stability and it is oxidized and degraded during the oxidation reaction.

Among the photocatalysts, TiO_2 has broadly used in photocatalytic water splitting reactions since it is stable, non-corrosive and environmentally benign as well as cost-effectiveness. Addition to them, it has suitable energy levels for water splitting reaction, however, it shows low efficiency under solar light since its band gap energy is around 3.2 eV and it is appropriate for UV light. Another reason of low efficiency is the photo-generated electrons in CB and VB holes of TiO_2 could recombine rapidly. Moreover, it has a high Gibbs free energy (ΔG= 237 kJ/mol) so the recombination of H_2 and O_2 is easier than the decomposition of water (Acar et al., 2014). Due to these reasons, TiO_2 is not much appropriate to the solar water-splitting reaction.

A suitable photocatalyst for the solar water-splitting reaction should meet some requirements. For instance, its band gap energy should be lower than 3 eV and it should be stable throughout the reaction. Moreover, its band edge potentials should be appropriate for overall solar water-splitting reaction.

In this thesis, it was aimed to produce hydrogen by photocatalytic oxidation since it is an effective, low-cost process and it does not require any special equipment, high pressure and temperature. Hence, it could be carried out milder conditions compared to other processes. Fossil fuels do not use in photocatalytic oxidation likewise SMR and coal gasification. Thus, photocatalytic oxidation does not depend on fossil fuels. It can be carried out using renewable and sustainable sources.

To choose or develop an appropriate photocatalyst for photocatalytic hydrogen production has several challenges which were mentioned previously. To overcome the mentioned problems, the photocatalysts should be stable, high crystallinity and their band gap energy has to be lower than 3 eV. Perovskite type catalysts (i.e. $LaFeO_3$, $BiFeO_3$ and $LaRuO_3$) are stable, recyclable and reusable. They have high crystallinity, high catalytic activity even at low catalyst loading and low band gap energy. Parida et al. studied over synthesis of $LaFeO_3$ by sol-gel auto-combustion and it was calcined at different temperatures varied between 500 °C and 900 °C. The study shows that band gap energies of $LaFeO_3$ varied between 2.07 eV and 2.11 eV depending on the calcination temperature. Hence, this catalyst is appropriate for the photocatalytic hydrogen production under solar light irradiation. Moreover, there is a relationship between the BET surface area, particle size and hydrogen production amount. The highest hydrogen production was observed in the presence of $LaFeO_3$ (calcined at 500 °C) with the highest BET surface and lowest

particle size (Parida et al., 2010). Hence, $LaFeO_3$ could be an appropriate option for photocatalytic hydrogen production under solar light irradiation. Xu and Shen studied over the synthesis of $BiFeO_3$ and its band gap energy varied between 2.6 eV and 2.7 eV depending on the annealing temperature (Xu and Shen, 2008). Hence, $BiFeO_3$ could also be an appropriate option for photocatalytic hydrogen production under solar light irradiation. Consequently, whereas $LaFeO_3$ was previously used, $BiFeO_3$ has not be used for photocatalytic hydrogen production under solar light irradiation. In this thesis, perovskite type catalysts ($LaFeO_3$, $BiFeO_3$ and $LaRuO_3$) were chosen to test their photocatalytic activity to produce hydrogen under solar light irradiation. By the help of these catalysts, the stability and band gap energy problems could be solved.

Another challenge in photocatalytic hydrogen production is that the chance of electron-hole recombination should be reduced. Archarya et al. studied over the synthesis of graphene supported $LaFeO_3$ nanosphere (NS). The study proved that the introduction of graphene to $LaFeO_3$ NS could lessen the chance of electron–hole recombination. In addition, the charge carriers' life time is extended. Consequently, the photocatalytic activity enhanced. It could be figured out that the excellent interfacial and mutual effect between RGO sheet and $LaFeO_3$ NS through the self-assembly tactic and the outstanding ability of the RGO to trigger charge transfer. Moreover, RGO sheet acts as a charge separator as well as an electron sink for the water reduction reaction. In addition, the RGO sheets allow the photocatalytic reactions to occur not only on the surface of LFO NS, but also on the RGO sheets with remarkably advanced reaction sites (Archarya et al., 2017). In this thesis, it was aimed to synthesize graphene supported $LaFeO_3$ and graphene supported $BiFeO_3$ and their catalytic activities have not been tested for hydrogen production by photocatalytic oxidation under solar light irradiation. According to the literature survey, $LaRuO_3$ and graphene supported $LaRuO_3$ have not been used to produce hydrogen by photocatalytic oxidation. In this thesis, it was also aimed to synthesize and use them for photocatalytic hydrogen production. However, there is no information about the band gap energy of this catalyst in literature. The only known property is the percentage of ionic character which is 53.5 (Viswanathan, 2003). The ionic character of the catalysts give information whether the usage of catalysts are appropriate or not for the photocatalytic oxidation production. Thus, very low value of the ionic character is not suitable since these semiconductors do not have the necessary band gap value of 1.23 V. This means the search for utilizing lower end of the visible region is not possible for direct

water splitting reaction. The percentage of ionic character of $LaRuO_3$ indicates that it can be used for photocatalytic hydrogen production.

In the context of the thesis, these catalysts was tested to produce hydrogen from SMS, nitrogen containing model solution (1,8- diazabicyclo[5.4.0]undec-7-ene (DBU) model solution), and sugar beet wastewater. Consequently, owing to perovskite type catalysts and graphene supported perovskite type catalysts, the mentioned challenges could be overcome during the photocatalytic hydrogen production.

CHAPTER 6

EXPERIMENTAL STUDY

Experimental study part includes synthesis and characterization study (SEM, BET, XRD, FT-IR and PL analysis) of perovskite type photocatalysts (LFO, BFO and LRO) and hybrid photocatalysts (GLFO, GBFO and GLRO). Additionally, XPS analysis was carried out for the determination of elemental compositions of LFO and GLFO.

Firstly, the investigation of photocatalytic activities of synthesized photocatalyst for hydrogen evolution from SMS were performed. In this context, the effective reaction parameters which are pH, catalyst loading and light over the photocatalytic activities of the synthesized catalysts were examined to determine the most promising catalysts for this process. After that, a general full factorial design was created to investigate the main and interaction effects of reaction parameters that are pH, graphene content of catalysts and catalyst loading throughout the photocatalytic hydrogen evolution using SMS. Additionally, the impacts of catalyst calcination temperature and initial hydrogen peroxide concentration were examined for the most promising catalyst. Subsequently, an experimental matrix was created based on Box Behnken model to optimize the reaction parameters (pH, catalyst loading and initial hydrogen peroxide concentration) for photocatalytic hydrogen evolution using SMS. Moreover, a kinetic study was performed at the optimum reaction conditions to investigate the reaction kinetic.

Secondly, the photocatalytic hydrogen production from real sugar beet wastewater was carried out in the presence of hybrid catalysts using the same experimental matrix which was used for optimization experiments of SMS. In this context, the reaction parameters (pH, catalyst loading and initial hydrogen peroxide concentration) were optimized for all hybrid catalysts. In addition, to understand the reaction kinetic, some experiments were performed at different reaction temperatures at the optimum reaction conditions.

Subsequently, the photocatalytic hydrogen evolution using nitrogen containing model solution which was composed of DBU was studied in the presence of hybrid catalysts and the same experimental matrix was used for the optimization of reaction

parameters (pH, catalyst loading and initial hydrogen peroxide concentration). Then, treatment of DBU was performed in HCW since it is a resistant compound and non-biodegradable. In this context, a general full factorial design was created to investigate the main and interaction effects of NaOH concentration, current density and reaction time. Additionally, the effects of initial DBU concentration and reaction temperature were investigated. A kinetic study was performed to comprehend the reaction kinetic and the intermediates formed throughout reaction were determined via GC-MS analysis.

6.1. Materials

The list of chemicals used in this thesis were given in Table 6.1.

Table 6.1. List of used chemicals during experimental study

Name	Manufacturer
Sucrose (microbiological grade)	Merck
Graphite (extra pure)	Merck
Sodium nitrate (≥99.5)	Merck
Lanthanum(III) nitrate hexahydrate ($La(NO_3)_3.6H_2O$) (analysis grade)	Merck
bismuth(III) nitrate pentahydrate ($Bi(NO_3)_3 \cdot 5H_2O$) (analysis grade)	Merck
iron(III) nitrate nonahydrate ($Fe(NO_3)_3 \cdot 9H_2O$) (analysis grade)	Merck
hydrogen peroxide (H_2O_2) 30 %,	Merck
hydrazine hydrate (80% solution in water)	Merck
sodium hydroxide	Merck
Ruthenium(III) chloride,	Sigma-Aldrich
Phosphoric acid (H_3PO_4)	Sigma-Aldrich
1,8-diazabicyclo[5.4.0]undec-7-ene (DBU),	Sigma-Aldrich
Potassium permanganate ($KMnO_4$, extra pure)	Tekkim
Ethylene glycol (extra pure)	Isolab
citric acid (≥99.7)	Isolab
Sugar beet wastewater	Eskişehir Sugar Factory, Turkey

6.2. Experimental Set-Up and Procedure

The experimental test set-up for photocatalytic experiments consists of a cylindrical glass reactor (V=1 L), a stimulated solar light lamp, a pump for circulation. A

gas analysis system (ABB - Advance Optima, AO2000) connected to gas outlet of the reactor was used to determine the number of produced gases which are H_2, CO, CO_2 and CH_4 during the reaction. The experimental setup for photocatalytic experiments is illustrated in Figure 6.1.

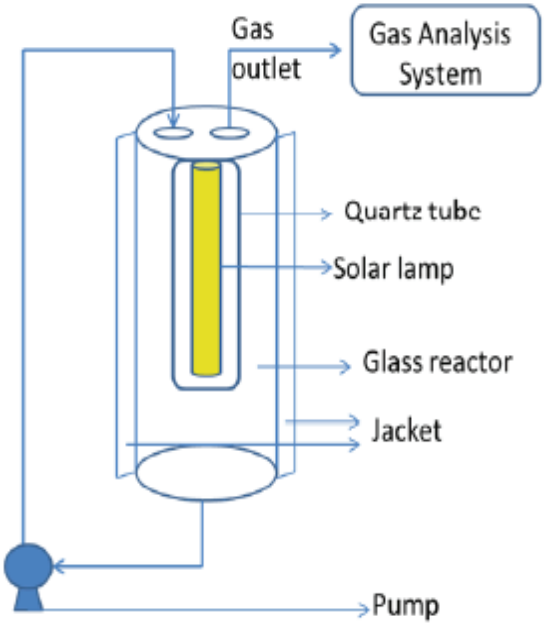

Figure 6.1. The experimental set-up for photocatalytic experiments

In SMS experiments, 1000 ppm SMS (500 mL) was used and the all reactions were performed for four hours under solar light illumination, however, in order to investigate the light effect, some experiments were carried in the dark. In a typical photocatalytic hydrogen evolution using SMS, firstly, the SMS was prepared at the desired pH value using HCl and NaOH solutions and then, the desired amount of catalyst and H_2O_2 were introduced. After that, the light was turned on so that the reaction started. During the reaction, the amounts of produced gases were monitored via gas analysis system and the experiments were terminated at the end of four hours.

In the context of the experimental study over SMS, firstly, the effects of solar light (under light and in the dark), pH of SMS (3 and 7.5) and catalyst loading (0.1 and 0.2 g/L) were investigated using perovskite type catalysts (LFO, BFO and LRO) and hybrid catalysts (GLFO, GBFO and GLRO). Then, the effects of $[H_2O_2]_0$ (0, 5 and 15 mM) and calcination temperature (500, 600, 700 and 800 °C) over the produced amount of

hydrogen were investigated in the presence of most promising catalyst. After that, a factorial design was created via Minitab 18 software to search the major and interaction of reaction parameters which are pH (3 and 7.5), catalyst loading (0.1 and 0.2 g/L), $[H_2O_2]_0$ (0 and 15 mM) and graphene content (0 and 20%) over the produced amount of hydrogen and the results were discussed statistically. In order to optimize the reaction factors (pH, catalyst loading and $[H_2O_2]_0$) for photocatalytic hydrogen evolution using SMS using most promising catalyst, an experimental matrix was created using Box Behnken model via Minitab 18 software so that the main and interaction of reaction parameters were clarified and the results were discussed statistically.

After completion of SMS experiments, the experimental study was continued with real sugar beet wastewater experiments. In real sugar beet wastewater experiments, 500 mL of real sugar beet wastewater was used and the experiments were carried out using hybrid photocatalysts under the solar light for four hours. In these experiments, the same experimental matrix which was created using Box Behnken model was used to search the impacts of pH, catalyst loading and $[H_2O_2]_0$ over the evolved hydrogen amount from sugar beet wastewater and the experimental results were analysed statistically to optimize the reaction conditions.

The liquid products of photocatalytic hydrogen evolution using the SMS were analyzed via HPLC to determine the degradation efficiency while the products of sugar beet wastewater were analyzed via TOC (Shimadzu TOC-Vcph (TNM-1/SSM-5000A) and GC-MS (Agilent 6890 N/5973 N Network, USA) to determine the removal percentage of organic compounds and to comprehend the reaction mechanism, respectively.

DBU model solution experiments for photocatalytic hydrogen production were performed using DBU containing solutions (6 mM) at the desired pH values and the pH of solutions was adjusted using HCl solution. The experiments were performed in the presence of best promising catalysts and the experimental procedure was same with SMS and sugar beet wastewater experiments. Moreover, same experimental matrix was used to optimize the reaction parameters and the experimental results were analyzed statistically.

The subcritical experiments were performed in a batch hydrothermal electrolysis reactor made of stainless steel (V=450 mL). A cylindrical titanium electrode (D:12 mm, L:94 mm) was specially designed for this reaction system and it was used as anode. The

cathode was the wall of reactor made of titanium. The experimental set-up for subcritical experiments was illustrated in Figure 6. 2.

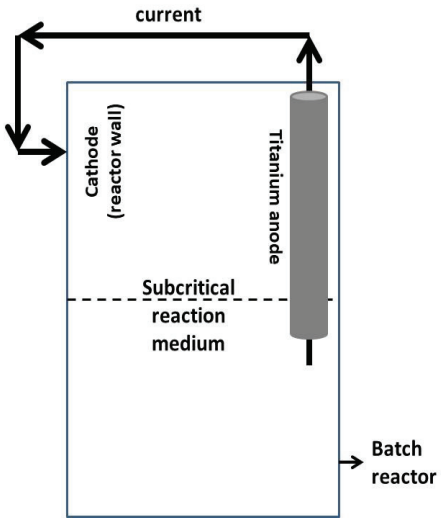

Figure 6.2. Experimental set-up for experiments under subcritical conditions

In a typical experiment under subcritical conditions, the batch reactor was filled with DBU solution (200 mL) and its concentration was 6 mM. Then, NaOH solution which is used as electrolyte was added into DBU solution at the desired concentrations. After that, the air in the reaction media was purged by nitrogen gas. Then, the mixture was continuously stirred and heated up to the desired reaction temperature. After reaching the desired temperature, no current was applied during hydrothermal degradation experiments while 1 A of constant current was applied in the hydrothermal electrolysis experiments. The reactions were carried out various time intervals between 30 and 90 minutes. After completion of reaction time, the heater was turned off and cooling water was started to circulate around the reactor. When the temperature reached 40 °C, the reactor was opened and liquid sample was taken and analyzed via TOC to investigate the removal efficiency under subcritical conditions.

In the context of experimental study over DBU treatment in HCW, the effects of reaction parameters that are the concentration NaOH (0.01 and 0.05 mM), reaction duration (30, 60 and 90 min), and current density (0 and 0.0027 mA/cm^2) were investigated by creating a general full factorial design via Minitab 18 software and the experimental results were analyzed statistically. Furthermore, the impacts of reaction

temperature (200, 240, and 280 °C) and $[DBU]_0$ (3, 6, and 12 mM) over the removal of DBU and TOC under subcritical conditions were searched. Additionally, a kinetic study was performed to understand the reaction kinetic and the intermediate products of the treatment of DBU in HCW were identified by gas chromatography-mass spectrometry (GC−MS) analysis.

6.3. HPLC Calibration Curves of Sucrose and DBU

The liquid product solution of SMS was analyzed via high-performance liquid chromatography (HPLC) to determine the sucrose conversion. HPLC analysis for sucrose was performed using a Rezex RCM Ca^{+2} column at 80 °C column temperature and distilled water was used as mobile phase. The calibration curve for sucrose analysis via HPLC is created using SMS at seven different sucrose concentration (10, 20, 50, 100, 200, 1000 and 2000 ppm) and obtained calibration curve is given in Figure 6.3.

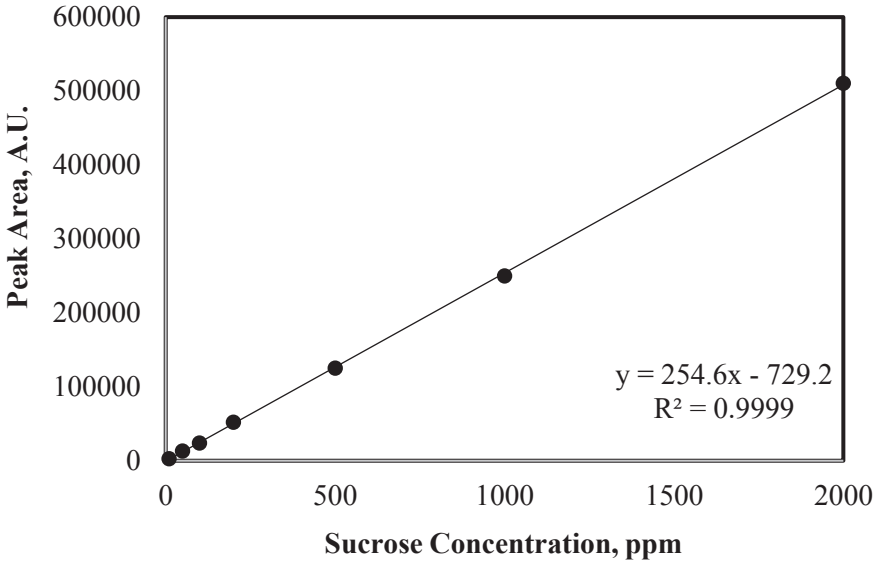

Figure 6.3. Sucrose calibration curve

The liquid product solution of DBU model solution was analyzed to determine DBU removal under subcritical conditions via HPLC analysis using C18 column and column temperature was 50 °C. In this analysis, a mobile phase consists of acetonitrile

(A phase) and the mixture of 0.001 vol % H_3PO_4 - ultra pure water (B phase) was used and a gradient method was used to analyze the samples and the details are given in Table 6. 2. In order to create the calibration curve of DBU, several DBU solutions at different concentrations (10, 20, 50, 100, and 200 ppm) were used and the calibration curve of DBU is given in Figure 6.4.

Table 6.2. Analysis conditions of DBU

Time (min)	B phase (%)
0	100
8	5
10	5
10.01	100
12	100

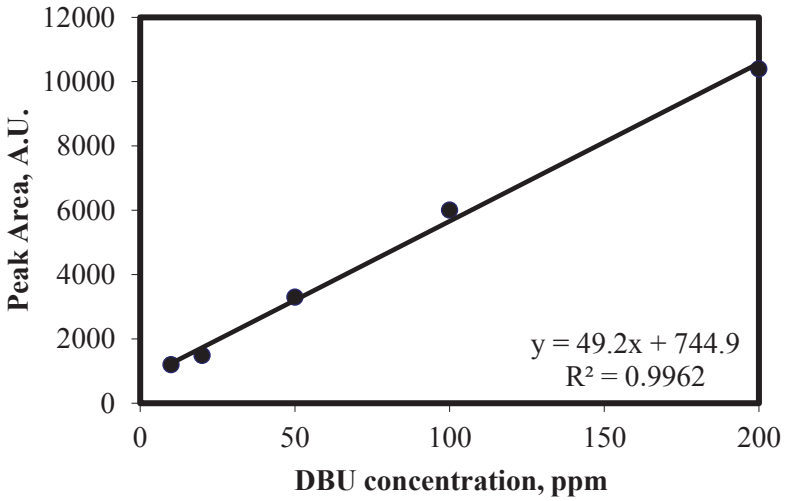

Figure 6.4. DBU calibration curve

6.4. Synthesis of Catalysts

In this context, firstly, graphene synthesis from graphite by chemical reduction was performed. Then, synthesis of perovskite type catalysts (LFO, BFO and LRO) and synthesis of perovskite type hybrid catalysts (GLFO, GBFO and GLRO) were performed. The synthesis procedures of graphene, perovskite type catalysts and hybrid catalysts were

developed based on literature and their preparation steps were explained at the following subtitles in detail.

6.4.1. Synthesis of Graphene

Based on the literature, chemical decomposition is the most appropriate method to obtain graphene based on the cost, labour and energy usage (Hu et al., 2014, Guo. et al., 2013). In this respect, it was decided to produce graphene by chemical separation method. The procedure for synthesis of graphene (on basis: 1 g) is as follows: (Liu et al., 2013)

0.5 grams of $NaNO_3$ and 25 ml of H_2SO_4 were added on 1 gram of graphite and hence, a solution was obtained. Then, the solution was kept in an ice bath to add 3 grams of $KMnO_4$ since addition of $KMnO_4$ cause a very exothermic reaction and the temperature must be below 20 °C. The obtained mixture was continued to stir in an ice bath at 35 °C for 40 minutes. Then, the mixture was added into distilled water (45 mL) and stirred for 20 minutes. After that, mixture of distilled water (140 ml) and H_2O_2 (10 ml) was prepared and the obtained mixture added into the hydrogen peroxide solution. After this step, the final mixture was kept at room temperature for one day and hence, graphene oxide (GO) formed. In order to remove sulphate and metal ions, the obtained GO was washed with 5% HCl solution. After washing step, obtained residue was calcinated in the furnace at 300 °C for 15 minutes. After calcination, 1 ml of hydrazine hydrate was added for reduction of 100 mg of GO and they were stirred at 80 °C for 6 hours. The final residue was dried under vacuum at 50 °C to obtain graphene.

6.4.2. Synthesis of Perovskite Type Catalysts

6.4.2.1. Synthesis of LFO

Considering the stoichiometric ratio, the precursors (lanthanum (III) nitrate and iron (III) nitrate) were separately dissolved in distilled water. After that, they were mixed

and stirred at room temperature for 1 hour. Hence, the mixture of precursor solution was achieved. Required amounts of $C_6H_8O_7$ based on the stoichiometric ratio (1.5 times of total moles of precursors) and $C_2H_6O_2$ (25 ml for 0.1 mol of one of the precursors) were mixed with distilled water. Then, the prepared solution consists of $C_2H_6O_2$ and $C_6H_8O_7$ was put into the precursor solution mixture. The obtained solution was heated up to 80 °C and it was kept at this temperature and continued to stir until the gel formation was observed. After that, the obtained gel was dried in the oven for 6 hours at 150 °C. Then, it was calcined in the furnace at different calcination temperatures (500, 600, 700 and 800 °C) (Rusevova et al., 2014). Preparation steps of LFO were shown in Figure 6.5.

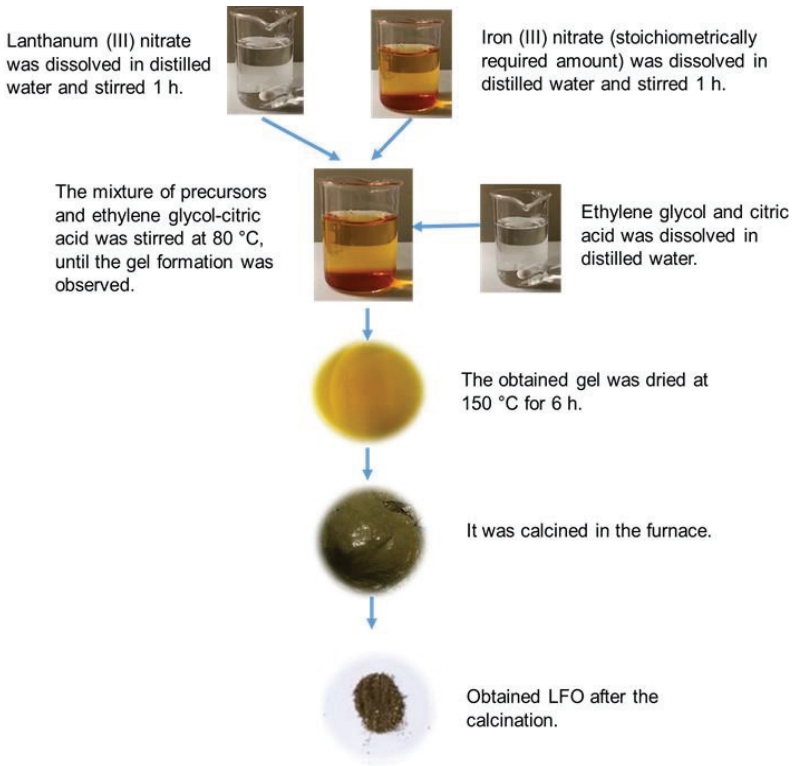

Figure 6.5. Synthesis of LFO

6.4.2.2. Synthesis of BFO

To synthesize BFO, the same procedure which was used for synthesis of LFO was followed using bismuth (III) nitrate instead of lanthanum (III) nitrate as precursor (Rusevova et al., 2014). Preparation steps of BFO were illustriated in Figure 6.6.

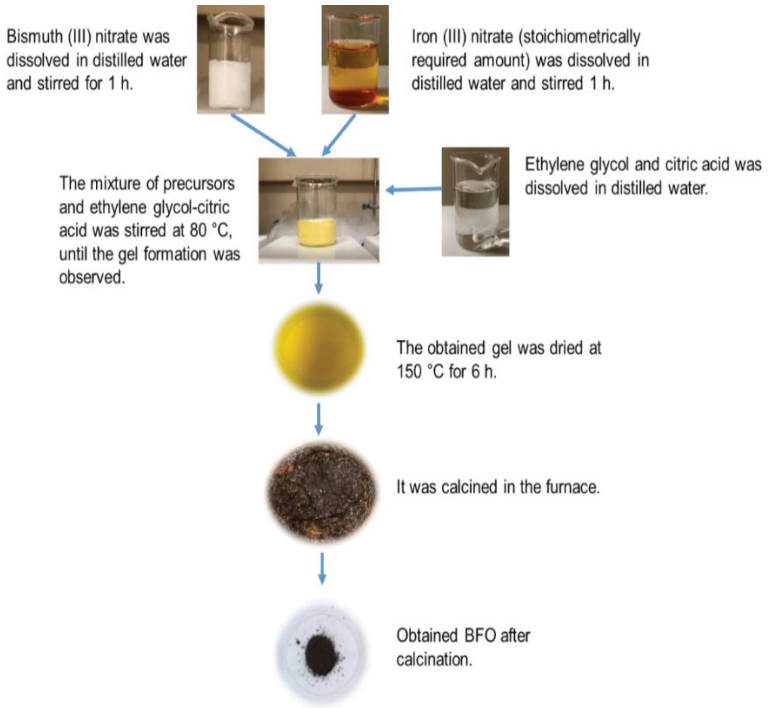

Figure 6.6. Synthesis of BFO

6.4.2.3. Synthesis of LRO

Pechini's citrate technique was modified for the synthesis of LRO. In the procedure, the ratios of citric acid to ruthenium chloride and ethylene glycol to citric acid were four and 1.38, respectively. Citric acid, ruthenium chloride and ethylene glycol were mixed at 50 °C and a mixture was obtained. Lanthanum nitrate was added into this mixture considering the stoichiometric ratio of ruthenium to lanthanum and then, it was kept at 50 °C and evaporation was continued for two days. After evaporation, obtained residual was dried at 150 °C for 24 hours. LRO was calcinated for four hours at 700 °C (Pietri et al., 2001).

6.4.3. Synthesis of Perovskite Type Hybrid Catalysts

The needed quantity of graphene was put into the ethanol-water solution and sonicated for two hours at room temperature to obtain graphene supported LFO, which

comprises 20% graphene by mass. After that, LFO which is calcined at 500 °C was put into obtained solution and stirred for two hours. After, it was centrifuged and dried at 70 °C for 12 hours. Finally, graphene supported LFO which was calcinated at 500 °C was synthesized. Additionally, LFO which was calcinated at 600, 700 and 800 °C was used to synthesize the hybrid catalysts. The same procedure was repeated with BFO and LRO to obtain perovskite type hybrid catalysts which were calcinated at different calcination temperatures (Rusevova et al., 2014; Afifah and Saleh, 2017).

CHAPTER 7

CHARACTERIZATION STUDY

This chapter comprises the analyses conditions of SEM-EDX, XRD, BET, FT-IR, TEM, XPS and PL analyses and the results of these catalyst characterization studies. Among these analyses, XPS was carried out for only most promising photocatalysts (LFO and GLFO) for hydrogen production. In addition, the results are discussed in detail and compared with literature.

7.1. Results of Characterization Study

Surface morphologies of all catalysts (LFO, GLFO, BFO, GBFO, LRO and GLRO) calcined at different calcination temperatures (500, 600, 700 and 800 °C) were searched via SEM analysis with FEI QUANTA 250 FEG model.

The synthesized catalysts were degassed at 350 °C for 3 hours and BET areas, pore sizes and pore volumes of these catalysts were determined via Micromeritics ASAP 2010. Additionally, N_2 adsorption-desorption isotherms were also obtained.

To confirm the perovskite structure of all synthesized catalysts, the crystalline structures of perovskite and hybrid catalysts were examined by Philips X'Pert diffractometer with CuKα radiation. The scattering angle 2θ was varied from 5° to 80° (step length: 0.02°).

KBr (potassium bromide) pellet technique was used to get infrared spectra of these catalysts at room temperature. The pellets were prepared with a sample amount of 0.1 mg catalyst and required amount of KBr to reach to total amount of 2000 mg. The FTIR spectra of perovskite and hybrid catalysts were retrieved between 400 and 2000 cm^{-1} of wavelength (resolution of 4 cm^{-1}) by an infrared spectrometer type Schimadzu FT-IR 8400S. The formation of bonds in perovskite structure of synthesized catalysts were investigated with this analysis.

PL analysis was carried out via Fluorescence Spectrometer (Edinburgh Instruments FLSP920) to comprehend the photocatalytic activities of all synthesized catalysts.

XPS (device: Thermo Scientific K-Alpha with a 180° hemispherical analyzer-128 channel detector and the X-ray source was Al Kα Monochromatic (1486.68 eV) and TEM (device: Jeol 2100F 200kV RTEM) analyses were performed for LFO and GLFO.

7.1.1. SEM Results

SEM analysis was carried out to investigate the surface morphology of all synthesized catalysts which are calcinated at 700 °C and their SEM diagrams were given in Figure 7. 1.

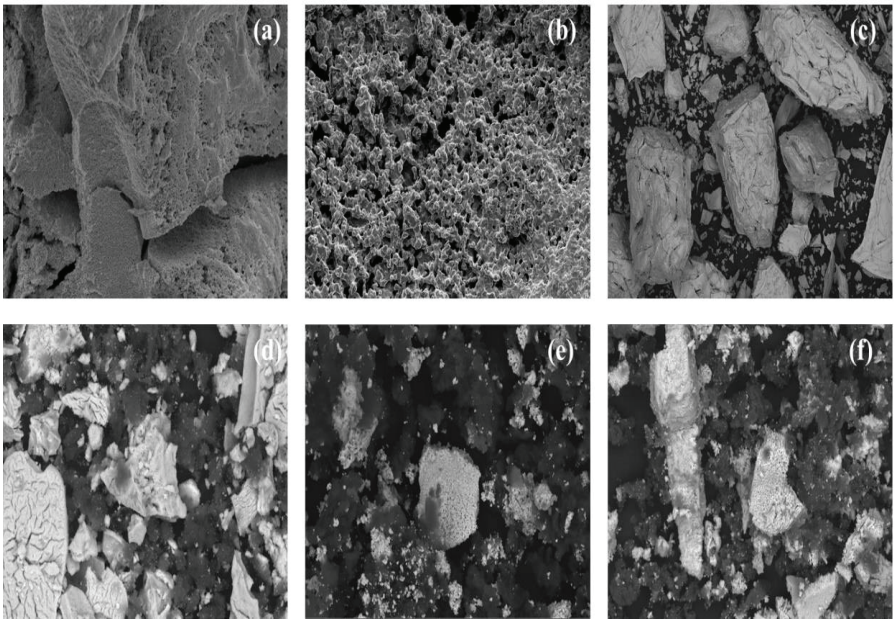

Figure 7.1. SEM diagrams of LFO (a), BFO (b), LRO (c), GLFO (d), GBFO (e) and GLRO (f) (Magnification: 1000x)

Additionally, GLFO is the most promising catalyst so that SEM diagrams of GLFO which was calcinated at various temperatures (500, 600, 700 and 800 °C) were given in Figure 7. 2. Based on the SEM diagrams of LFO, GLFO, BFO, GBFO, LRO and

GLRO catalysts which were calcined at 700 °C, it is clearly seen that they had a very porous structure and nanocrystals were agglomerated. Incorporation of graphene did not cause any change in the morphology of perovskite catalysts and graphene was homogeneously distributed. Therefore, the similar results were found in many studies (Dükkancı, 2016; Samran et al., 2019; Kiani et al., 2018). Based on Figure 7. 2., as the calcination temperature increased, the porous structure became more prominent and the particle size reduces. The perovskite structure was conserved up to 800 °C of calcination temperature and there was no change in the structure of GLFO which are calcined at different temperatures after graphene was introduced. Futhermore, EDS spectrum and EDX mapping of GLFO which was calcinated at 700 °C was given in Figure 7. 3.

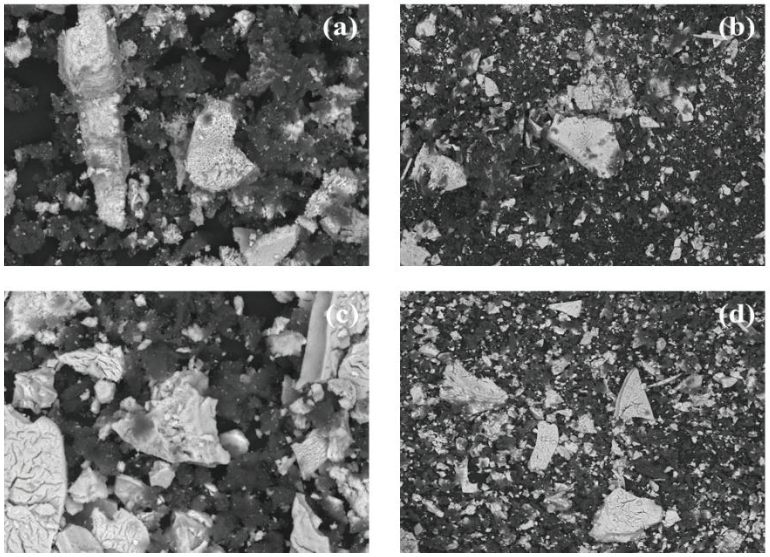

Figure 7.2. SEM diagrams of GLFO calcinated at different temperatures, 500 °C (a), 600 °C (b), 700 °C (c) and 800 °C (d)

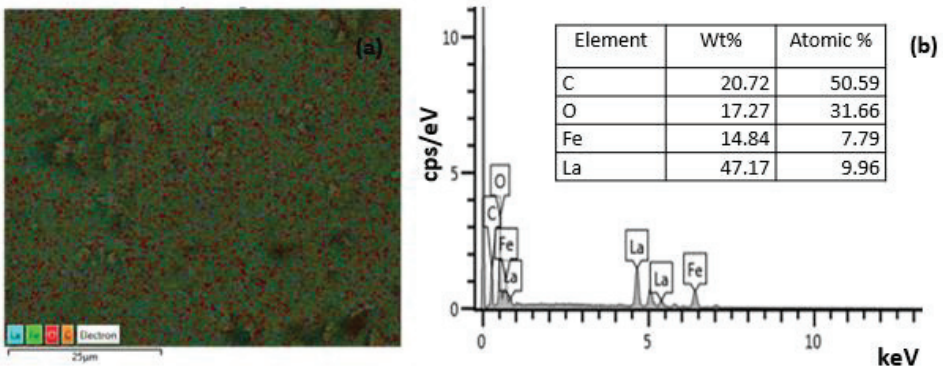

Figure 7.3. EDX mapping of GLFO (a) and EDS spectrum of GLFO (b)

The weight percentage of graphene in GLFO catalyst was confirmed by the help of EDS analysis and the elemental compositions of elements (La, Fe and O) in GLFO were determined. In this study, the ratio of La/Fe was found as 1.13. In literature, Kucharczyk et al. synthesized LFO which was calcinated at 700 °C and the La/Fe ratio was determined as 1.12 for this calcination temperature while Cho et al. determined as 1.18 (Kucharczyk et al., 2019, Cho et al., 2009). Thus, it could be decuded that the results of SEM analysis are in line with literature.

7.1.2. XRD Results

XRD analysis was carried out to comprehend the structures of synthesized catalysts and their XRD diagrams of perovskite catalysts and hybrid catalysts were given in Figure 7. 4. and Figure 7. 5., respectively. It is reported in a plenty of studies in the literature that perovskite type catalysts has the characteristic peaks at certain 2θ values (22.63 °, 32.22 °, 39.73 °, 46.21 °, 57.45 °, 67.42 °, 72.12 °, and 76.69 °) and observation of these peaks at given 2θ values are attributed to the orthorhombic structure of perovskite type catalysts (Dükkancı, 2016; Kucharczyk et al., 2019).

As a result, it is clearly observed in XRD diagrams of perovskite and hybrid catalysts that the characteristic peaks of these catalysts were observed at these 2θ values and hence they had orthorhombic structures. Moreover, it was seen in many studies that 2θ values of BFO were compatible with the literature (Hussain et al., 2013; Yotburut et al., 2017; Shariq et al., 2013). Graphene has an amorphous structure and its characteristic peak is near 21° (Hu et al., 2014). Based on Figure 7.5, it could be deduced that graphene was successfully synthesized.

According to the XRD patterns of LFO and GLFO, during the synthesis of perovskite and hybrid catalysts, iron oxide and lanthanum oxide did not form. Whereas some impurities were observed in XRD pattern of BFO, no impurities were observed in the XRD pattern of GBFO, LRO and GLRO. Furthermore, the broadness of these characteristic peaks proved that the nanocrystalline nature of perovskite and hybrid catalysts. Consequently, it could be concluded that the synthesis of them was successfully achieved.

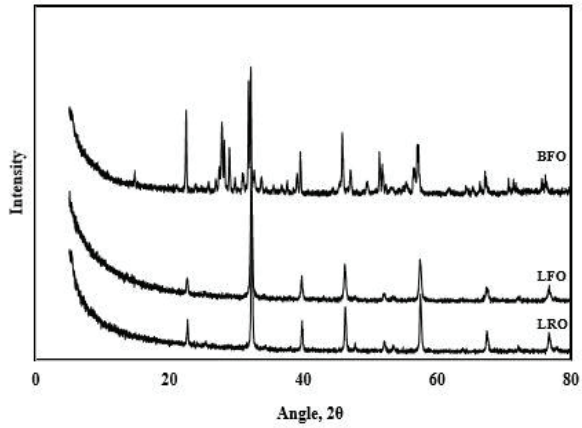

Figure 7.4. XRD diagram of perovskite catalysts

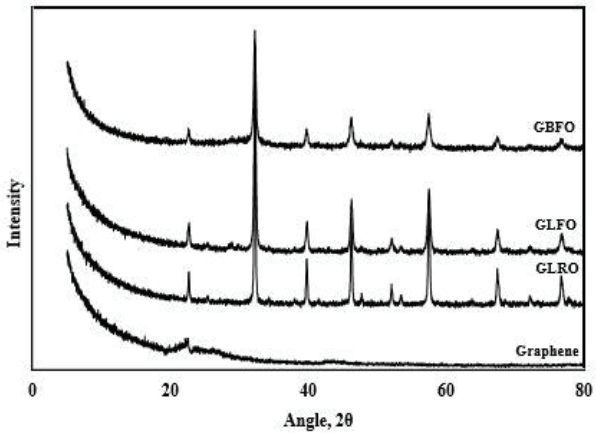

Figure 7.5. XRD diagram of graphene and hybrid catalysts

7.1.3. FT-IR Results

FT-IR analysis was carried out for LFO, GLFO, BFO and GBFO in order to confirm the formation of Fe-O (around 550 cm^{-1}) and O-Fe-O (around 400 cm^{-1}) bonds in the structure of perovskite type catalysts and FT-IR diagrams of them were given in Figure 7. 6. The presence of Fe-O stretching vibration and O–Fe–O bending vibration mode of FeO_6 octahedron in the structure of the perovskite catalysts showed that the catalyst synthesis was successfully accomplished (Dukkancı, 2016; Kucharczyk et al., 2019; Cho et al., 2009).

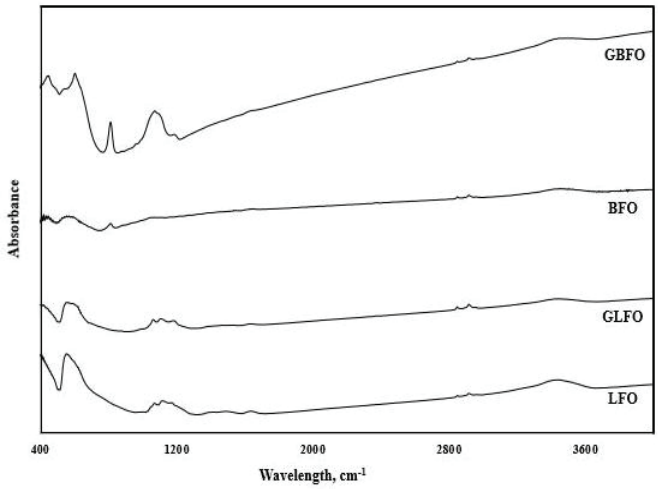

Figure 7.6. FT-IR diagram of synthesized catalysts

It is clearly seen in Figure 7. 6. that characteristic bonds of perovskite structure formed and thus, the perovskite structure was successfully obtained. Moreover, the results supported the XRD results of synthesized catalysts. The results are confirmed that the perovskite and hybrid type of catalysts were successfully synthesized. The broad peak aligning between 1000 and 1290 cm^{-1} refer to the stretching mode of carbonate ions and thus, they could form because of the exposure of them to ambient air (Feng et al., 2011). The asymmetric and symmetric C−H stretching vibrations of the methyl and methylene radicals originated from lipidic compounds are observed between 2800 and 3000 cm^{-1} and these peaks were observed in Figure 4.6. because of the contamination of them throughout analysis (Guerra et al., 2014). In addition, the wide band around 3400 cm^{-1} indicated that the hydroxyl groups are adsorbed on the surface (Dukkancı 2016).

7.1.4. BET Results

BET areas of all synthesized catalysts were listed in Table 7. 1. Introduction of graphene caused an increase the BET areas of synthesized catalysts and among them, GLRO had the highest BET area whereas BFO had the lowest BET area. Pietri et al. reported that the BET area of LRO is found as 2 m^2/g, however, LRO which is synthesized in this study has relatively higher BET surface area (Pietri et al., 2001). Moreover, the BET surface of LRO increased by the incorporation of graphene. Pore size of LRO and

GLRO were found as 5.63 nm and 4.90 nm, respectively. Pore volume of LRO and GLRO were determined as 0.017 cm^3/g and 0.026 cm^3/g. Hence, incorporation of graphene caused an increase in pore volume whereas it caused a decrease in pore size of the catalyst.

Table 7.1. BET areas of synthesized catalysts

	Perovskite Catalysts			Hybrid Catalysts		
	LFO	**BFO**	**LRO**	**GLFO**	**GBFO**	**GLRO**
BET areas [m^2/g]	9.67	1.19	22.65	15.33	2.62	27.59

In literature, BET surface area of the $LaFeO_3$ catalyst calcined at 700 °C was reported as 3.61 m^2/g (Dükkancı, 2016). However, the surface area of LFO catalyst which was calcined at 700 °C was determined to be 9.67 m^2/g. Moreover, GLFO had 15.33 m^2/g BET area and by incorporation of graphene, the catalyst had a wider surface area. Pore sizes of LFO and GLFO was found as 5.46 nm and 5.03 nm, respectively. Moreover, pore volumes of LFO and GLFO was found as 0.01 cm^3/g and 0.2 cm^3/g, respectively. Therefore, incorporation of graphene leads to an enhancement in the surface area and pore volume of hybrid catalysts whereas a reduction was observed for pore sizes of the catalyst. Consequently, lanthanum-based catalysts were found to have a higher surface area than bismuth-based ones. The N_2 adsorption-desorption isotherms of perovskite catalysts and hybrid catalysts were shown in Figure 7. 7. and Figure 7. 8., respectively.

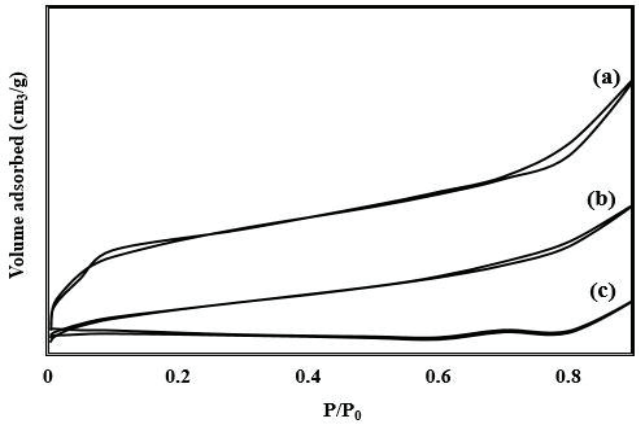

Figure 7.7. N_2 isotherms of perovskite catalysts: LRO (a), LFO (b) and BFO (c)

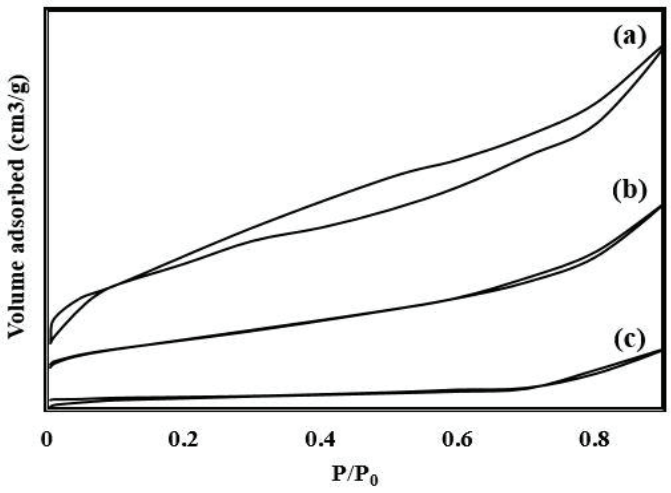

Figure 7.8. N_2 isotherms of hybrid catalysts: GLRO (a), GLFO (b) and GBFO (c)

Based on the results, all catalysts demonstrated a type IV isotherm and they have a type H1 hysteresis loop in the relative pressure (P/P_0) range of 0.4–0.9. Consequently, this hysteresis loop refers that all synthesized catalysts were mesoporous.

7.1.5. PL Results

Photoluminescence (PL) analysis is a crucial technique to grasp the recombination process of photo-excited charge carriers. Additionally, it suggests an idea anent the life span of electron-hole pairs. The semiconductor photocatalysts are illuminated with a light source as a photon energy source in a representative PL analysis and this photon energy must be higher than the band gap of semiconductor photocatalysts so that the polarisation which could be defined by Bloch equations could be started. After initiation of polarisation, firstly, electrons (e^-) and holes (h^+) form in the conduction band. Subsequently, they form in valance band with finite momenta. Because to coulomb scattering and phonon interaction, the excitons' momentum and energy relax, and the peaks in the PL diagram have a reduced intensity, indicating slower charge pair recombination and a longer life period of e^- and h^+ pairs (Acharya et al., 2017; Wu et al., 2018; Hongfang et al., 2016; Li et al. 2015). The PL spectras of all synthesized catalysts were given in Figure 7.9.

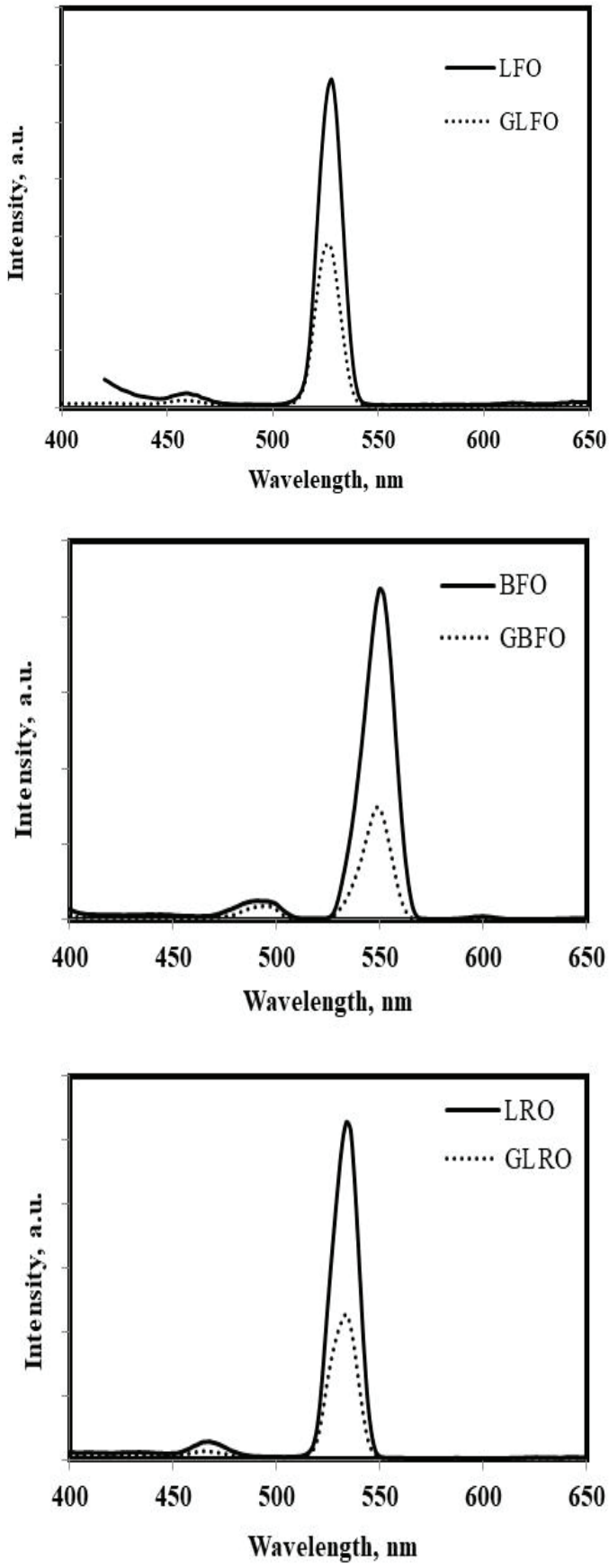

Figure 7.9. PL spectras of all synthesized catalysts

LFO and GLFO gave a peak at 528 and 526 nm, respectively. Based on PL spectra of BFO and GBFO, it was seen that BFO had a peak at 552 nm and GBFO had a peak at 550 nm. Additionally, LRO had a peak at 536 nm while GLRO had a peak at 534 nm. Therefore, addition of graphene caused a small shift in peaks compared to perovskite catalysts and it implies that the hybrid catalysts needed lower photon energy for photocatalytic hydrogen production.

PL analysis gave a brief idea about the photocatalytic activities of synthesized catalysts. According to the results of PL analysis, the incorporation of graphene caused a decrease in the intensities of peaks for all synthesized catalysts and thus, it implied that hybrid catalysts could show better photocatalytic activity than perovskite catalysts. Whereas BFO had the highest peak intensity, GLFO had the lowest peak intensity. Therefore, the highest hydrogen evolution efficiency must be achieved using GLFO and the lowest hydrogen evolution must be obtained in the presence of BFO. Consequently, among all synthesized catalysts, the most promising solar-driven photocatalyst is GLFO based on PL analysis.

7.1.6. XPS Results

XPS analysis was used to determine the surface elemental composition of LFO and GLFO and the results were given in Figure 7. 10. and Figure 7. 11. According to XPS spectras, La $3d_{5/2}$ was responsible for the two peaks at 835.7 eV and 839 eV and the main peak of La $3d_{5/2}$ was the peak at 835.7. A core hole with an electron transferred from O 2p valence band to an empty La 4f orbit caused the other peak of La $3d_{5/2}$. Additionally, the results were in accordance with literature (Lee et al., 2014; Xiao et al., 2015; Thirumalairajan et al., 2013). The spin and orbit splitting of the Fe (2p) components were $Fe2p_{3/2}$ and $Fe2p_{1/2}$ were located in XPS spectras of LFO and GLFO at 711.8 and 724.3 eV, respectively. In literature, similar results were reported in many studies (Lee et al., 2014; Xiao et al., 2015; Thirumalairajan et al., 2013; Yang et al., 2006).

The peak of O1s which located at 530.7 eV in XPS spectras of LFO and GLFO had higher intensity compared to other elements since its composition was higher than the other elements. The peak of C-C component of graphene was observed at 284.5 eV.

In Figure 4.11 (a), the shake-up satellite of the graphene owing to the π-π transitions placed at 291.1 eV as a weak peak and the results were in accordance with literature (Moreau et al., 2010; Kidambi et al., 2013; Villar-Rodil et al., 2009).

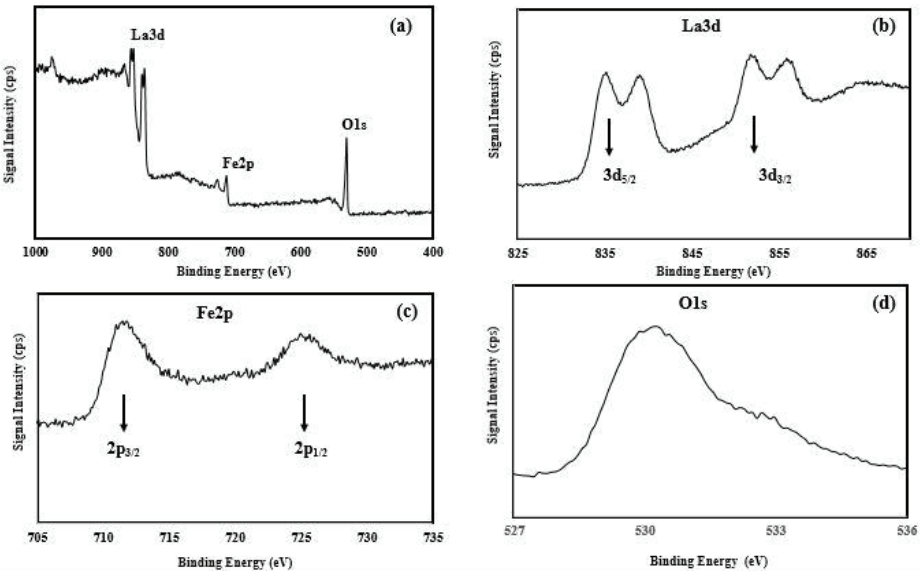

Figure 7.10. XPS spectra of LFO (a), La $3d_{5/2}$ (b), Fe2p (c), O1s (d)

Based on XPS analysis of GLFO, the binding energies of La3d5, Fe2p and O1s were determined and results were listed in Table 7. 2. According to Table 7. 2., introduction of graphene brought about a shift in binding energies of La3d5, Fe2p and O1s and hence, it pointed out that there was an electronic interaction between LFO crystals and graphene. Therefore, it could be concluded that graphene supported LFO was successfully synthesized.

Table 7.2. Binding energies of components

Components	**Binding Energy (eV) of LFO**	**Binding Energy (eV) of GLFO**	**Δ (eV)**
La3d5	835.2	835.9	0.7
Fe2p	711.8	712.6	0.8
O1s	530.37	531.5	1.2

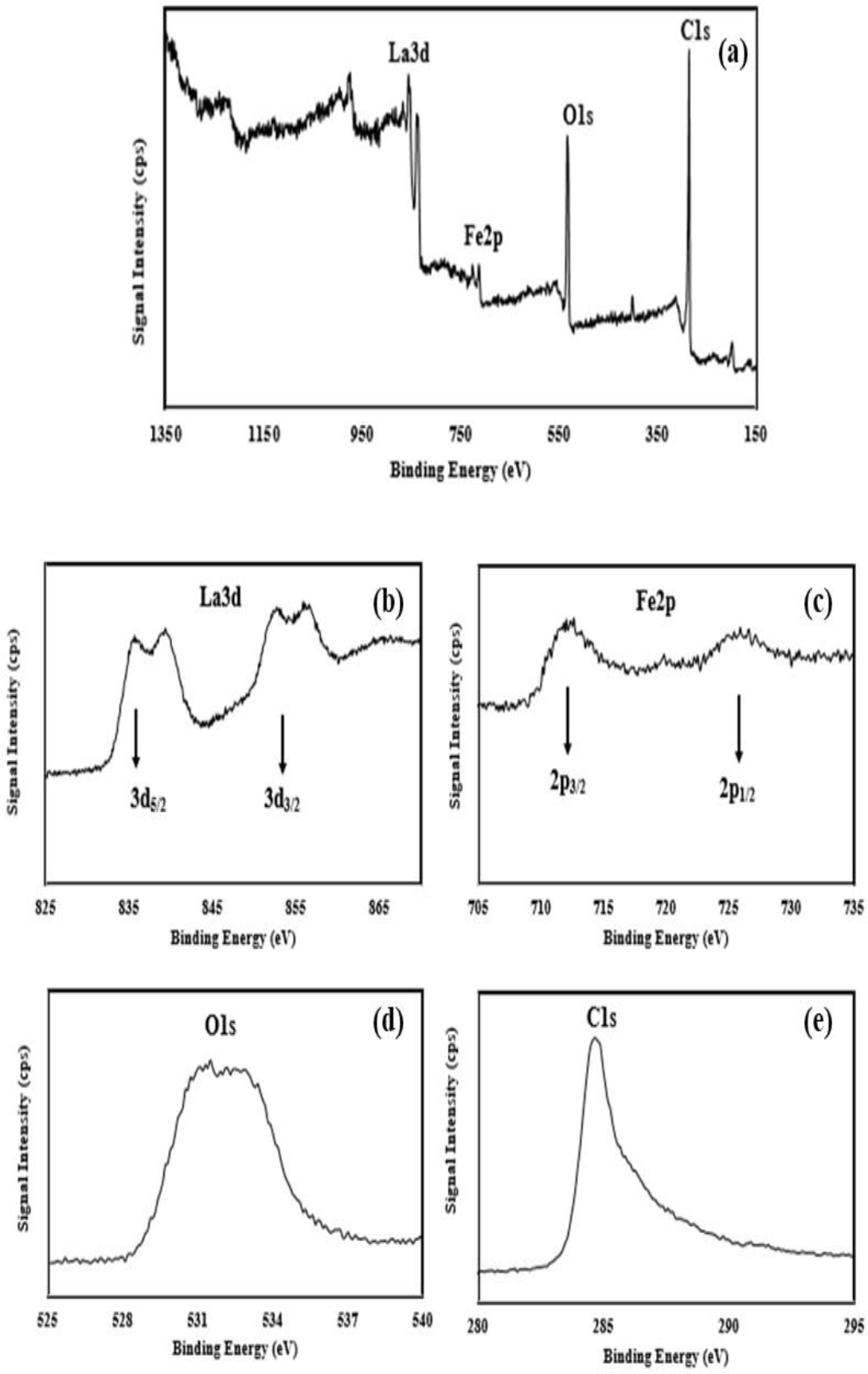

Figure 7.11. XPS spectra of GLFO (a), La $3d_{5/2}$ (b), Fe2p (c), O1s (d) and C1s (e)

7.1.7. TEM Results

The internal morphologies of LFO and GLFO were investigated via TEM analysis and the results were given in Figure 7. 12.

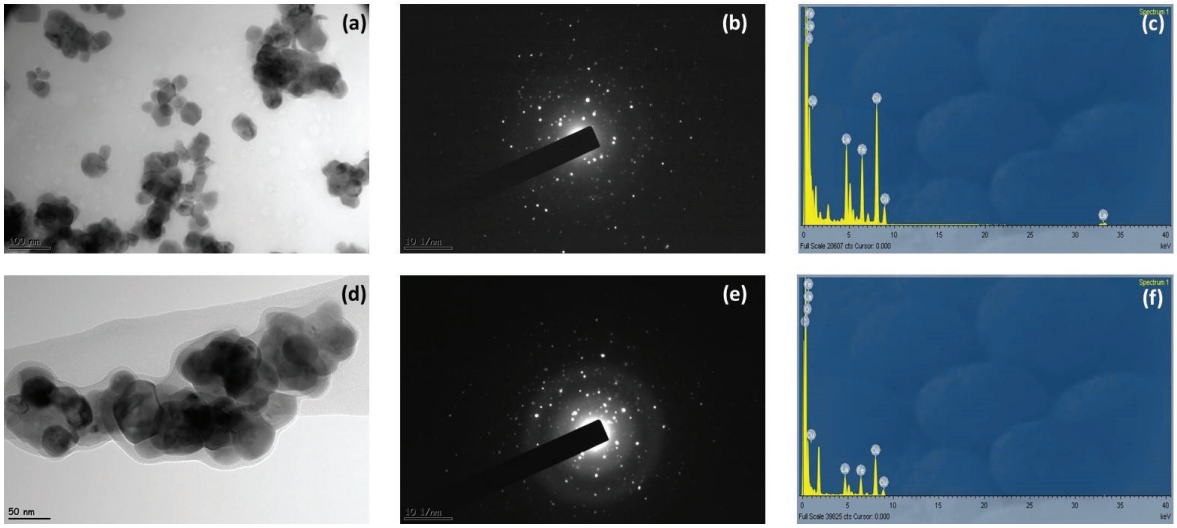

Figure 7.12. TEM images of LFO (a) and GLFO (d), SAED pattern of LFO (b) and GLFO (e), EDS pattern of LFO (c) and GLFO (f)

According to the results, the catalysts (LFO and GLFO) were not suitable for permeability of electron and very rough agglomerates are seen in TEM images. Yet, a dispersed distribution was viewed in TEM images. In addition, TEM image of GLFO showed that LFO was covered with a graphene layer. According to TEM images of GLFO, because of the interplanar spacing of LFO, it was possible to determine that crystal lattice fringes had an interfringe distance. Many research in the literature have reported similar findings (Acharya et al.,2017; Ren et al., 2016; Hao et al., 2020). The incorporation of graphene did not occur any change in perovskite structure. Moreover, XRD results supported the TEM results. Therefore, the introduction of graphene was successfully accomplished. SAED patterns prove their poly-crystallinity characteristics. Besides, these patterns confirmed that the orthorhombic structure of LFO was successfully accomplished. The results were inconsistence with the literature (Acharya et al., 2017, Lee et al., 2013, Ren et al., 2016). In EDS spectrum results, La, Fe and O elements were determined for LFO and the XPS and SEM-EDS spectrum results confirm

the existence of these elements. Furthermore, the elements (La, Fe, O and C) were seen in the EDS spectrum and SEM-EDS spectrum of GLFO and XPS results supported this finding. Yet, some impurities were observed in TEM-EDS spectrums of LFO and GLFO.

Consequently, the characterization study of synthesized catalysts showed that the synthesize of perovskite and hybrid catalysts were successfully accomplished. Moreover, the most promising catalyst for photocatalytic hydrogen evolution from SMS, real sugar beet wastewater and DBU model solution was specified as GLFO so that firstly, LFO and GLFO were tested for hydrogen evolution via photocatalytic oxidation.

CHAPTER 8

PHOTOCATALYTIC HYDROGEN PRODUCTION FROM SUCROSE MODEL SOLUTION

The photocatalytic performances of perovskite and hybrid catalysts over the evolution of hydrogen from SMS were searched to choose most promising photocatalyst. In the context of experimental study for hydrogen evolution from SMS, firstly, the effects of solar light, pH of sucrose solution and catalyst loading over the produced hydrogen amount were examined in the presence of all synthesized catalysts to get a brief idea about their photocatalytic activities.

Firstly, hydrogen production from distilled water was investigated at pH of 3 and 7.5 solar light illumination to determine the amount of hydrogen from distilled water and the obtained hydrogen amounts were varied between 371 and 526 $\mu mol/g_{cat}$ depending on the reaction conditions. These experiments were also performed in the presence of hydrogen peroxide (15 mM) for all synthesized catalysts and the obtained hydrogen amounts were varied between 798 and 912 $\mu mol/g_{cat}$.

To clarify the effect of solar light on the photocatalytic hydrogen evolution from SMS, the synthesized catalysts (LFO, GLFO, BFO, GBFO, LRO and GLRO) were tested in the presence and absence of solar light at the following conditions: pH 7.5, catalyst loading 0.1 g/L, 1000 ppm of SMS and 4 hours of reaction time. The results were given in Figure 8.1 (a) and (b) for no light and solar light irradiation, respectively.

In the absence of light, very low hydrogen production was achieved and among these catalysts, LFO and GLFO showed relatively higher efficiency compared to other ones. On the other hand, usage of solar light caused considerable increase in the produced hydrogen amount and hence, the hydrogen production could be achieved in the presence of these perovskite and hybrid catalysts under solar light irradiation. Additionally, hybrid catalysts showed higher catalytic efficiency than perovskite catalysts. Slightly higher hydrogen production amounts were obtained in the presence of LFO and GLFO with respect to other catalysts and PL results of these catalysts support the experimental results. Therefore, the subsequent experiments were performed under solar light irradiation since

higher hydrogen yields could be achieved due to usage of photon energies by photocatalyst to degrade organic pollutants in wastewaters.

After completing the light effect experiments, the effect of catalyst loading (0.1 and 0.2 g/L) over the hydrogen production from SMS (1000 ppm) was investigated at 7.5 of pH for 4 hours of reaction duration in the presence of all synthesized catalysts and the results were represented in Figure 8. 2. Increasing amount of catalyst loading for all catalysts caused a decrease in the produced hydrogen amounts. However, in all cases, hybrid catalysts showed higher photocatalytic activities in terms of produced hydrogen amounts than perovskite catalysts. Therefore, it could be deduced that the supporting with graphene enhanced their photo-catalytic activities. Additionally, it implies that introduction of graphene causes a decrease in the probability of recombination of electrons and holes while it enhances the efficiency of separation. After the investigation of catalyst loading effect, the effect of pH (3 and 7.5) was investigated using 0.1 g/L of catalyst loading for each catalyst and obtained results were given in Figure 8.3.

Based on the results, all catalysts showed higher photocatalytic activity in acidic reaction media compared to pH of 7.5 since pH of 3 is lower than their pH_{zpc} and hence their surfaces can charge below their pH_{zpc} so that the evolved hydrogen amounts enhanced. Among them, LFO and GLFO showed a significant increase in the produced amount of hydrogen.

As a result, LFO and GLFO were chosen as the most promising catalysts to produce hydrogen from SMS based on the experimental results as well as PL results.

Full Factorial Design (FFD) was used to build an experimental design via Minitab 2018 statistical analysis program to comprehend the effects of reaction parameters that are initial pH of SMS, catalyst loading, graphene content and $[H_2O_2]_0$ over the hydrogen evolution via photocatalytic oxidation using most promising catalysts (LFO and GLFO). A statistical analysis was carried out to comprehend the main impacts of them and their interactions with each other. Uncoded values of these factors were listed in Table 8.1.

The experimental design matrix and the obtained experimental results were listed in Table 8.2. The obtained hydrogen amounts varied between 2882.29 and 3388.34 $\mu mol/g_{cat}$. Addition of hydrogen peroxide led to an increase over produced hydrogen amount and higher hydrogen amounts were observed in the presence of GLFO. For instance, a considerable increase over produced hydrogen amount was observed using 15 mM of hydrogen peroxide at pH 3 and 7.5 in the presence of LFO and GLFO (0.1 g/L catalyst loading).

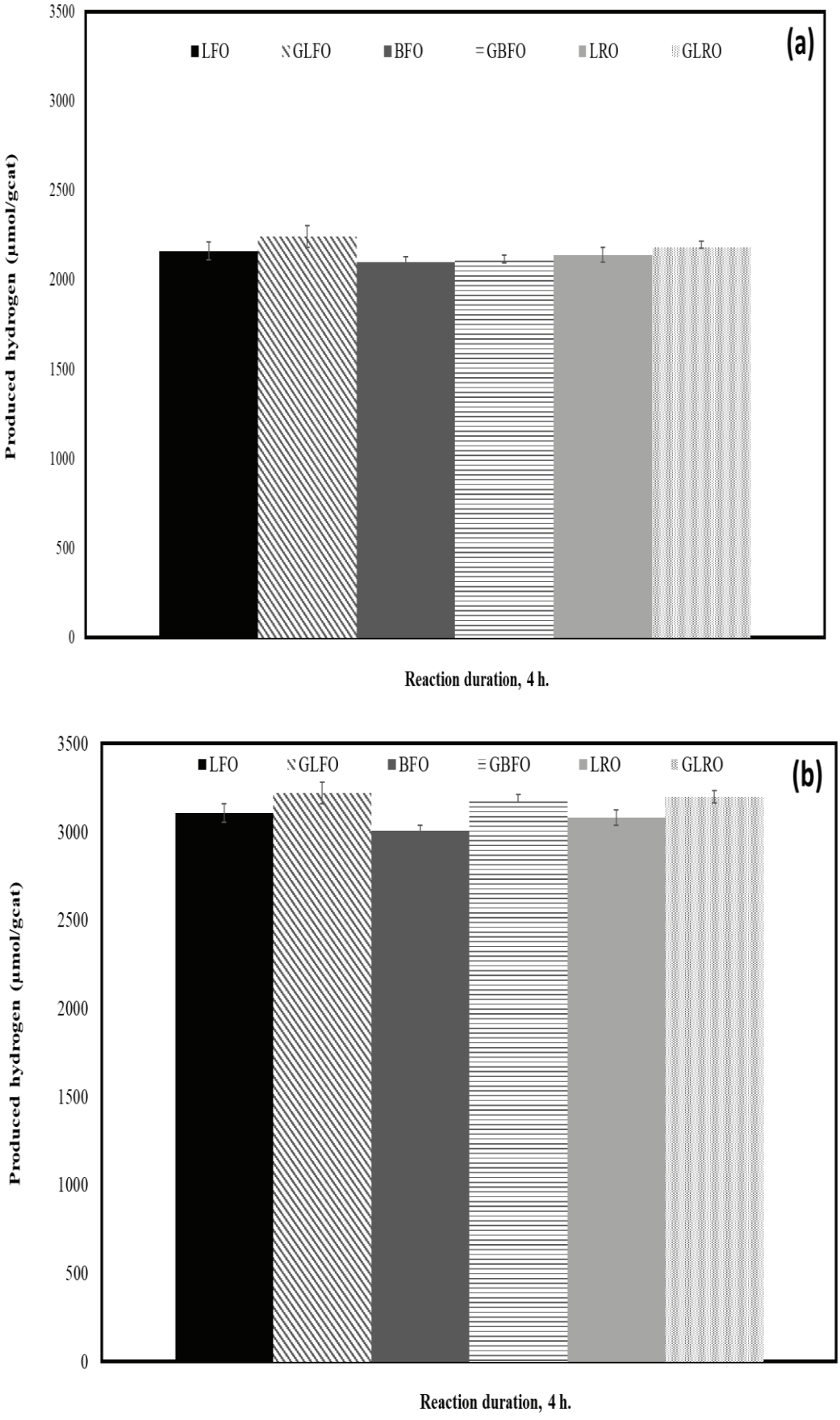

Figure 8.1. Photocatalytic activity of perovskite and hybrid catalysts (a) no light, (b) solar light irradiation

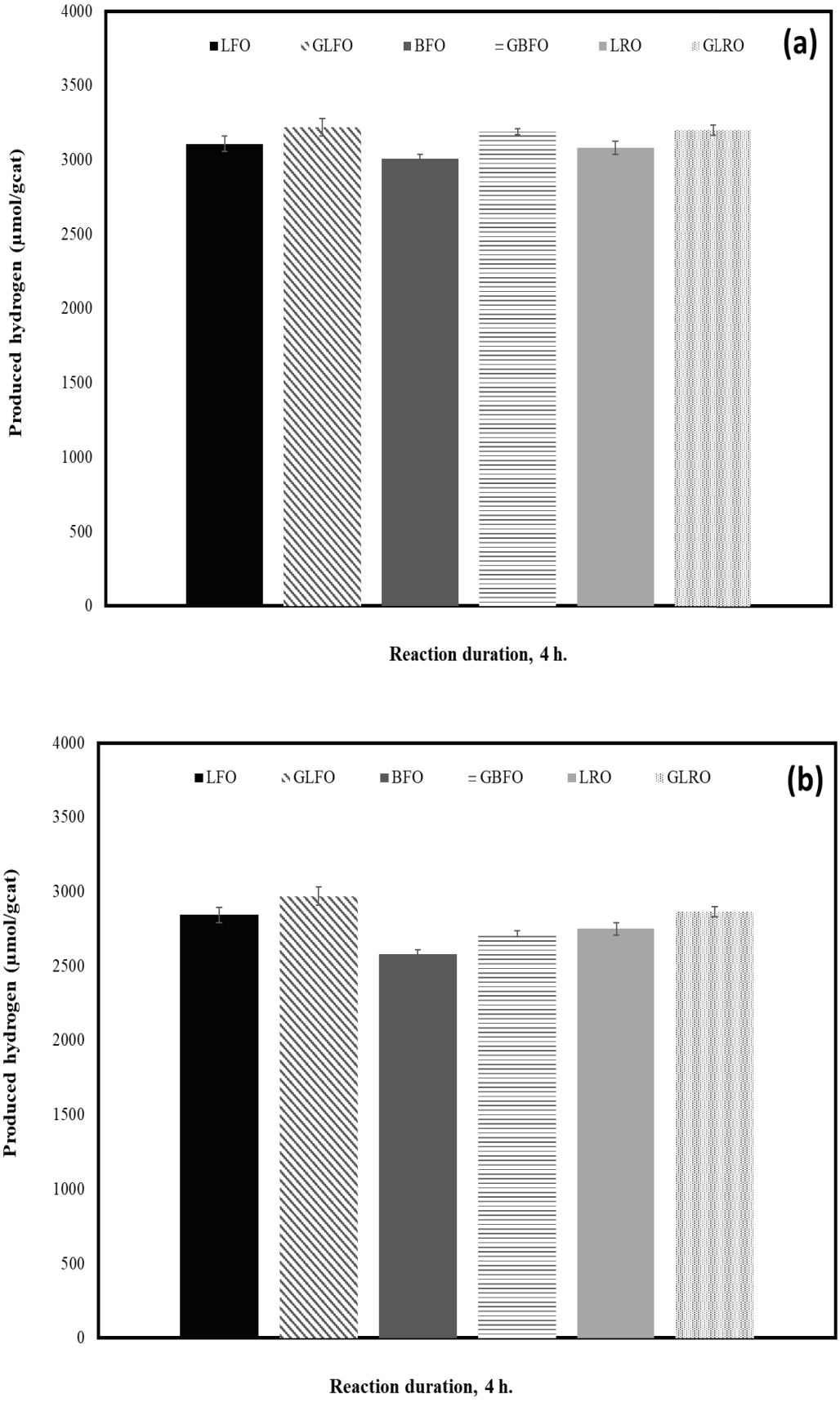

Figure 8.2. Catalyst loading effect for all catalysts; 0.1 g/L (a) and 0.2 g/L (b)

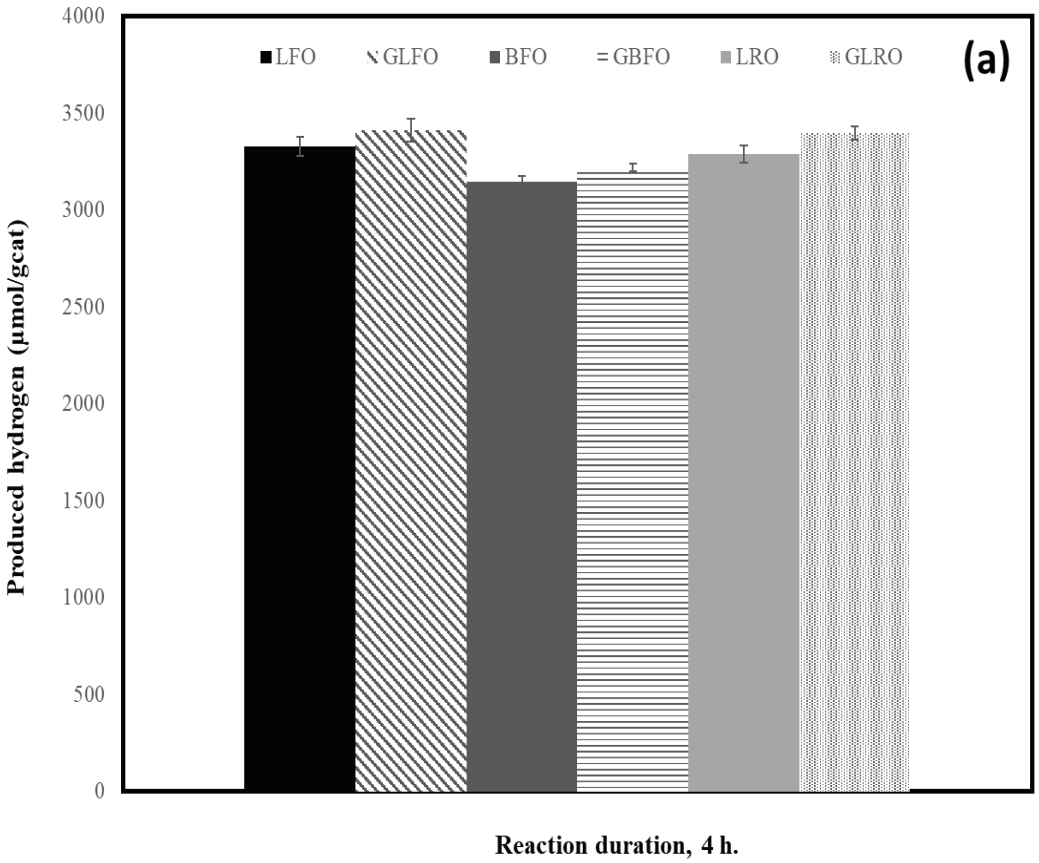

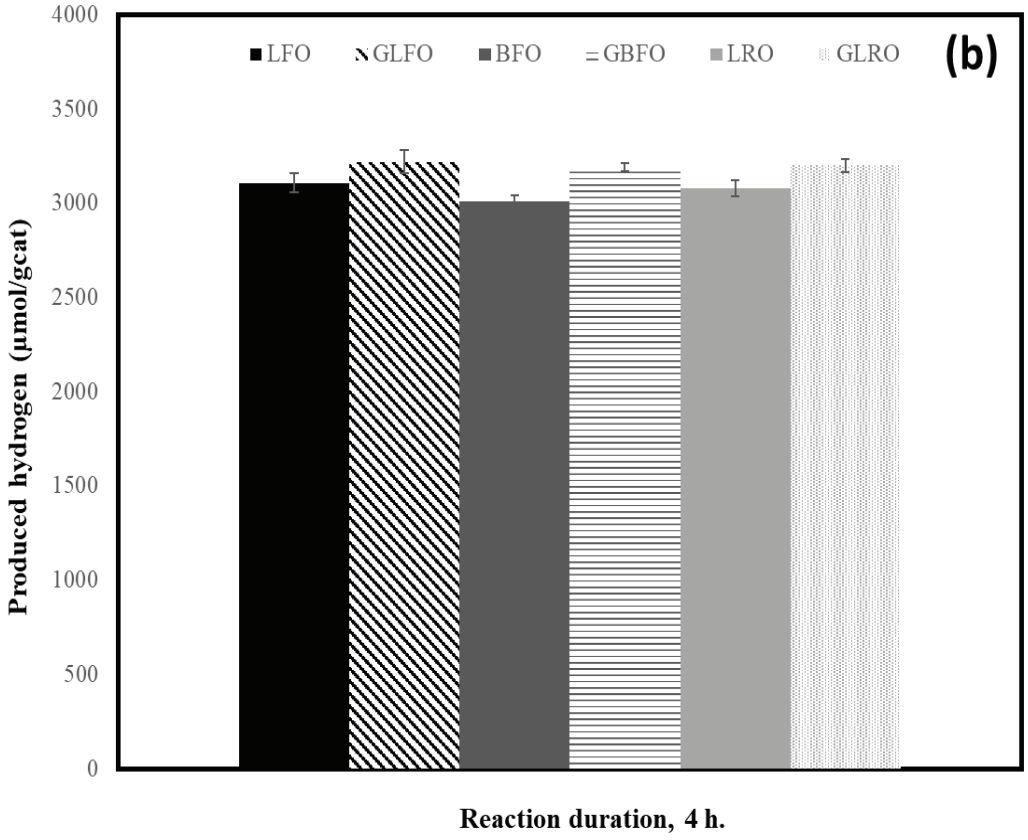

Figure 8.3. pH effect for all catalysts; pH of 7.5 (a) and pH of 3 (b)

Table 8.1. Uncoded values of factors

Factors	**Uncoded values**
pH (A)	3 and 7.5
Catalyst Loading (B)	0.1 and 0.2 g/L
$[H_2O_2]_0$ (C)	0 and 15 mM
Graphene content (D)	0 and 0.2

The reaction parameters are labelled as A, B, C and D in this experimental design for initial pH of SMS, catalyst loading of LFO and GLFO, $[H_2O_2]_0$ and graphene content of catalysts, respectively. ANOVA table of the experimental matrix for FFD was given in Table 8. 3. Based on the obtained results, p-values which are less than $\alpha = 0.05$ of each factor are given individually to comprehend the main effects and interactions between the reaction factors. The value of R^2 for this model is determined as 86.53 % and thus, it could be implied that the model is well fit to the evolved hydrogen amount experimentally.

Based on the ANOVA table, graphene content (D) had a considerable impact over the evolved hydrogen amount whereas other main factors did not affect statistically. Among 2-way interactions, A*C had an impact over the produced amount of hydrogen and hence they show a synergetic effect for hydrogen evolution via photocatalytic oxidation. Additionally, the 3-way interactions (A*B*C, A*C*D, and B*C*D) had an impact over the obtained hydrogen amount statistically. The residual plots and Pareto chart for obtained hydrogen amount were given in Figure 8.4. and Figure 8.5., respectively.

Residual values indicate the gap between the predicted and experimentally obtained hydrogen amounts and if all of them is near to the straight line, namely, any outlier is not observed, then it could be said that the normally distributed (Safa and Bahatti, 2011). Figure 8. 4. shows that the experimental points were reasonably aligned between -100 and +100 with a normal distribution. Pareto Chart explains that individual and interaction effects of factors and the vertical line (t-value) means the magnitude of minimum statistically significant effect in a certain confidence level.

Table 8.2. Uncoded design matrix of reaction parameters and evolved hydrogen amount

A	B	C	D	Produced Hydrogen (μmol/g_{cat})
3	0.1	0	0.2	3118.81
7.5	0.2	15	0.2	3157.32
7.5	0.2	0	0.2	2970.30
7.5	0.2	15	0.2	2970.30
3	0.1	15	0	3102.31
3	0.2	15	0.2	2959.30
3	0.2	0	0.2	3327.83
3	0.1	0	0	3327.83
7.5	0.1	0	0.2	2700.77
7.5	0.1	15	0	3063.81
3	0.1	15	0.2	2926.29
3	0.2	0	0.2	3322.33
3	0.2	15	0	3322.33
7.5	0.2	0	0.2	2992.30
3	0.1	15	0	3245.32
7.5	0.1	0	0	3107.81
7.5	0.2	15	0	3245.32
3	0.1	0	0	3322.33
3	0.2	0	0	3289.33
3	0.2	15	0.2	2882.29
3	0.2	0	0	3063.81
7.5	0.1	15	0.2	3388.34
7.5	0.1	15	0.2	3355.34
7.5	0.1	0	0.2	2893.29
3	0.1	15	0.2	3025.30
7.5	0.2	0	0	3344.33
3	0.1	0	0.2	3212.32
7.5	0.1	0	0	3283.83
7.5	0.1	15	0	3256.33
7.5	0.2	0	0	3245.32
3	0.2	15	0	3245.32
7.5	0.2	15	0	3267.33

Table 8.3. Statistical Analysis for Evolved Hydrogen (α=0.005)

Source	DoF	SS	MS	F-Value	P-Value
Model	15	815002	54333	6.85	0.000
Linear	4	209167	52292	6.60	0.002
A	1	6358	6358	0.80	0.384
B	1	2364	2364	0.30	0.593
C	1	378	378	0.05	0.830
D	1	200067	200067	25.23	0.000
2-Way Interactions	6	221647	36941	4.66	0.006
A*B	1	4	4	0.00	0.983
A*C	1	186392	186392	23.51	0.000
A*D	1	1831	1831	0.23	0.637
B*C	1	25430	25430	3.21	0.092
B*D	1	3873	3873	0.49	0.495
C*D	1	4119	4119	0.52	0.481
3-Way Interactions	4	384153	96038	12.11	0.000
A*B*C	1	36323	36323	4.58	0.048
A*B*D	1	26686	26686	3.37	0.085
A*C*D	1	205321	205321	25.89	0.000
B*C*D	1	115823	115823	14.61	0.002
4-Way Interactions	1	34	34	0.00	0.949
A*B*C*D	1	34	34	0.00	0.949
Error	16	126864	7929		
Total	31	941865			

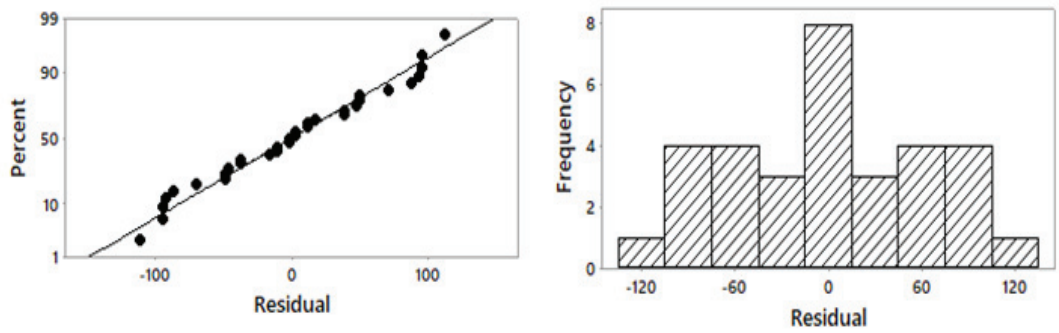

Figure 8.4. Residual plots for produced hydrogen amount

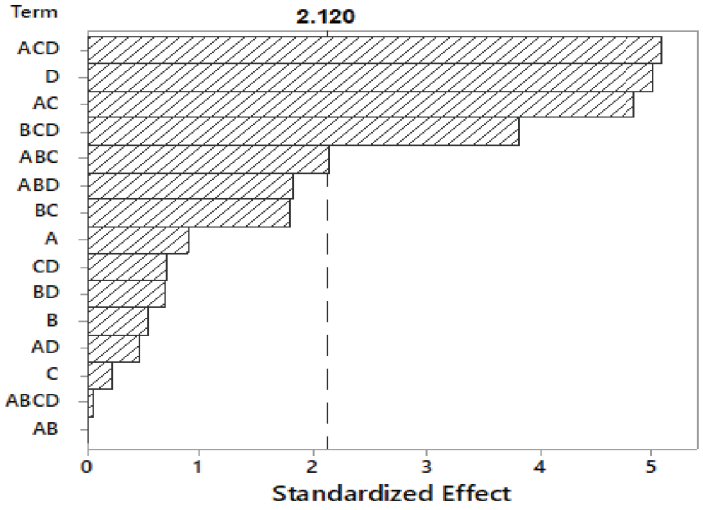

Figure 8.5. Pareto chart for the effecting factor over hydrogen production

In this experimental design, t-value is 2.120 and thus, the factors, which have higher t-values than 2.120, are statistically significant impact over the obtained hydrogen amount in 95 % of confidence level. Since $F_{0.05,1,16} = 4.49$, all the factors with F value higher than 4.49 affect the obtained hydrogen amount statistically. Hence, the most important factor was the interaction of A*C*D and among the main effects, D had a considerable effect over the obtained hydrogen amount. Furthermore, the interactions of A*C, B*C*D, A*B*C had an impact over the obtained hydrogen amount. Interaction plots of the factors for produced hydrogen amount were shown in Figure 8.6.

Due to the level of an experimental factor, the changes in the level of other factors explain via an interaction plot since an interaction can amplify or lessen the major effects and interaction of reaction parameters. Based on Figure 8. 6., A*C and B*C had an impact over the produced hydrogen amount.

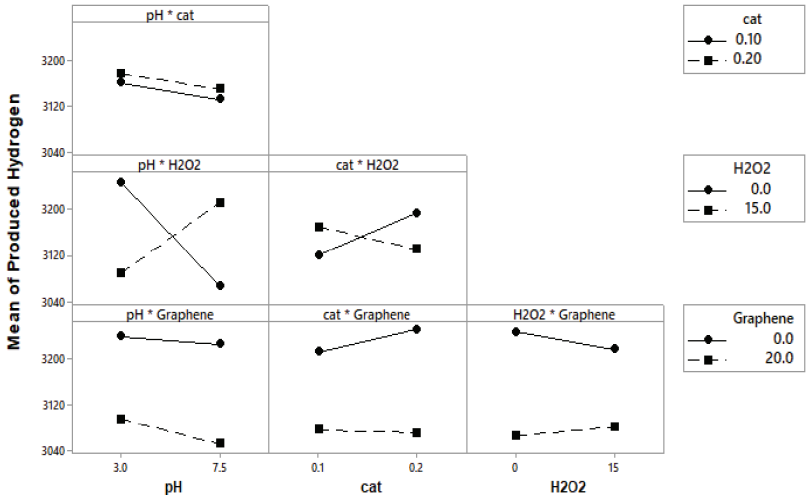

Figure 8.6. Interaction plots of the reaction parameters for hydrogen evolution

The model was reduced with the elimination of A*B*D and A*B*C*D terms due to the hierarchy of terms in the model and hence, a general equation was obtained to evaluate the predicted hydrogen amount and this equation was given in Equation 8.

$$\text{Produced Hydrogen Amount} = 3530 - 46.6A - 1836B - 45C - 3.3D + 303A*B + 5.8A*C - 3.9A*D + 295B*C + 98.3B*D + 0.07C*D - 39.9A*B*C + 0.48A*C*D - 16.04B*C*D \quad (\mathbf{Eq.\ 8})$$

Calcination Temperature Effect:

The calcination temperature of catalyst (T_{cal}) is another important parameter that affect the evolved hydrogen amount and the impact of calcination temperature of GLFO was searched at four different T_{cal} (500, 600, 700 and 800 °C) since the most promising catalyst was GLFO based on the statistical analysis. The effect of T_{cal} was investigated using 0.1 g/L of GLFO at 3 of pH and results were given in Figure 8. 7.

The evolved hydrogen amounts were similar for GLFO calcinated 500 and 600 °C of T_{cal} and much lower than 700 and 800 °C of T_{cal}. The highest hydrogen evolution (3228.82 μmol/g_{cat}) was achieved using GLFO calcined at 700 °C. It could be attributed that the GLFO catalyst calcined at 700 °C has more crystalline structure and results of XRD analysis support these findings.

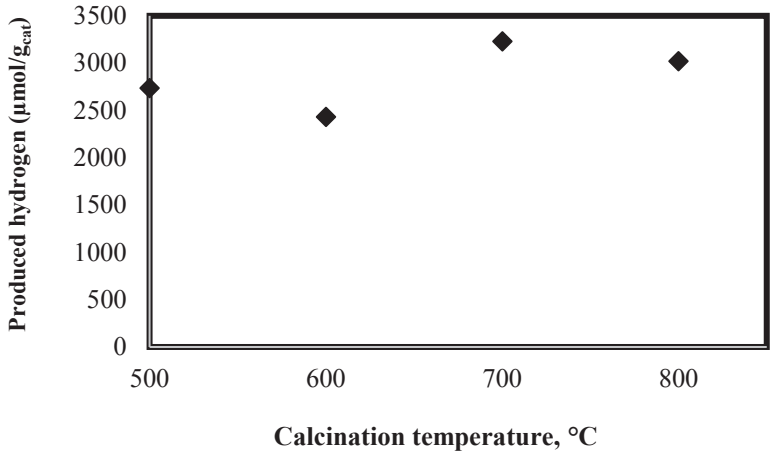

Figure 8.7. Produced hydrogen amount vs. calcination temperature

Reusabilty of GLFO:

In order to comprehend the reusability of this catalyst, re-use experiments were performed and the produced hydrogen amounts achieved after each cycle are given in Figure 8. 8. After 5 re-uses, GLFO conserved its photocatalytic activity almost ~94 % in terms of the produced hydrogen amount. Consequently, GLFO can be used several times in photocatalytic hydrogen production without any considerable activity loss. In literature, it was reported that LFO conserved its 88 % of degradation efficiency in 3rd cycle (Feng et al., 2020). Another study shows that LFO conserved its 90 % of degradation efficiency in 4th cycle (Babu et al., 2017). Therefore, it could be deduced that incorporation of graphene caused an enhancement in terms of degradation efficiency and stability.

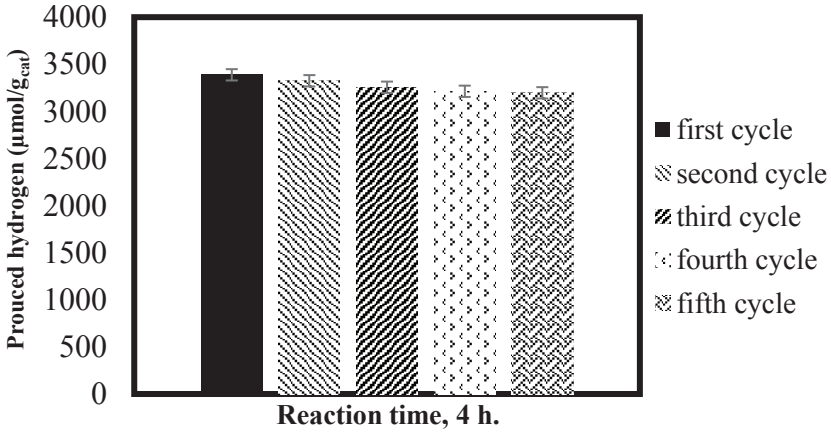

Figure 8.8. Re-uses of GLFO

8.1. Photocatalytic Hydrogen Production with GLFO

The experiments for optimization of reaction conditions for SMS was performed using the best promising catalyst (GLFO). In this context, a Box Behnken design was created by Minitab 18 software with six repeats at centre to optimize the reaction parameters which are pH (A), catalyst loading (B), and $[H_2O_2]_0$ (C) for the photocatalytic hydrogen evolution from SMS using GLFO. While uncoded values of factors and experimental results were given in Table 8.4. and Table 8.5., respectively.

Table 8.4. Uncoded values of reaction parameters

Factors			**Level of factors**
pH	A	3	7.5
Catalyst loading	B	0.1	0.2
Initial H_2O_2 concentration	C	0	15

Table 8.5. Uncoded design matrix of reaction parameters and evolved hydrogen amount

A	**B**	**C**	**Produced Hydrogen (µmol/g_{cat})**
3	0.15	0	3245.32
7.5	0.15	15	3305.83
5.25	0.15	7.5	3377.34
7.5	0.15	0	3003.30
3	0.1	7.5	3102.31
5.25	0.15	7.5	3470.85
7.5	0.1	7.5	3052.81
5.25	0.2	0	3102.31
5.25	0.1	15	3388.34
3	0.2	7.5	3206.82
5.25	0.15	7.5	3399.34
5.25	0.15	7.5	3443.34
5.25	0.10	0	3069.31
5.25	0.15	7.5	3520.35
5.25	0.15	7.5	3509.35
7.5	0.2	7.5	3058.31
5.25	0.2	15	3503.85
3	0.15	15	3459.85

The produced hydrogen amounts from SMS using GLFO for this experimental matrix changed between 3003.30 and 3520.35 μmol/g_{cat}. The mean value of produced hydrogen from SMS was determined as 3289.94 μmol/g_{cat} and the standard deviation (uncertainty) was found as 60.7 μmol/g_{cat}. ANOVA table of this experimental design was given in Table 8. 6.

Table 8.6. ANOVA table for GLFO

Source	DF	Adj SS	Adj MS	F-Value	P-Value
Model	9	554705	61634	18.27	0.0002
Linear	3	243932	81311	24.10	0.0002
A	1	44113	44113	13.08	0.0068
B	1	8354	8354	2.48	0.1542
C	1	191464	191464	56.75	0.0001
Square	3	304684	101561	30.10	0.0001
A*A	1	141967	141967	42.08	0.0002
B*B	1	123153	123153	36.50	0.0003
C*C	1	1656	1656	0.49	0.5034
2-Way Interaction	3	6089	2030	0.60	0.6320
A*B	1	2451	2451	0.73	0.4188
A*C	1	1936	1936	0.57	0.4704
B*C	1	1702	1702	0.50	0.4977
Error	8	26991	3374		
Lack-of-Fit	3	10264	3421	1.02	0.4567
Pure Error	5	16727	3345		
Total	17	581696			

In this table, p-values (less than $\alpha = 0.05$) of each factor are given individually to consider the interactions between the parameters. Based on the ANOVA table, whereas the main effects of A and C had a significant impact over the produced hydrogen amount, B did not affect the produced hydrogen amount statistically. Moreover, produced hydrogen amount was depended on A*A and B*B. However, 2-way interactions of reaction parameters did not affect the produced hydrogen amount. If the p-value of lack-of-fit is larger than $\alpha = 0.05$, it could be concluded that the model is well fitted to data. Thus, according to the ANOVA table, the p-value of lack-of-fit (0.4567) was higher than the value of α (0.05) so that the model was well fitted to obtained experimental data.

Additionally, the R-sq of model was determined as 95.36% and hence, it could be concluded that the model was well fit to the observed response. The residual plots for hydrogen production were given in Figure 8. 9. Based on normal probability plot and histogram, it could be said that the data was normally distributed between -80 and +60. The Pareto Chart was given in Figure 8. 10.

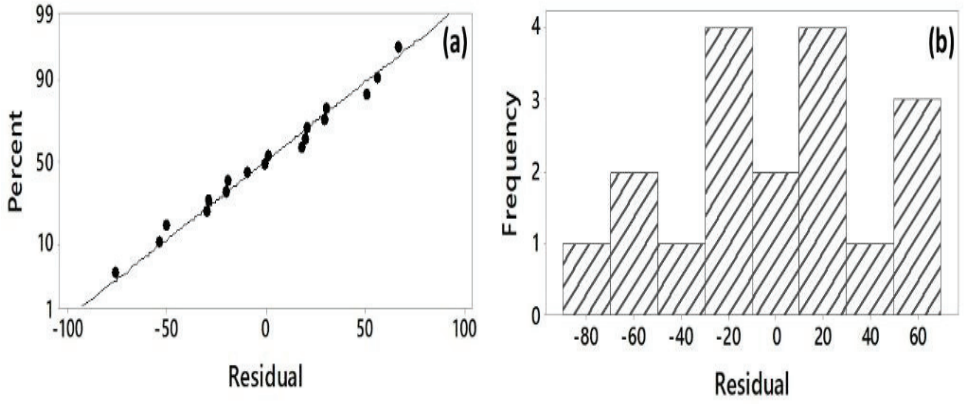

Figure 8.9. Residual plots for hydrogen production

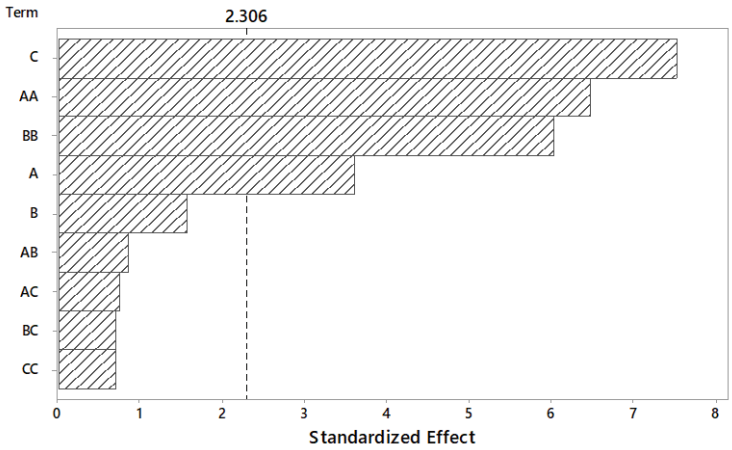

Figure 8.10. Pareto chart for the effecting factor over hydrogen production

According to Pareto Chart, the vertical line (t-value: 2.306) in the chart indicates the minimum statistically significant effect magnitude for confidence level of 95 %. Thus, the main effect of C was the most important factor for the photocatalytic hydrogen evolution since hydrogen peroxide form radicals to decompose sucrose and obtained hydrogen amount was depended on the degraded amount of sucrose. Additionally, among

the main factors, A had also a major effect over produced hydrogen amount since the pH affect the catalyst activity. Moreover, the squares of A and B affected the amount of produced hydrogen amount. Yet, 2-way interactions of factors did not have any considerable impact over the produced hydrogen amount. Considering the hierarchy, the insignificant terms were eliminated and an equation for empirically determination of the produced hydrogen amount was obtained and the regression equation (Eq. 9) was given below.

$$\text{Produced Hydrogen Amount} = 848 + 344.8\,A + 21018\,B + 20.63\,C - 35.98\,A*A - 67907\,B*B \quad (\textbf{Eq. 9})$$

8.2. Photocatalytic Hydrogen Production with GBFO

The same experimental matrix was also used to investigate the photocatalytic activity of GBFO for photocatalytic hydrogen production from SMS. The results of uncoded design table for the factors and produced hydrogen amounts were given in Table 8. 7. The mean value of produced hydrogen from SMS using GBFO was 2846.23 μmol/g_{cat} and the standard deviation (uncertainty) was found as 21.3 μmol/g_{cat}. ANOVA table of this experimental design was given in Table 8. 8. to consider the interactions between factors based on p-values of each factor.

Based on ANOVA table, the most significant term was the C*C and the main effects of A, B and C were strongly effective over the produced hydrogen amount. Moreover, B*C was also effective over the produced hydrogen amount. The other terms did not have any effect over the produced hydrogen statistically. The value of R^2 for this model were calculated as 98.82 % and hence, it could be deduced that the model is well fit to the observed response.

The normal probability plot and histogram diagram were given in Figure 8. 11. and experimental points were reasonably aligned suggesting normal distribution between -60 and +60. Pareto Chart was given in Figure 8. 12 to comprehend the individual and interaction effects of factors. Based on Pareto Chart, t-value is 2.31 in a confidence level of 95 %. Thus, C*C was the most important parameter and all main factors had also a

major effect over the photocatalytic hydrogen production. Moreover, B*C had a synergistic effect over produced hydrogen amount.

Table 8.7. Uncoded design table for reaction parameters and evolved hydrogen amount

A	B	C	Produced Hydrogen (µmol/g_{cat})
3	0.15	0	2717.27
7.5	0.15	15	2579.76
5.25	0.15	7.5	2700.77
7.5	0.15	0	2755.78
3	0.1	7.5	2552.26
5.25	0.15	7.5	3102.31
7.5	0.1	7.5	2568.76
5.25	0.2	0	2590.76
5.25	0.1	15	3514.85
3	0.2	7.5	2728.77
5.25	0.15	7.5	2739.27
5.25	0.15	7.5	2673.27
5.25	0.10	0	2970.30
5.25	0.15	7.5	3459.85
5.25	0.15	7.5	2662.27
7.5	0.2	7.5	2783.28
5.25	0.2	15	2508.25
3	0.15	15	3025.30

Table 8.8. ANOVA table for GBFO

Source	DF	Adj SS	Adj MS	F-Value	P-Value
Model	9	960091	106677	74.18	0.000001
Linear	3	506630	168877	117.43	0.000001
A	1	354132	354132	246.25	0.000000
B	1	121179	121179	84.26	0.000016
C	1	31319	31319	21.78	0.001609
Square	3	433900	144633	100.57	0.000001
A*A	1	74	74	0.05	0.825932
B*B	1	3301	3301	2.30	0.168244
C*C	1	414035	414035	287.90	0.000000
2-Way Interaction	3	19561	6520	4.53	0.038800
A*B	1	4728	4728	3.29	0.107381
A*C	1	2731	2731	1.90	0.205529
B*C	1	12102	12102	8.42	0.019863
Error	8	11505	1438		
Lack-of-Fit	3	9447	3149	7.65	0.025725
Pure Error	5	2057	411		
Total	17	971596			

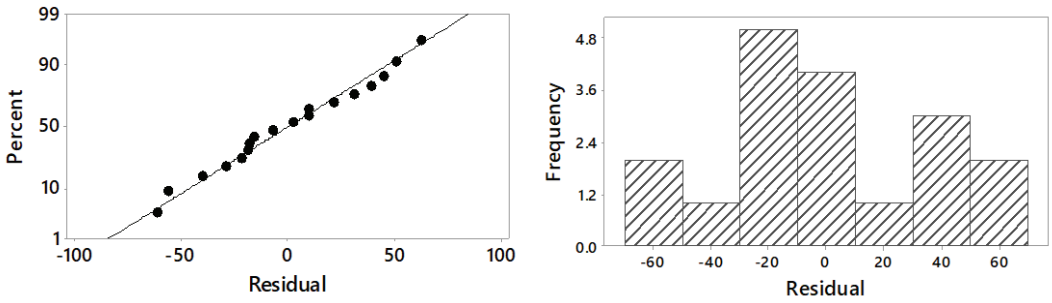

Figure 8.11. Residual plots for hydrogen production using GBFO

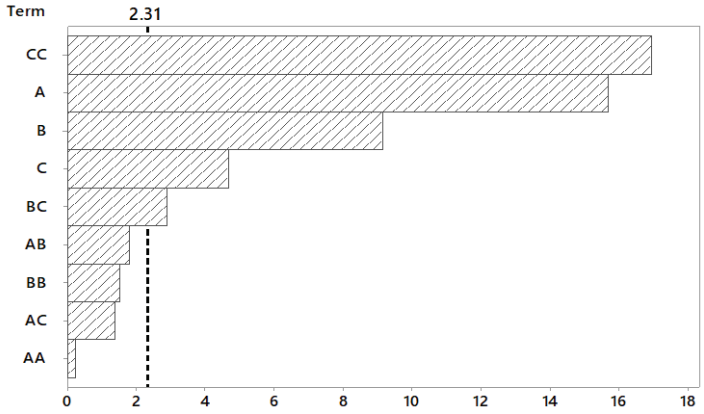

Figure 8.12. Pareto chart for the effecting factor over hydrogen production using GBFO

Considering the hierarchy, the insignificant terms were eliminated and an equation for empirically determination of the produced hydrogen amount was obtained and the regression equation (Eq. 10) was given below.

$$\text{Produced Hydrogen} = 2913.2 - 93.51\,A + 3562\,B - 52.6\,C + 5.532\,C*C - 146.7\,B*C \quad (\textbf{Eq. 10})$$

8.3. Photocatalytic Hydrogen Production with GLRO

The same Box Behnken design was also used to search photocatalytic efficiency of GLRO for hydrogen evolution from SMS and the results for this experimental matrix was given in Table 8. 9.

The highest hydrogen production was achieved as 3404.84 μmol/g_{cat} at the following reaction conditions: 5.25 of pH, 0.15 g/L of GLRO and 7.5 mM of $[H_2O_2]_0$. The mean value of produced hydrogen from SMS using GLRO was 3138.67 μmol/g_{cat} and the standard deviation (uncertainty) was found as 34.3 μmol/g_{cat}. ANOVA table of this experimental matrix was given in Table 8. 10. p-values (less than α=0.05) of each factor are given separately in this table to comprehend the interactions between the factors.

Table 8.9. Uncoded design table for reaction parameters and evolved hydrogen amount

A	B	C	Produced Hydrogen (μmol/g_{cat})
3	0.15	0	3030.80
7.5	0.15	15	3179.32
5.25	0.15	7.5	3382.84
7.5	0.15	0	2805.28
3	0.1	7.5	2678.77
5.25	0.15	7.5	3410.34
7.5	0.1	7.5	2865.79
5.25	0.2	0	3047.30
5.25	0.1	15	3135.31
3	0.2	7.5	3085.81
5.25	0.15	7.5	3338.83
5.25	0.15	7.5	3415.84
5.25	0.10	0	2898.79
5.25	0.15	7.5	3404.84
5.25	0.15	7.5	3349.83
7.5	0.2	7.5	2887.79
5.25	0.2	15	3322.33
3	0.15	15	3256.33

According to ANOVA table, the main effects and the square of all factors (A, B and C) were significant over the produced hydrogen amount. Among two-way interaction terms, A*B had a synergistic effect over produced hydrogen amount and the other terms did not have any effect over the produced hydrogen statistically. The value of R^2 for this model was determined as 98.84 % and hence, the model showed well fit to the observed response. The residual plots for this model were given in Figure 8. 13.

Table 8.10. ANOVA table for GLRO

Source	DF	Adj SS	Adj MS	F-Value	P-Value
Model	9	874526	97170	75.60	0.00000
Linear	3	210295	70098	54.54	0.00001
A	1	8714	8714	6.78	0.03143
B	1	67910	67910	52.84	0.00009
C	1	133671	133671	104.00	0.00001
Square	3	630624	210208	163.55	0.00000
A*A	1	284963	284963	221.72	0.00000
B*B	1	255119	255119	198.50	0.00000
C*C	1	7344	7344	5.71	0.04383
2-Way Interaction	3	33607	11202	8.72	0.00668
A*B	1	31958	31958	24.87	0.00107
A*C	1	1278	1278	0.99	0.34782
B*C	1	371	371	0.29	0.60587
Error	8	10282	1285		
Lack-of-Fit	3	4932	1644	1.54	0.31423
Pure Error	5	5350	1070		
Total	17	884808			

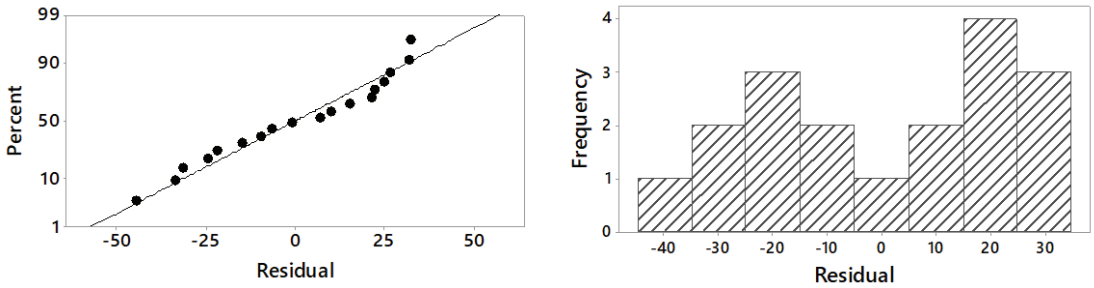

Figure 8.13. Residual plots for hydrogen production using GLRO

Based on the residual plots, it could be deduced that the experimental points were reasonably aligned with a normal distribution between -40 and +30. Pareto Chart for this experimental design was given in Figure 8. 14. Based on the results, t-value is equal to 2.31 in a confidence level of 95 %. Therefore, the square of A (A*A) and the square of B (B*B) were the most important parameters for the photocatalytic hydrogen evolution from SMS using GLRO. Additionally, the square of C (C*C) was also an effective parameter. Besides, all main factors had also a major effect over produced hydrogen

amount. Moreover, two-way interaction of A and B factors had synergistic effect over produced hydrogen amount.

Considering the hierarchy, the insignificant terms were eliminated and an equation for empirically determination of the produced hydrogen amount was obtained and the regression equation (Eq. 11) was given below.

$$\text{Produced Hydrogen} = -1179 + 634.5\,A + 35029\,B + 28.18\,C - 50.48\,A*A - 96718\,B*B - 0.729\,C*C - 795\,A*B \quad (\textbf{Eq. 11})$$

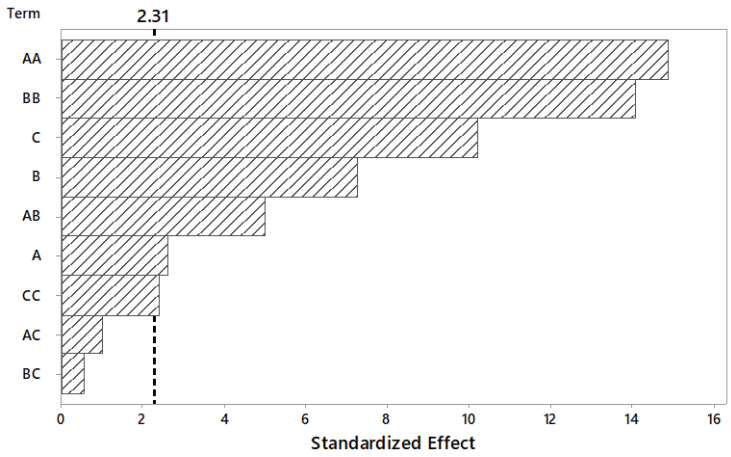

Figure 8.14. Pareto chart for the effecting factor over hydrogen production using GLRO

8.4. Kinetic Study

The effect of reaction temperature over produced hydrogen amount from SMS was investigated at three different reaction temperature (25, 35 and 45 °C) in the presence of most promising catalyst (GLFO). Experiments lasted for 1 hour using 1000 ppm of SMS and the values of overall TOC removal % are listed in Table 8. 11. TOC removal % values for each 15 minutes were given in Figure 8. 15.

The first and second order reaction models based on TOC removal % were used to analyze obtained data to figure out the reaction kinetic mechanism for hydrogen production from SMS using GLFO. Whereas the R^2 values for first order reaction model were very low, the R^2 values for second order reaction model were higher and it could be concluded that this reaction follow observed second order reaction. As reaction

temperature rised reaction rate constants increased. The linearized form of obtained data was given in Figure 8. 16. and the R^2 values and reaction rate kinetic constants for this reaction model was given in Table 8. 12. The Arrhenius plot of lnk versus 1/T was given in Figure 8. 17. and activation energy for this observed reaction was calculated as 27.25 kJ/mol.

Table 8.11. TOC removal % for sucrose model solution

Temperature, °C	Produced Hydrogen [µmol/g_{cat}]	TOC removal, %
25	874.59	26.90
35	1089.11	32.37
45	1287.13	36.14

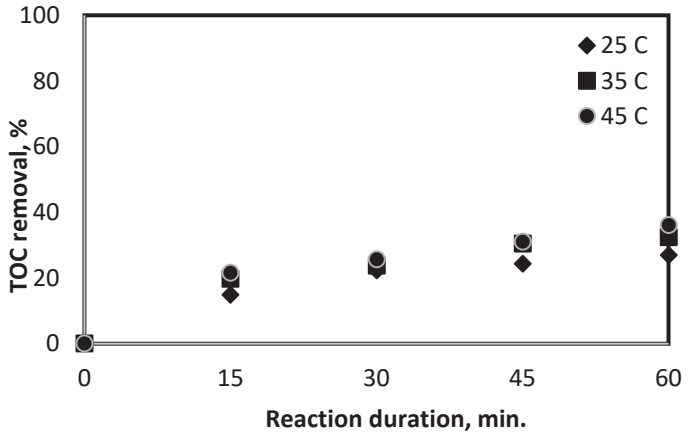

Figure 8.15. TOC removal % for sucrose model solution

Table 8.12.R^2 values for reaction models

Temperature, °C	R^2, Second Order	Reaction rate constants, $ppm^{-1}min^{-1}$
25	0.95	0.00002
35	0.96	0.00003
45	0.97	0.00004

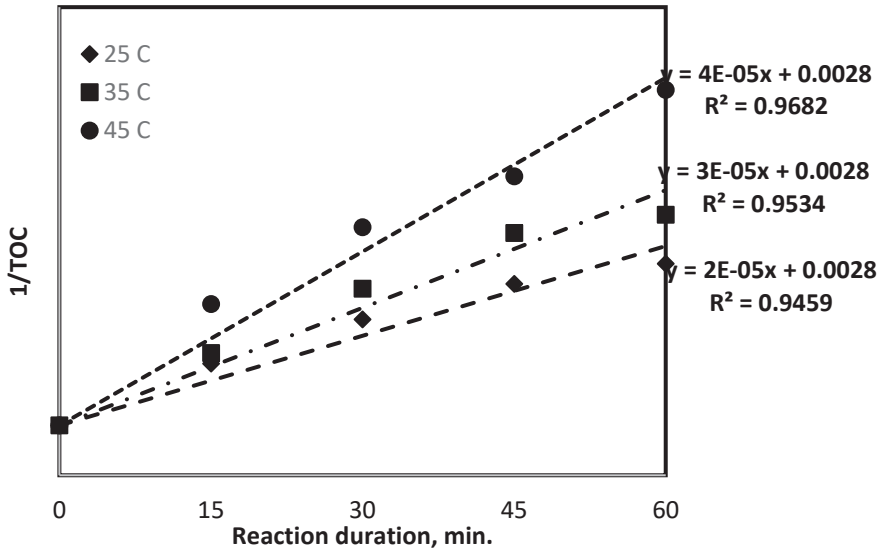

Figure 8.16.Linerazed data for sucrose model solution

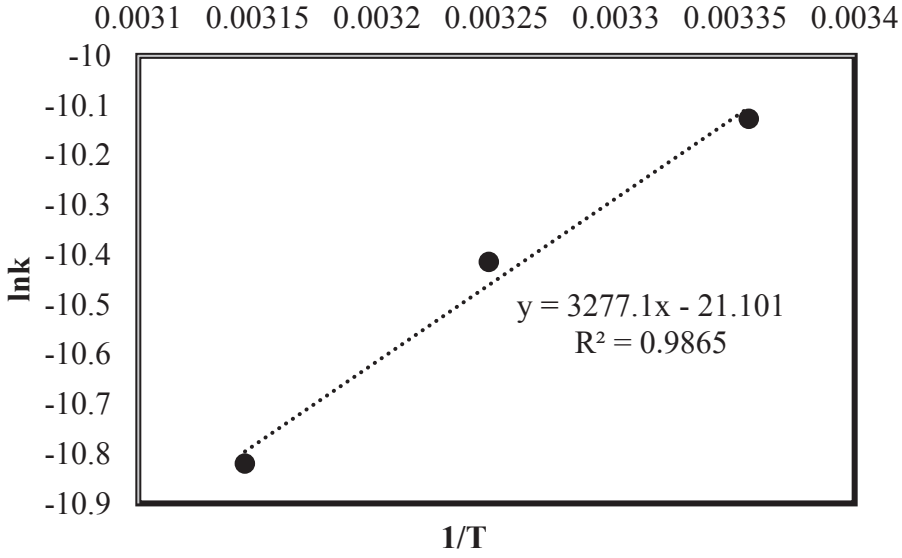

Figure 8.17.lnk vs 1/T

CHAPTER 9

PHOTOCATALYTIC HYDROGEN PRODUCTION FROM REAL SUGAR BEET WASTEWATER

This chapter comprises the characterization study (ICP-MS and HPLC analysis) of real sugar beet wastewater and optimization study for reaction parameters including pH, catalyst loading and initial hydrogen peroxide concentration via Box Behnken statistical model for the produced hydrogen amount from real sugar beet wastewater in the presence of hybrid catalysts (GLFO, GBFO and GLRO). Additionally, all produced gases (H_2, CO, CO_2, CH_4) from SMS and real sugar beet wastewater were listed to compare results.

The last part is the kinetic study for the produced hydrogen amount from real sugar beet wastewater at three different temperatures (25, 35 and 45 °C) in the presence of the most promising hybrid catalyst (GLFO).

9.1. Characterization of Real Sugar Beet Wastewater

The elemental analysis of real sugar beet wastewater which was supplied from Sugar Factory located in Eskişehir, Turkey was carried out via ICP-MS (Agilent 7500 ce) analysis and the elemental composition of real sugar beet wastewater was given in Table 9. 1.

Additionally, some published studies related to sugar beet wastewater and its pulp is also given in this table for comparison with literature. Based on the results, all elements in sugar beet wastewater (supplied from Eskişehir Sugar Factory) were not detected in these studies reported in literature. Consequently, it could be concluded that each sugar beet wastewater has specific characteristic.

Sucrose content of real sugar beet wastewater was determined via HPLC analysis and it was found as 22 ppm.

Table 9.1. Elemental analysis of sugar beet wastewater

Elements	Sugar beet wastewater [mg/L]	Sugar beet factory wastewater [mg/L] (Güven et al., 2009)	Sugar beet processing wastewater (Alkaya and Demireri 2011b) [mg/L]	Sugar beet pulp (Suhartini et al., 2014) [mg/L]
TKN (N)	51.8	53.23	10	1952.28
Phosphorus (P)	-	4.77	2.7	56.1
Potassium (K)	157.8	-	-	471.24
Cobalt (Co)	0.9607	-	-	0.00045
Iron (Fe)	5.203	-	-	2.92
Molybdenum (Mo)	0.1064	-	-	0.00045
Nickel (Ni)	1.654	-	-	0.02
Selenium (Se)	1.785	-	-	0.00017
Calcium (Ca)	579.4	906	378±5.7	-
Magnesium (Mg)	99.51	-	-	-

9.2. Photocatalytic Hydrogen Production with GLFO

After completion of the experiments for optimization of reaction conditions for SMS in the presence of best promising catalyst which is GLFO, the experiments were carried out using real sugar beet wastewater. In this context, the same Box Behnken design was used for sugar beet wastewater experiments likewise the experimental design for SMS. The results of uncoded design table for the reaction parameters and results are given in Table 9. 2.

The mean value of produced hydrogen from sugar beet wastewater was 4216.17 μmol/g_{cat} and the standard deviation (uncertainty) was found as 559.18 μmol/g_{cat}. The highest hydrogen production was achieved as 7035.20 μmol/g_{cat} from sugar beet wastewater at 7.5 of pH and in the presence of GLFO catalyst at a 0.15 g/L of catalyst loading. The obtained highest hydrogen amount from sugar beet wastewater was more than twice the amount of hydrogen obtained from the SMS under the same reaction conditions. Additionally, TOC analysis was performed for sugar beet wastewater experiments and the highest TOC removal was also observed at the same reaction reactions. The factors are defined as A, B and C for pH, catalyst loading, $[H_2O_2]_0$, respectively. ANOVA table of this experimental matrix was given in Table 9. 3. In this table, p-values (less than $\alpha = 0.05$) of each factor are given individually to consider the interactions between the parameters.

Table 9.2. Uncoded design table for reaction parameters and evolved hydrogen amount

A	B	C	Produced Hydrogen (µmol/g_{cat})	TOC Removal, %
3	0.15	0	5566.56	97.60
7.5	0.15	15	5060.51	97.40
5.25	0.15	7.5	4048.40	93.77
7.5	0.15	0	7035.20	99.73
3	0.1	7.5	6837.18	98.27
5.25	0.15	7.5	4460.95	96.57
7.5	0.1	7.5	6078.11	97.94
5.25	0.2	0	3547.85	92.28
5.25	0.1	15	4680.97	97.31
3	0.2	7.5	3498.35	81.02
5.25	0.15	7.5	4196.92	95.77
5.25	0.15	7.5	3448.84	75.63
5.25	0.10	0	4543.45	97.07
5.25	0.15	7.5	5066.01	97.42
5.25	0.15	7.5	4075.91	94.29
7.5	0.2	7.5	3063.81	53.88
5.25	0.2	15	3096.81	55.81
3	0.15	15	6688.67	97.99

Based on the ANOVA table, while the main effect of initial hydrogen peroxide concentration and pH were not effective over produced hydrogen amount, catalyst loading showed a main effect over the produced hydrogen amount. Additionally, produced hydrogen amount was depended on square of pH and square of catalyst loading. Same parameters were also effective to produce hydrogen from SMS. Furthermore, among the 2-way interactions of reaction parameters, pH and $[H_2O_2]_0$ had a synergetic effect over the produced hydrogen amount from the sugar beet wastewater. If the p-value of lack-of-fit is larger than $\alpha = 0.05$, it could be concluded that the model is well fitted to data. Thus, according to the ANOVA table, the p-value of lack-of-fit (0.196) was higher than the value of α (0.05) so that the model was well fitted to obtained experimental data. Additionally, the R^2 of model was determined as 87.80% and hence, the model is well fit to the observed response. However, this value was lower than the R-sq of model for SMS. The residual plots and Pareto chart for hydrogen evolution were given in Figure 9.1. and Figure 9. 2., respectively.

Table 9.3. ANOVA table for GLFO

Source	DF	Adj SS	Adj MS	F-Value	P-Value
Model	9	24245322	2693925	6.40	0.008
Linear	3	10373423	3457808	8.21	0.008
A	1	228872	228872	0.54	0.482
B	1	9974573	9974573	23.69	0.001
C	1	169978	169978	0.40	0.543
Square	3	11361410	3787137	8.99	0.006
A*A	1	8392524	8392524	19.93	0.002
B*B	1	2348603	2348603	5.58	0.046
C*C	1	1025319	1025319	2.43	0.157
2-Way Interaction	3	2510488	836829	1.99	0.195
A*B	1	26330	26330	0.06	0.809
A*C	1	2397558	2397558	5.69	0.044
B*C	1	86600	86600	0.21	0.662
Error	8	3368905	421113		
Lack-of Fit	3	1949791	649930	2.29	0.196
Pure Error	5	1419115	283823		
Total	17	27614227			

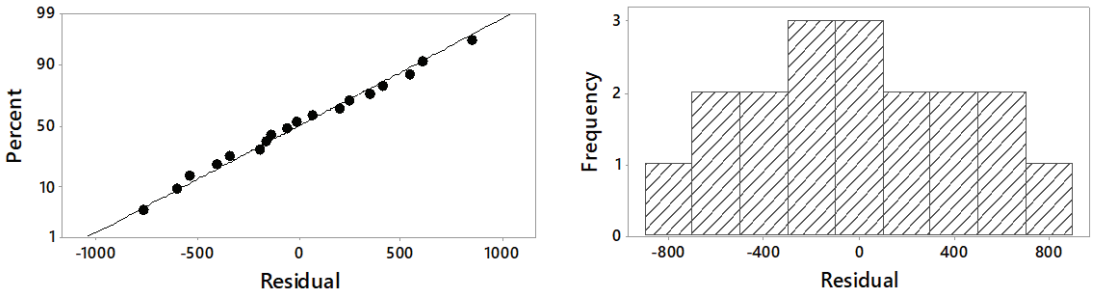

Figure 9.1. Residual plots for hydrogen production

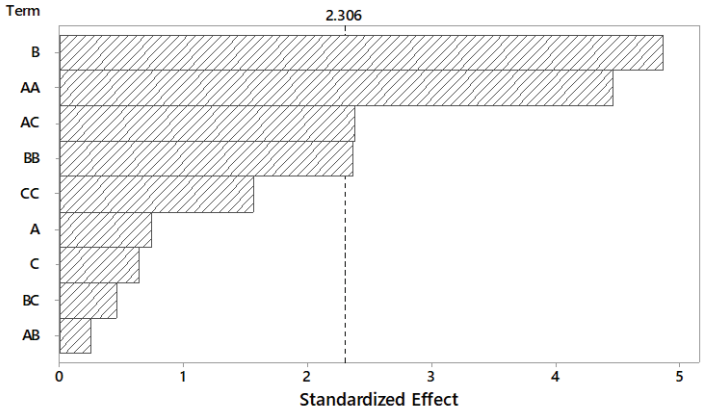

Figure 9.2. Pareto chart for the effecting factor over hydrogen production

The difference between the experimentally produced and predicted hydrogen amounts are clarified with residual values. In residual plot, if all points are near the straight line, then it could be deduced that the data is normally distributed. Figure 9.1. showed that the experimental points were reasonably aligned suggesting normal distribution in the range of -800 and +800. The normal distribution range had become a larger interval compared to SMS results. The individual and interaction effects of parameters are explained by the Pareto Chart and Figure 9. 2. indicates that the vertical line (t-value: 2.306) in the chart implies the minimum statistically important impact magnitude in a confidence level of 95 %.

Therefore, the main effect of B was the most important factor for the photocatalytic hydrogen evolution from sugar beet wastewater. Besides, the squares of A and B affected the amount of produced hydrogen and these results were similar to SMS results. Moreover, among the 2-way interactions of factors, A and C had a synergetic effect over the evolved hydrogen amount from sugar beet wastewater. However, the two-way interaction effects were not observed for SMS experiments. Consequently, an equation for empirically determination of the produced hydrogen amount from sugar beet wastewater was obtained and the regression equation (Eq. 12) was given below.

$$Produced\ Hydrogen = 7859 - 2716A + 64861B + 151C + 273.9A * A - 293454B * B + 8.62C * C + 721A * B - 45.9A * C - 392B * C \quad \textbf{Eq. 12}$$

9.3. Kinetic Study

The effect of reaction temperature over produced hydrogen amount from real sugar beet wastewater was searched at three different reaction temperature (25, 35 and 45 °C) in the presence of most promising catalyst (GLFO). Kinetic study experiments lasted for 1 hour and the values of overall TOC removal % are listed in Table 9.4. Kinetic study experiments lasted for 1 hour and the values of overall TOC removal % values for each 15 minutes were given in Figure 9. 3.

The first and second order reaction models were used to analyze obtained data to figure out the reaction kinetic mechanism for hydrogen production from real sugar beet

wastewater in the presence of GLFO. Whereas the R^2 values for second order reaction model were very low, the R^2 values for first order reaction model were higher and it could be concluded that this reaction followed observed 1st order reaction kinetic model and the R^2 values and reaction rate kinetic constants for this reaction model was given in Table 9. 5.

Table 9.4. TOC removal % for sucrose model solution

Temperature, °C	**Produced Hydrogen [µmol/g_{cat}]**	**TOC removal, %**
25	1105.61	25.25
35	1353.14	28.96
45	1947.19	41.48

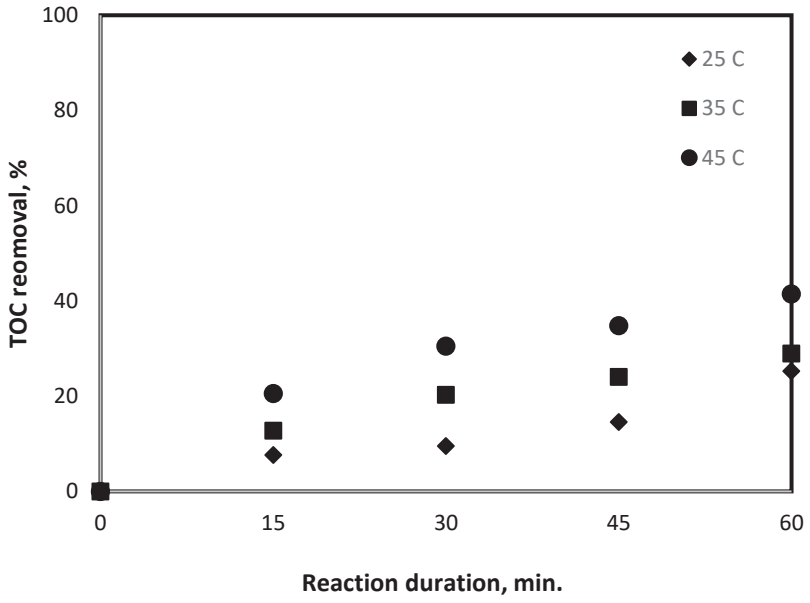

Figure 9.3. TOC removal % for sugar beet wastewater

As reaction temperature rised reaction rate constants increased. The linearized form of obtained data and the Arrhenius plot of lnk versus 1/T were given in Figure 9. 4. And Figure 9. 5., respectively. Besides, the activation energy for this observed reaction was determined as 32 kJ/mol.

Table 9.5. R^2 values for reaction models

Temperature (T), °C	R^2 of First Order Reaction Model	Reaction rate constants, min^{-1}
25	0.93	0.0043
35	0.94	0.0062
45	0.91	0.0097

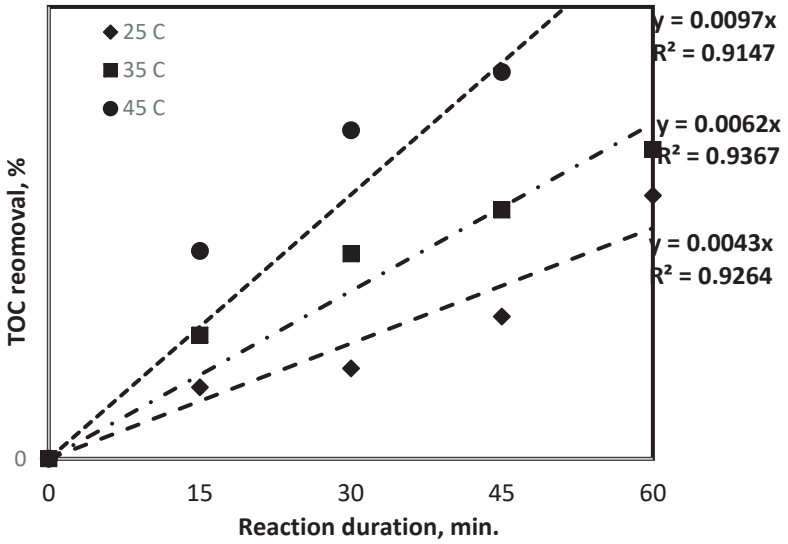

Figure 9.4. Linerazed data for sugar beet wastewater

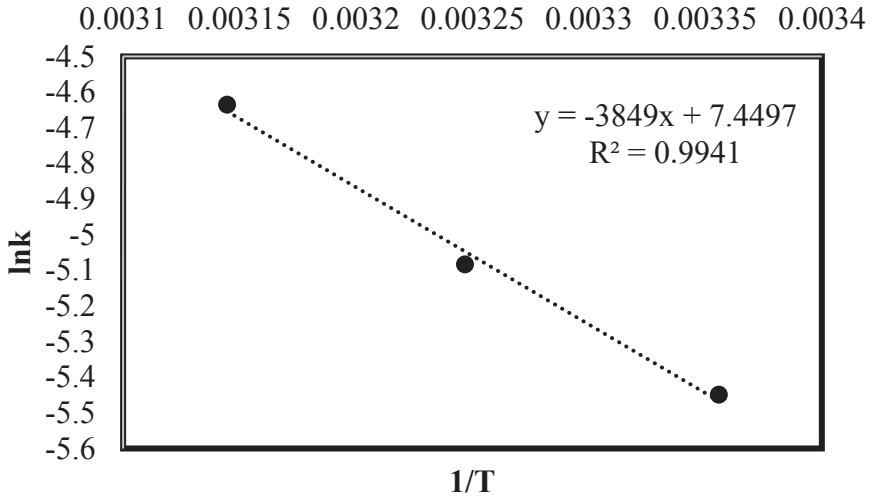

Figure 9.5. lnk vs 1/T

9.4. Photocatalytic Hydrogen Production with GBFO

Hydrogen evolution from real sugar beet wastewater was also investigated in the presence of another hybrid catalyst (GBFO) in order to compare the photocatalytic activities of all synthesized hybrid catalysts. In this context, the same Box Behnken experimental design matrix was used and the results of uncoded design table for the reaction parameters and produced hydrogen amounts from real sugar beet wastewater in the presence of GBFO were given in Table 9. 6.

The evolved hydrogen amounts in the presence of GBFO varied between 2777.78 and 6617.16 μmol/g_{cat}. The mean value of evolved hydrogen from sugar beet wastewater in the presence of GBFO was 3506.60 μmol/g_{cat} and the standard deviation (uncertainty) was found as 468.48 μmol/g_{cat}. The highest hydrogen production was achieved as 6617.17 μmol/g_{cat} from sugar beet wastewater at 3 of pH and using 0.1 g/L of GBFO catalyst and 7.5 mM H_2O_2. The obtained highest hydrogen amount (6617.16 μmol/g_{cat}) from real sugar beet wastewater was more than twice the amount of hydrogen obtained from the SMS under the same reaction conditions.

To comprehend the main effect and their interaction with each other's, the experimental data were analysed with Minitab 18 software. The parameters are defined as A, B and C for pH, catalyst loading, $[H_2O_2]_0$, respectively. ANOVA table of this experimental matrix was given in Table 9. 7. and p-values (less than $\alpha = 0.05$) of each reaction parameter are given individually to consider the interactions between the parameters. Based on Table 9. 7., the main impact of A and C did not affect the produced hydrogen amount, however, catalyst loading showed a main effect over the evolved hydrogen amount. Moreover, square of pH was also effective over the produced hydrogen amount. Other parameters were not effective on the evolved hydrogen amount in the presence of GBFO statistically. Based on the ANOVA table, the p-value of lack-of-fit (0.079) was found as higher than the value of α (0.05). Hence, it could be deduced that the model was well fitted to obtained experimental data. In addition, the R-sq of model was determined as 86.35 % and hence, it could be concluded that the model was well fit to the observed response.

The residual plots for hydrogen production from real sugar beet wastewater in the presence of GBFO was given in Figure 9. 6. and Pareto Chart was given in Figure 9. 7.

Table 9.6. Uncoded design table for reaction parameters and evolved hydrogen amount

A	B	C	Produced Hydrogen (µmol/g_{cat})
3	0.15	0	5489.55
7.5	0.15	15	4471.95
5.25	0.15	7.5	3564.36
7.5	0.15	0	6089.11
3	0.1	7.5	6617.16
5.25	0.15	7.5	3245.32
7.5	0.1	7.5	5429.04
5.25	0.2	0	3674.37
5.25	0.1	15	4031.90
3	0.2	7.5	3338.83
5.25	0.15	7.5	3822.88
5.25	0.15	7.5	3124.31
5.25	0.10	0	4295.93
5.25	0.15	7.5	4207.92
5.25	0.15	7.5	3074.81
7.5	0.2	7.5	2777.78
5.25	0.2	15	3173.82
3	0.15	15	6435.64

The normal probability plot (Figure 9. 6a) implies that the data was normally distributed. Additionally, Figure 9. 6b shows that the experimental points were aligned in the range of -600 and +800. The normal distribution range extended in a larger interval compared to results of SMS. The main and interaction effects of reaction parameter were elucidated via Pareto Chart and the minimum statistically important impact magnitude for 95 % confidence level was shown with the vertical line in Figure 9. 7. Thus, the parameter, which has higher magnitude than this vertical line, was statistically effective over hydrogen evolution from sugar beet wastewater in the presence of GBFO. In addition, t-value is equal to 2.306 in this confidence level. Therefore, among the main effects, the only effective parameter was B for the photocatalytic hydrogen production from sugar beet wastewater using GBFO. Besides, the squares of A affected the produced hydrogen amount. However, other parameters were not effective statistically. An equation for empirically determination of the produced hydrogen amount from sugar beet wastewater using GBFO was obtained and the regression equation (Eq. 13) was given below.

$$Produced\ Hydrogen = 11701 - 3065\,A + 22951\,B + 17C + 282.6A*A - 158691B*B + 12.16\,C*C + 1393\,A*B - 38.0\,A*C - 158\,B*C \qquad \textbf{Eq. 13}$$

Table 9.7. ANOVA table for GBFO

Source	DF	Adj SS	Adj MS	F-Value	P-Value
Model	9	22089149	2454350	5.62	0.012
Linear	3	8331329	2777110	6.36	0.016
A	1	1211588	1211588	2.78	0.134
B	1	6862106	6862106	15.73	0.004
C	1	257634	257634	0.59	0.464
Square	3	12002961	4000987	9.17	0.006
A*A	1	8933569	8933569	20.47	0.002
B*B	1	686803	686803	1.57	0.245
C*C	1	2042335	2042335	4.68	0.062
2-Way Interaction	3	1754859	584953	1.34	0.328
A*B	1	98302	98302	0.23	0.648
A*C	1	1642571	1642571	3.76	0.088
B*C	1	13986	13986	0.03	0.862
Error	8	3490951	436369		
Lack-of-Fit	3	2494876	831625	4.17	0.079
Pure Error	5	996075	199215		
Total	17	25580099			

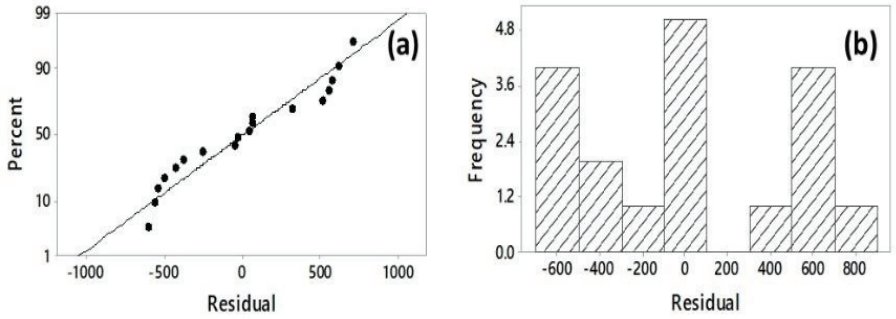

Figure 9.6. Residual plots for hydrogen production

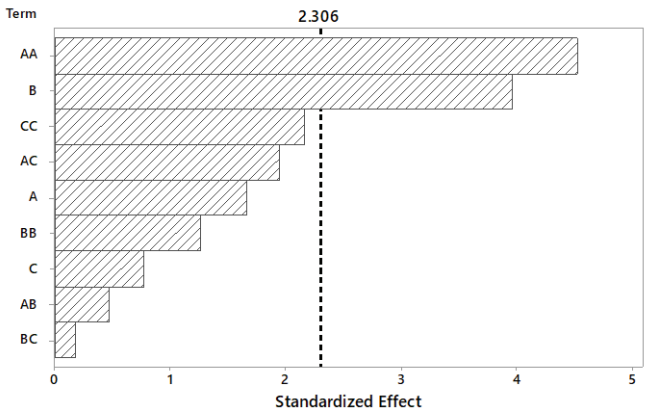

Figure 9.7. Pareto chart for the effecting factor over hydrogen production

9.5. Photocatalytic Hydrogen Production with GLRO

Hydrogen evolution from real sugar beet wastewater was also performed using GLRO to equate the photocatalytic efficiencies of all synthesized hybrid catalysts for hydrogen production. In this scope, the same Box Behnken experimental design matrix was used and the results of uncoded design table for the reaction parameters and produced hydrogen amounts from real sugar beet wastewater using GLRO were given in Table 9. 8.

Table 9.8. Uncoded design table for reaction parameters and evolved hydrogen amount

A	B	C	Produced Hydrogen (µmol/g_{cat})
3	0.15	0	5521.19
7.5	0.15	15	4867.04
5.25	0.15	7.5	3895.23
7.5	0.15	0	6645.35
3	0.1	7.5	6758.27
5.25	0.15	7.5	3236.56
7.5	0.1	7.5	5685.54
5.25	0.2	0	3587.91
5.25	0.1	15	4353.46
3	0.2	7.5	3526.85
5.25	0.15	7.5	4186.37
5.25	0.15	7.5	3892.17
5.25	0.10	0	4391.01
5.25	0.15	7.5	4076.32
5.25	0.15	7.5	4793.62
7.5	0.2	7.5	2913.81
5.25	0.2	15	3124.16
3	0.15	15	6772.56

The evolved hydrogen amounts in the presence of GLRO were distributed between 2913.81 and 6772.56 µmol/g_{cat}. These values were higher than the obtained hydrogen amounts using GBFO while almost same results were achieved in the presence of GLFO. Furthermore, it was expected results based on the results of PL analysis for these catalysts. The mean value of evolved hydrogen from sugar beet wastewater in the

presence of GLRO was 4013.38 μmol/g_{cat} and the standard deviation (uncertainty) was determined as 529.98 μmol/g_{cat}. The highest hydrogen evolution was obtained as 6772.56 μmol/g_{cat} from sugar beet wastewater at 3 of pH and in the presence of 0.15 g/L of GLRO and 15 mM H_2O_2. The obtained highest hydrogen amount (6772.56 μmol/g_{cat}) from sugar beet wastewater using GLRO was more than twice the amount of hydrogen obtained from the SMS under the same reaction conditions. To clarify the main effect and interaction of the reaction parameters with each other's, the experimental data were analysed statistically. The factors are defined as A, B and C for pH, catalyst loading, $[H_2O_2]_0$, respectively. ANOVA table of this experimental design was given in Table 9. 9. In this table, p-values (less than $\alpha = 0.05$) of each reaction parameter are given individually to account for the interactions between the parameters.

Table 9.9. ANOVA table for GBFO

Source	DF	Adj SS	Adj MS	F-Value	P-Value
Model	9	22935030	2548337	6.09	0.009
Linear	3	8964259	2988086	7.14	0.012
A	1	760841	760841	1.82	0.214
B	1	8071258	8071258	19.29	0.002
C	1	132160	132160	0.32	0.590
Square	3	11577791	3859264	9.22	0.006
A*A	1	8523058	8523058	20.37	0.002
B*B	1	2076506	2076506	4.96	0.057
C*C	1	1275205	1275205	3.05	0.119
2-Way Interaction	3	2392981	797660	1.91	0.207
A*B	1	52829	52829	0.13	0.732
A*C	1	2294740	2294740	5.48	0.047
B*C	1	45412	45412	0.11	0.750
Error	8	3347946	418493		
Lack-of-Fit	3	2073184	691061	2.71	0.155
Pure Error	5	1274762	254952		
Total	17	26282976			

The main effect of A and C did not affect the produced hydrogen amount, however, catalyst loading showed a main effect over the evolved hydrogen amount. Moreover, square of pH was also effective over the produced hydrogen amount. Similar results were also observed using other hybrid catalysts (GLFO and GBFO). Among the two-way interaction, A*C had a significant effect over the evolved hydrogen amount from

real sugar beet wastewater using GLRO. Therefore, the pH and hydrogen peroxide showed a synergetic effect during the degradation of organic compounds in the real sugar beet wastewater and concomitant hydrogen evolution. However, other parameters did not affect the evolved hydrogen amount in the presence of GLRO statistically. The p-value of lack-of-fit (0.155) is higher than the value of α (0.05) and thus, it could be infered that the model was well fitted to the experimental data. In addition, the R^2 of model was determined as 87.26 % and hence, it could be educed that the model is well fit to the evolved hydrogen amount. The residual plots for hydrogen production was given in Figure 9. 7. and Pareto Chart was given in Figure 9. 8. The normal probability plot (Figure 9. 8a) implies that the data was normally distributed. Additionally, Figure 9. 8b shows that the experimental points were aligned in the range of -800 and +800.

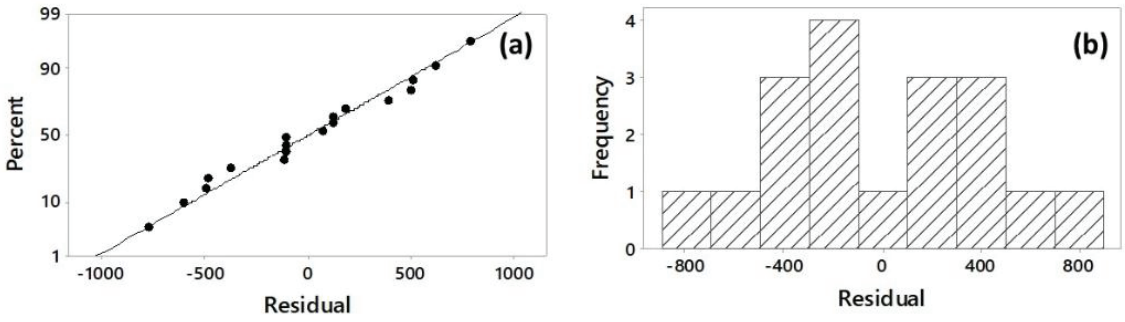

Figure 9.8. Residual plots for hydrogen production

The normal distribution range has extended in a larger interval compared to results of SMS. Pareto Chart clarifies the main and interaction effects of reaction parameters and the minimum statistically significant effect magnitude for 95 % confidence level was shown with the vertical line in Pareto Chart. Thus, the parameter, which has higher magnitude than this vertical line, is statistically effective over hydrogen evolution from sugar beet wastewater in the presence of GLRO. In addition, t-value is equal to 2.306 in this confidence level.

Therefore, among the main effects, the only effective parameter was B for the photocatalytic hydrogen production from sugar beet wastewater using GLRO. Whereas the squares of A and 2-way interaction of A and C affected the evolved hydrogen amount, other parameters were not effective statistically.

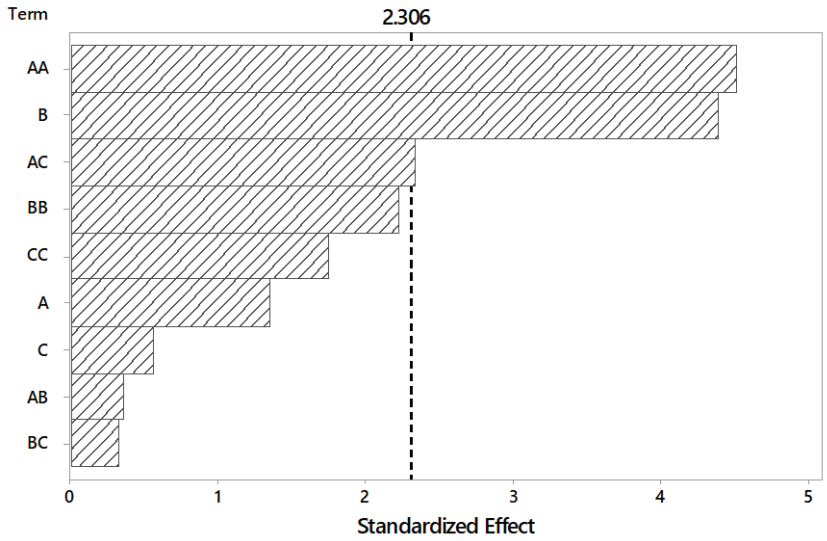

Figure 9.9. Pareto chart for the effecting factor over hydrogen production

An equation for empirically determination of the produced hydrogen amount from sugar beet wastewater using GLRO was obtained and the regression equation (Eq. 14) was given below.

$$Produced\ Hydrogen = 8533 - 2852A + 59459B + 117C + 276.1A * A - 275932B * B + 9.61C * C + 1022\ A * B - 44.9A * C - 284B * C \qquad \textbf{Eq. 14}$$

9.6. Comparison of Produced Gases Amounts

In this study, the effects of pH (A), catalyst loading (B) and initial hydrogen peroxide concentration (C) over produced hydrogen amounts from SMS and sugar beet wastewater were investigated and the experimental data were statistically analysed to comprehend the effective parameters for photocatalytic hydrogen production in the presence of hybrid catalysts. The comparison table for the produced hydrogen amounts from SMS and sugar beet wastewater based on catalyst type (GLFO, GBFO and GLRO) was given in Table 9. 10.

Based on the results, the pH of sucrose solution had a main effect over the produced hydrogen amount from SMS while the square of pH had an impact over the

produced hydrogen amount from real sugar beet wastewater in the presence of all catalyst. In the photocatalytic oxidation process, initial pH of solution, which contain an organic compound, is an important parameter since it affects the formation of hydroxyl radicals. For instance, hydroxyl radicals attack the organic molecules in wastewaters so that less harmless and/or harmless compounds form and hence, the wastewater could be treated and reused. Additionally, the formation of hydrogen can enhance in acidic conditions due to the higher concentration of hydrogen ions in the reaction media since hydrogen is evolved by excited electrons and hydrogen ions that are absorbed on the surface of photocatalysts (Estahbanati et al., 2019; Badawy et al. 2011; Enzweiler et al., 2020).

According to experimental results of SMS, relatively higher hydrogen amounts were observed around 5.25 of pH. However, due to the agglomeration of hybrid catalysts, the available surface of hybrid catalysts reduced and it might cause a decrease in the hydrogen production amounts at same conditions.

The initial hydrogen peroxide concentration is another important parameter in this process since the degradation of organic molecules are achieved by the help of hydroxyl radicals. The reaction mechanism of formation of hydroxyl radical were given in the following equations (Ghaly et al., 2007; Silva and Faria, 2010):

$$H_2O_2 + O_2^- \rightarrow OH\cdot + OH^- + O_2\cdot \qquad \textbf{Eq. 15}$$

$$H_2O_2 + hv \rightarrow 2OH \qquad \textbf{Eq. 16}$$

$$H_2O_2 + e^- \rightarrow OH^- + OH\cdot \qquad \textbf{Eq. 17}$$

$$H_2O_2 + 2e^- \rightarrow 2OH^- \qquad \textbf{Eq. 18}$$

$$H_2O_2 + 2h^+ \rightarrow O_2 + 2H^+ \qquad \textbf{Eq. 19}$$

$$OH\cdot + H^+ + e^- \rightarrow H_2O \qquad \textbf{Eq. 20}$$

$$H_2O_2 + OH\cdot \rightarrow HO_2\cdot + H_2O \qquad \textbf{Eq. 21}$$

$$HO_2\cdot + OH\cdot \rightarrow H_2O + O_2 \qquad \textbf{Eq. 22}$$

Based on Eq. 17 and 18, it could be said that hydrogen peroxide can act as a scavenger for VB-holes. Additionally, based on Eq. 20-22, it could be deduced that it could act as a scavenger for OH·. Because of these reasons, the concentration of hydrogen peroxide should be optimized. Considering the results, it could be confirmed that initial hydrogen peroxide concentration was an important factor for produced hydrogen amount from SMS using all hybrid catalysts since it had a main effect statistically.

The metal oxides have positively charged surfaces and hence, as the pH of solution decreases, the adsorbed H_2O_2 concentration on the surface of metal oxides enhances (Pan et al., 2020). For instance, the obtained hydrogen amounts from SMS using GLFO and 15 mM of hydrogen peroxide were 3459.85 and 3305.83 $\mu mol/g_{cat}$ at 3 and 7.5 of pH, respectively. Additionally, the obtained hydrogen amounts from real sugar beet wastewater using GLFO and 15 mM of hydrogen peroxide were 6688.67 and 5060.51 $\mu mol/g_{cat}$ at 3 and 7.5 of pH, respectively. Consequently, it implied that the hydrogen peroxide was highly adsorbed on the surface of this hybrid catalyst in acidic conditions, and hence, the produced hydrogen amount increased in acidic reaction media. Additionally, based on the results of Box Behnken model, the synergetic effect of pH and initial hydrogen peroxide concentration over produced hydrogen amount from real sugar beet was observed in the presence of GLFO and GLRO. The synergetic effect of them depends on the other reaction parameters such as TOC and concentration of organic substances in the wastewater streams (Dionysiou et al., 2004). Thus, to observe the synergetic effect of them, the appropriate reaction conditions were provided for GLFO and GLRO. The main effects of A and C were statistically effective over the produced hydrogen amount from SMS. However, they did not have a main effect, while main effect of catalyst loading had a main impact over the produced hydrogen amount from real sugar beet wastewater. Hence, catalyst loading became an important factor for hydrogen production from real sugar beet wastewater. In addition, catalyst loading was also an important parameter for the produced hydrogen amount from SMS.

The catalyst loading affects the distribution of light and the excess amount of catalyst could cause penetration of light so that the obtained hydrogen amount decreases. So, the catalyst loading should be optimized in photocatalytic oxidation process (Bednarczyk et al., 2018; Enzweiler et al., 2020).

The produced gases amount from SMS and real sugar beet wastewater based on catalyst types were given in Table 9. 11. and Table 9. 12., respectively.

Table 9.10. The comparison table for produced hydrogen amount based on catalyst type

Reaction Conditions			Produced Hydrogen (µmol/g_{cat})					
			Sucrose Model Solution			Sugar beet wastewater		
A	**B**	**C**	**GLFO**	**GBFO**	**GLRO**	**GLFO**	**GBFO**	**GLRO**
3	0.15	0	3245.32	2717.27	3030.80	5566.56	5489.55	5521.19
7.5	0.15	15	3305.83	2579.76	3179.32	5060.51	4471.95	4867.04
5.25	0.15	7.5	3377.34	2700.77	3382.84	4048.40	3564.36	3895.23
7.5	0.15	0	3003.30	2755.78	2805.28	7035.20	6089.11	6645.35
3	0.1	7.5	3102.31	2552.26	2678.77	6837.18	6617.16	6758.27
5.25	0.15	7.5	3470.85	3102.31	3410.34	4460.95	3245.32	3236.56
7.5	0.1	7.5	3052.81	2568.76	2865.79	6078.11	5429.04	5685.54
5.25	0.2	0	3102.31	2590.76	3047.30	3547.85	3674.37	3587.91
5.25	0.1	15	3388.34	3514.85	3135.31	4680.97	4031.90	4353.46
3	0.2	7.5	3206.82	2728.77	3085.81	3498.35	3338.83	3526.85
5.25	0.15	7.5	3399.34	2739.27	3338.83	4196.92	3822.88	4186.37
5.25	0.15	7.5	3443.34	2673.27	3415.84	3448.84	3124.31	3892.17
5.25	0.10	0	3069.31	2970.30	2898.79	4543.45	4295.93	4391.01
5.25	0.15	7.5	3520.35	3459.85	3404.84	5066.01	4207.92	4076.32
5.25	0.15	7.5	3509.35	2662.27	3349.83	4075.91	3074.81	4793.62
7.5	0.2	7.5	3058.31	2783.28	2887.79	3063.81	2777.78	2913.81
5.25	0.2	15	3503.85	2508.25	3322.33	3096.81	3173.82	3124.16
3	0.15	15	3459.85	3025.30	3256.33	6688.67	6435.64	6772.56
Effective parameters based on Box Behnken model			A, C AA, BB	A, B, C BC, CC	A, B, C AB, AA BB, CC	B, AA BB, AC	B, AA	B, AA, AC
R^2 values of model			95.36%	98.82%	98.84%	87.80%	86.35%	87.26%

Methane production from SMS was not observed whereas methane production was observed in a few experiments which were carried out using real sugar beet wastewater. For instance, the methane production was observed in the presence of GLFO and GBFO at the same reaction conditions (pH=7.5, catalyst loading=0.2 g/L, $[H_2O_2]_0$=7.5 mM). However, methane production was observed at the following two reaction conditions (pH=5.25, catalyst loading=0.1 g/L, $[H_2O_2]_0$=15 mM and pH=5.25, catalyst loading=0.15 g/L, $[H_2O_2]_0$=7.5 mM).

In all experiments, the production of CO and CO_2 from SMS and real sugar beet wastewater was observed. While the produced CO amounts from SMS varied between 352 and 825 μmol/g_{cat}, the produced CO amounts from real sugar beet wastewater were changed in the range of 649 and 847 μmol/g_{cat}. The produced amounts of CO_2 from SMS varied between 1106 and 1579 μmol/g_{cat}, whereas the produced amounts of CO_2 from real sugar beet wastewater were changed in the range of 11155 and 102536 μmol/g_{cat}. Therefore, the produced amounts of CO and CO_2 from real sugar beet wastewater was higher than the produced amounts of them from SMS since the real sugar beet wastewater contains different organic compounds as well as sucrose.

Therefore, it could be deduced that the degradation of sucrose and organic pollutants in sugar beet wastewater is achieved successfully. The degradation of them, in other words, the treatment of wastewater and hydrogen production was achieved simultaneously so that it could be said that the organic compounds in real wastewater could be used as electron donors for hydrogen production by photocatalytic oxidation and hence, the electron donor cost could be reduced using wastewater for photocatalytic hydrogen production.

The uncertainty values for all produced gases from SMS and real sugar beet solution in the presence of all hybrid catalysts were given in Table 9. 13.

The obtained CO_2 amounts for real sugar beet wastewater in the presence of all hybrid catalysts were relatively higher compared to SMS and thus, the uncertainty values for CO_2 in the presence of all hybrid catalysts were also relatively higher for real sugar beet wastewater. Additionally, the uncertainty values for the obtained hydrogen amount from real sugar beet wastewater using all hybrid catalyst increased.

Table 9.11. The produced gases from sucrose model solution based on catalyst type

			GLFO				GBFO				GLRO			
Reaction Conditions			**Produced Gases ($\mu mol/g_{cat}$)**				**Produced Gases ($\mu mol/g_{cat}$)**				**Produced Gases ($\mu mol/g_{cat}$)**			
A	**B**	**C**	H_2	CO	CO_2	CH_4	H_2	CO	CO_2	CH_4	H_2	CO	CO_2	CH_4
3	0.15	0	3245	352	1480	0	3218	743	1254	0	3031	737	1166	0
7.5	0.15	15	3306	737	1452	0	2849	781	1172	0	3179	765	1161	0
5.25	0.15	7.5	3377	776	1478	0	2668	759	1139	0	3383	759	1205	0
7.5	0.15	0	3003	710	1155	0	2690	682	1106	0	2805	748	1150	0
3	0.1	7.5	3102	633	1243	0	2734	765	1166	0	2679	710	1166	0
5.25	0.15	7.5	3471	754	1568	0	2690	765	1177	0	3410	732	1232	0
7.5	0.1	7.5	3053	616	1238	0	2437	737	1221	0	2866	737	1205	0
5.25	0.2	0	3102	633	1326	0	3119	732	1210	0	3047	699	1200	0
5.25	0.1	15	3388	765	1337	0	3053	726	1199	0	3135	710	1194	0
3	0.2	7.5	3207	726	1249	0	3086	743	1183	0	3086	743	1183	0
5.25	0.15	7.5	3399	792	1529	0	2717	809	1199	0	3339	770	1216	0
5.25	0.15	7.5	3443	809	1535	0	2701	776	1161	0	3416	787	1243	0
5.25	0.10	0	3069	721	1205	0	2800	748	1188	0	2899	743	1205	0
5.25	0.15	7.5	3520	825	1579	0	2717	759	1155	0	3405	743	1221	0
5.25	0.15	7.5	3509	809	1557	0	2679	770	1177	0	3350	737	1200	0
7.5	0.2	7.5	3058	748	1452	0	2651	765	1177	0	2888	770	1227	0
5.25	0.2	15	3504	759	1469	0	3152	737	1216	0	3322	770	1227	0
3	0.15	15	3460	583	1568	0	3273	743	1276	0	3256	743	1216	0

Table 9.12. The produced gases from sugar beet wastewater based on catalyst type

			GLFO				GBFO				GLRO			
Reaction Conditions			**Produced Gases (µmol/g_{cat})**				**Produced Gases (µmol/g_{cat})**				**Produced Gases (µmol/g_{cat})**			
A	**B**	**C**	H_2	CO	CO_2	CH_4	H_2	CO	CO_2	CH_4	H_2	CO	CO_2	CH_4
3	0.15	0	5567	732	101909	363	5490	737	102536	0	5521	725	100819	0
7.5	0.15	15	5061	737	23647	0	4472	649	22624	0	4867	712	23356	0
5.25	0.15	7.5	4048	682	61469	0	3564	682	53878	0	3895	678	58795	0
7.5	0.15	0	7035	671	27558	0	6089	671	26579	0	6645	672	27357	0
3	0.1	7.5	6837	704	32090	0	6617	693	31546	0	6758	702	31486	0
5.25	0.15	7.5	4461	737	70490	0	3245	682	53047	0	3237	695	62896	0
7.5	0.1	7.5	6078	732	26717	22	5429	671	25820	0	5686	711	25414	0
5.25	0.2	0	3548	666	17992	0	3674	666	18355	0	3588	663	18129	0
5.25	0.1	15	4681	677	78801	0	4032	682	76485	0	4354	681	77983	386
3	0.2	7.5	3498	688	53047	0	3339	677	52965	0	3527	677	52834	0
5.25	0.15	7.5	4197	704	65671	0	3823	671	63449	0	4186	696	64875	0
5.25	0.15	7.5	3449	704	63284	0	3124	671	64340	0	3892	697	63786	0
5.25	0.10	0	4544	693	58845	0	4296	699	59676	0	4391	694	59172	0
5.25	0.15	7.5	5066	726	71738	0	4208	655	70765	0	4076	696	70961	412
5.25	0.15	7.5	4076	726	82041	0	3075	682	64356	0	4794	713	74859	0
7.5	0.2	7.5	3064	847	11612	391	2778	671	11155	473	2914	698	11514	0
5.25	0.2	15	3097	688	47739	0	3174	671	46309	0	3124	672	47019	0
3	0.15	15	6689	660	87002	0	6436	704	88042	0	6773	687	87685	0

Table 9.13. Uncertanity values for all produced gases

	Sucrose model solution				Real sugar beet wastewater			
Catalyst type	**H_2**	**CO**	**CO_2**	**CH_4**	**H_2**	**CO**	**CO_2**	**CH_4**
GLFO	60.71	27.12	38.07	-	559.18	21.18	7856.99	-
GBFO	21.29	19.75	17.01	-	468.57	11.22	7200.22	-
GLRO	34.25	22.32	17.01	-	529.94	11.64	6134.64	176.54

CHAPTER 10

PHOTOCATALYTIC HYDROGEN PRODUCTION FROM NITROGEN CONTAINING MODEL SOLUTION (DBU)

1,8-Diazabicyclo[5.4.0]undec-7-ene (DBU) is a nitrogen containing compound and it is generally found in various industrial wastewaters such as pharmaceutical and textile. In addition, it has toxic effects over human and environment. To analyze the effectiveness of photocatalytic degradation on such toxic and stable compound, DBU solution was selected as a model solution of nitrogen containing wastewaters. Therefore, both treatment efficiency of DBU and hydrogen production from DBU via photocatalytic oxidation have been studied in the presence of GLFO, GBFO and GLRO catalysts. In this context, the same experimental matrix was used and the obtained hydrogen amounts are listed in Table 10. 1.

Table 10.1. Hydrogen production from DBU model solution

			Produced Hydrogen Amounts (μmol/g_{cat})		
A	**B**	**C**	**GLFO**	**GBFO**	**GLRO**
3	0.15	0	2761.28	2590.76	1798.68
7.5	0.15	15	2574.26	2178.22	2200.22
5.25	0.15	7.5	2832.78	1787.68	2101.21
7.5	0.15	0	2189.22	1996.70	2244.22
3	0.1	7.5	2013.20	2722.77	2332.23
5.25	0.15	7.5	2744.77	1809.68	2046.20
7.5	0.1	7.5	1914.19	1908.69	2095.71
5.25	0.2	0	1826.18	2926.29	2194.72
5.25	0.1	15	2370.74	2178.22	2062.71
3	0.2	7.5	1881.19	2904.29	2673.27
5.25	0.15	7.5	2898.79	1875.69	2145.21
5.25	0.15	7.5	3058.31	1864.69	2150.72
5.25	0.1	0	2057.21	2051.71	1991.20
5.25	0.15	7.5	2667.77	1930.69	2024.20
5.25	0.15	7.5	2755.78	2057.21	2079.21
7.5	0.2	7.5	1886.69	2040.70	2689.77
5.25	0.2	15	1875.69	3118.81	2563.26
3	0.15	15	3041.80	2920.79	2299.23

Table 10.2. ANOVA table for GLFO

Source	DF	Adj SS	Adj MS	F-Value	P-Value
Model	9	3184069	353785	10.91	0.00130
Linear	3	390780	130260	4.02	0.05136
A	1	160493	160493	4.95	0.05673
B	1	98033	98033	3.02	0.12022
C	1	132253	132253	4.08	0.07807
Square	3	2770400	923467	28.49	0.00013
A*A	1	93885	93885	2.90	0.12720
B*B	1	2493100	2493100	76.91	0.00002
C*C	1	6316	6316	0.19	0.67060
2-Way Interaction	3	22889	7630	0.24	0.86930
A*B	1	2731	2731	0.08	0.77902
A*C	1	2731	2731	0.08	0.77902
B*C	1	17427	17427	0.54	0.48435
Error	8	259327	32416		
Lack-of-Fit	3	163451	54484	2.84	0.14504
Pure Error	5	95876	19175		
Total	17	3443396			

The obtained hydrogen amounts were relatively lower compared to SMS and sugar beet wastewater in terms of all catalysts. Among them, relatively higher yields were obtained in the presence of GLFO. Based on the results, the highest hydrogen amounts were achieved as 3058.31, 3118.81, 2689.77 μmol/g_{cat} in the presence of GLFO, GBFO, and GLRO, respectively. The uncertainty values for GLFO, GBFO and GLRO were determined as 145.34, 102.14, 53.96 μmol/g_{cat}, respectively. According to the results, GLRO showed the lowest photocatalytic efficiency to produce hydrogen from DBU model solution while GLFO and GBFO showed similar activity. ANOVA tables for each hybrid catalysts, GLFO, GBFO and GLRO, are given in Table 10. 2., Table 10. 3., and Table 10. 4., respectively. In these tables, A, B and C were used for pH, catalyst loading and $[H_2O_2]_0$, respectively.

Based on Table 10. 2., only B*B was effective over the hydrogen evolution from DBU model solution using GLFO catalyst. The value of R^2 for this model was determined as 92.47 % and the model showed well fit to the observed response.

Table 10.3. ANOVA table for GBFO

Source	DF	Adj SS	Adj MS	F-Value	P-Value
Model	9	3183573	353730	8.12	0.004
Linear	3	1788412	596137	13.69	0.002
A	1	1135752	1135752	26.08	0.001
B	1	566427	566427	13.01	0.007
C	1	86234	86234	1.98	0.197
Square	3	1387944	462648	10.62	0.004
A*A	1	140887	140887	3.24	0.110
B*B	1	466098	466098	10.70	0.011
C*C	1	547844	547844	12.58	0.008
2-Way Interaction	3	7216	2405	0.06	0.982
A*B	1	613	613	0.01	0.909
A*C	1	5514	5514	0.13	0.731
B*C	1	1089	1089	0.03	0.878
Error	8	348386	43548		
Lack-of-Fit	3	301040	100347	10.60	0.013
Pure Error	5	47346	9469		
Total	17	3531959			

Table 10.4. ANOVA table for GLRO

Source	DF	Adj SS	Adj MS	F-Value	P-Value
Model	9	883331	98148	13.08	0.001
Linear	3	438342	146114	19.47	0.000
A	1	2001	2001	0.27	0.620
B	1	335857	335857	44.75	0.000
C	1	100484	100484	13.39	0.006
Square	3	332792	110931	14.78	0.001
A*A	1	91263	91263	12.16	0.008
B*B	1	196120	196120	26.13	0.001
C*C	1	43772	43772	5.83	0.042
2-Way Interaction	3	112197	37399	4.98	0.031
A*B	1	16005	16005	2.13	0.182
A*C	1	74135	74135	9.88	0.014
B*C	1	22057	22057	2.94	0.125
Error	8	60046	7506		
Lack-of-Fit	3	46829	15610	5.91	0.042
Pure Error	5	13217	2643		
Total	17	943377			

According to Table 10. 3., the effective factors were specified as A, B, C*C and B*B. Especially, main factors, A and B, strongly affected the produced hydrogen amount. The value of R^2 for this model was determined as 90.14 %. According to Table 10. 4., the factors, B, C, A*A, B*B, C*C and A*C, had impact on the produced hydrogen amount from DBU model solution using GLRO. 2-way interaction (A*C), namely, a synergistic effect of A and C was only observed using GLRO. The R^2 of this model was found as 93.64 %.

Residual plots and histogram diagrams for GLFO, GBFO and GLRO are given in Figure 10. 1. and the obtained data showed normal distributions for each hybrid catalysts. Additionally, no outlier was observed for them. While the experimental data aligned between -200 and +200 for GLFO and GBFO, the experimental data aligned in the range of -100 and +100 for GLRO. Pareto Charts of hybrid catalysts that were used for hydrogen production from DBU model solution are given in Figure 10. 2.

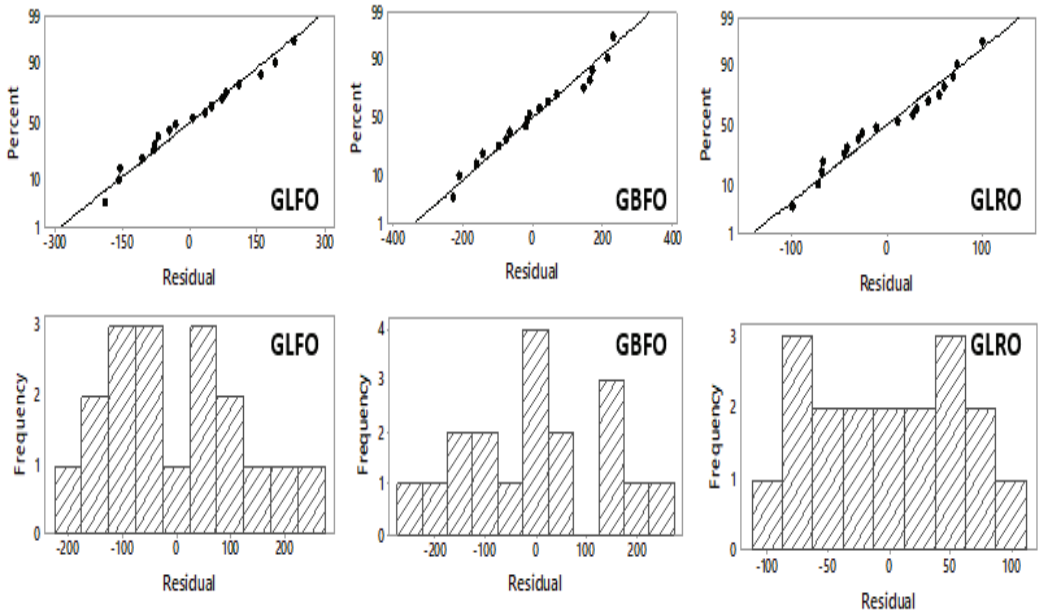

Figure 10.1. Normal probablity and histogram plots for all hybrid catalysts

Based on the results, t-value was 2.306 for all of them and the terms passed the t-value became statistically significant for these models. The most effective factors were B*B, A and B for GLFO, GBFO and GLRO, respectively. Therefore, it could be said that the catalyst loading should be considered to optimize the produced hydrogen amount from DBU model solution for all hybrid catalysts (GLFO, GBFO and GLRO).

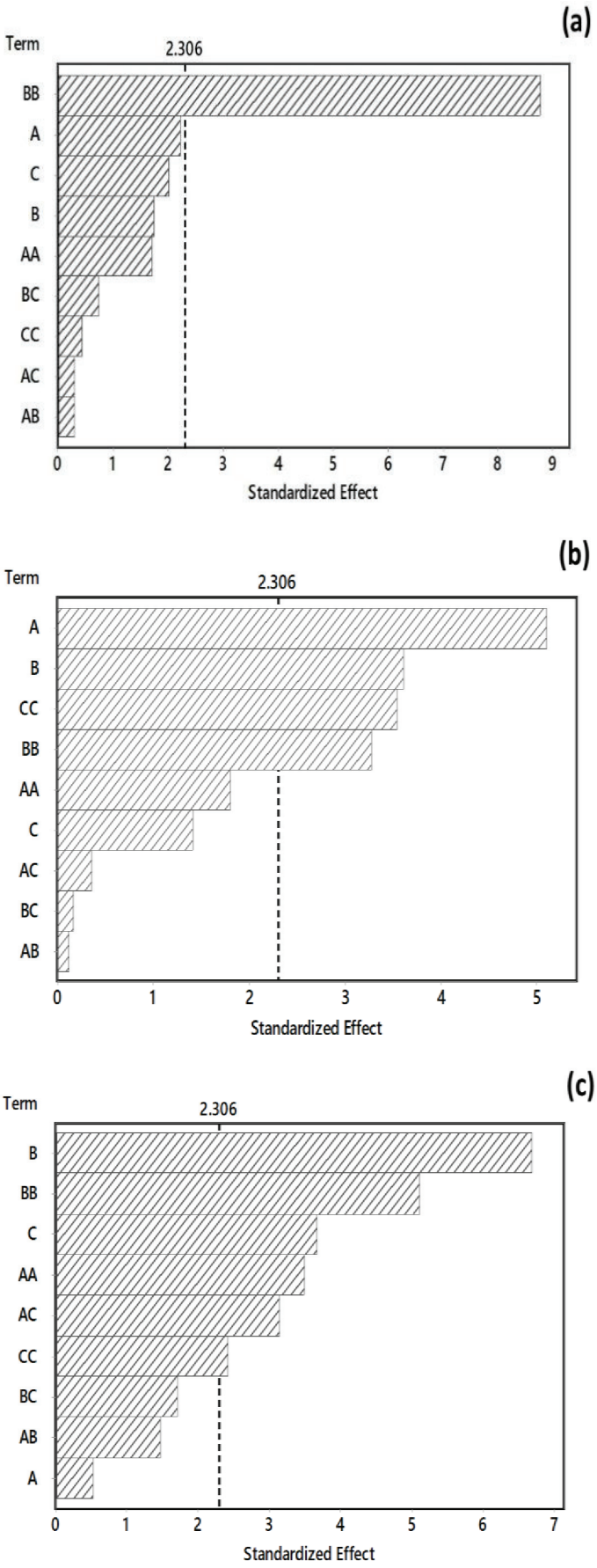

Figure 10.2. Pareto Charts for hybrid catalysts; GLFO (a), GBFO (b), GLRO (c)

The A and C had a synergetic impact over the evolved hydrogen amount for GLRO and their values should be considered to avoid from the scavenging effect and enhance the degradation efficiency of DBU. The equations for predicted hydrogen amount in the presence of GLFO, GBFO and GLRO are given in equation 23, 24 and 25, respectively.

$$Produced\ hydrogen\ (using\ GLFO) = -4233 + 195\,A + 88591B + 45.6C - 29A * A - 302347B * B - 0.68\,C * C + 232A * B + 1.55A * C - 176B * C \quad (\boldsymbol{Eq.23})$$

$$Produced\ hydrogen\ (using\ GBFO) = 6015 - 507\,A - 33650B + 75.7C + 35.5A * A + 130730B * B + 6.30\,C * C - 110\,A * B - 2.20A * C + 44B * C \quad (\boldsymbol{Eq.24})$$

$$Produced\ hydrogen\ (using\ GLRO) = 4271 - 317\,A - 25779B + 54.3C + 28.57A * A + 84800B * B - 1.781\,C * C + 562A * B - 8.07A * C + 198B * C \quad (\boldsymbol{Eq.25})$$

10.1. Treatment of DBU Model Solution in Hot Compressed Water

In the previous section, the results of DBU treated by photocatalytic oxidation to produce hydrogen were given. Due to low TOC conversion via photocatalytic oxidation, the DBU and TOC conversions were also investigated after DBU solution was treated in a hybrid method that combines wet oxidation in Hot Compressed Water (HCW) with electrolysis. This method can be used for wastewater treatment and production of value-added chemicals by degradation of biomass and/or wastes. For instance, in literature, it was used for treatment of organic compounds such as Orange G, glycerol and biodiesel containing wastewaters (Yuksel et al., 2011b; Yuksel et al., 2010; Yuksel et al., 2011a).

In addition, it was used for cellulose degradation to produce value-added chemicals such as furfural, formic acid, 5-HMF and levulinic acid etc. (Akın and Yuksel, 2016).

Electrochemical oxidation is widely used for wastewater treatment in the presence of chloride ion catalysts and Fenton's reagents. Although electrochemical oxidation could be performed at atmospheric pressure and temperature, it is a slow reaction due to the some limitations in terms of reaction kinetic (Sasaki et al., 2010). In order to overcome the limitations and to enhance the conversion, it can be performed under subcritical conditions because water undergoes some physicochemical changes at subcritical conditions. For instance, the solubility of organic compounds and ionic product increase while dielectric constant decreases. Additionally, highly-reactive hydroxyl radicals form throughout the reaction (Yuksel et al., 2011a; Yuksel et al., 2011b). Moreover, there is no need to use any catalyst and oxidizer because HCW acts as a catalyst due to the physicochemical changes and oxygen generation could be controlled (Yuksel et al., 2011a).

Usage of current accelerates the degradation of organic compounds in this hybrid method (Yuksel et al., 2011a). Usage of HCW minimizes the required energy for electrolysis and applying current near critical point of water favors reaction progress (Yuksel et al., 2011a; Yuksel et al., 2011b). Consequently, this hybrid method was chosen due to the economical feasibility.

In this context, a full factorial design was builded to analyse main and interaction effects of reaction parameters which were NaOH concentration (A), current density (B), reaction duration (C) over the conversions of DBU and TOC in HCW. The experimental design matrix and the results are given in Table 10.5.

According to the results, the highest DBU removal was achieved as 97.4% at the following reaction conditions: 0.05 M of NaOH concentration, 0.0027 mA/cm^2 of current density and 90 minutes of reaction duration. To comprehend the main and interaction of affecting reaction parameters ANOVA table of experimental design was created with a 95% of confidence level and it is given in Table 10.6. The R^2 of model was determined as 76.59% and it could be concluded that the model is well fit to the observed response.

According to ANOVA table, p-values of 2-way and 3-way interactions of reaction were higher than 0.05 and hence, they did not statistically show a significant impact over DBU removal. Therefore, these terms were eliminated to modify the model and reduced ANOVA table for the experimental design is given in Table 10.7.

Table 10.5. Experimental Design and Response as Percent Removal of DBU

NaOH conc., M	Current density, mA/cm^2	Reaction time, min.	DBU removal, %
0.01	0	30	82.9
0.05	0	30	84.6
0.05	0	60	87.3
0.05	0	90	90.3
0.01	0.0027	90	72.3
0.05	0.0027	30	94.6
0.01	0	90	79.1
0.01	0.0027	30	76.9
0.01	0.0027	90	84.7
0.05	0.0027	90	96.7
0.05	0	60	88.7
0.01	0	60	79.6
0.05	0.0027	60	95.5
0.01	0.0027	60	78.3
0.01	0	30	56.9
0.01	0.0027	30	62.7
0.05	0	30	83.5
0.05	0.0027	90	97.4
0.05	0.0027	60	97.1
0.05	0	90	88.9
0.05	0.0027	30	95.3
0.01	0	90	68.9
0.01	0.0027	60	78.3
0.01	0	60	61.2

Based on ANOVA table for reduced model, whereas A and B have a main impact over DBU removal, reaction duration does not have a main impact over DBU removal. Pareto chart for the main factors of reaction parameters are given in Figure 10. 3.

Table 10.6. Statistical Analysis Results for DBU Removal

Source	DoF	SS	MS	F-Value	P-Value
Model	11	2424.99	220.45	3.57	0.019
Linear	4	2344.92	586.23	9.49	0.001
A	1	1981.98	1981.98	32.08	0.000
B	1	252.85	252.85	4.09	0.066
C	2	110.09	55.04	0.89	0.436
2-Way Interactions	5	49.46	9.89	0.16	0.973
A*B	1	34.32	34.32	0.56	0.470
A*C	2	7.05	3.53	0.06	0.945
B*C	2	8.09	4.05	0.07	0.937
3-Way Interactions	2	30.61	15.31	0.25	0.784
A*B*C	2	30.61	15.31	0.25	0.784
Error	12	741.33	61.78		
Total	23	3166.33			

Table 10.7. Statistical Analysis Results for DBU Removal (Reduced Model)

Source	DoF	SS	MS	F-Value	P-Value
Model	4	2344.92	586.23	13.56	0.000
Linear	4	2344.92	586.23	13.56	0.000
A	1	1981.98	1981.98	45.85	0.000
B	1	252.85	252.85	5.85	0.026
C	2	110.09	55.04	1.27	0.303
Error	19	821.41	43.23		
Lack-of-Fit	7	80.07	11.44	0.19	0.983
Pure Error	12	741.34	61.78		
Total	23	3166.33			

The vertical line in Pareto chart means that the t-value is 2.093 for 12 degrees of freedom in 95% confidence level and hence, the magnitude of lowest statistically significant effect is equal to this value. $F_{0.05,1,12}$ is equal to 4.75 and thus, if F value of factors is higher than 4.75, it indicates that they are statistically significant for DBU removal. Therefore, based on the Pareto chart, while A and B are statistically significant reaction parameters over DBU removal, C is not a significant reaction parameter. Residual and histogram plots are given in Figure 10. 4.

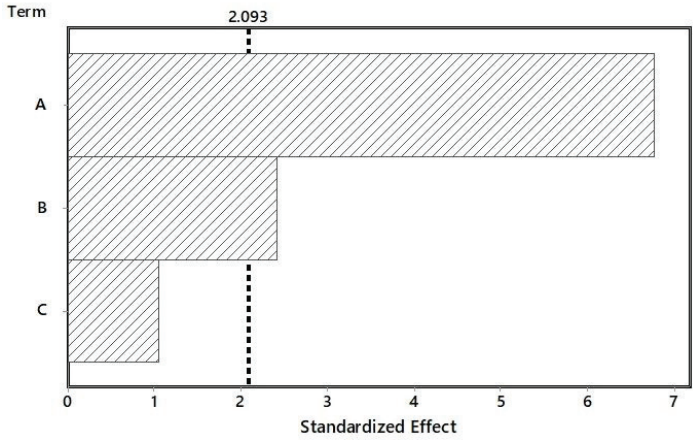

Figure 10.3. Pareto chart for DBU removal

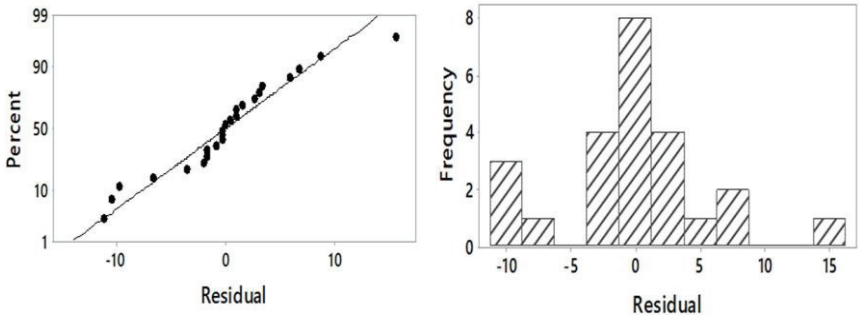

Figure 10.4. Residual and histogram plot for DBU removal

Residual plot explains whether the data normally distributed or not. In the plot, the points represent the difference between experimental and predicted DBU removal values. If these points are near the straight line, then it indicates that the data is normally allocated (Safa and Bhatti, 2011). Based on Figure 10. 4., the points are reasonably

aligned suggesting normal distribution between -10 and +10. However, an outlier was also observed.

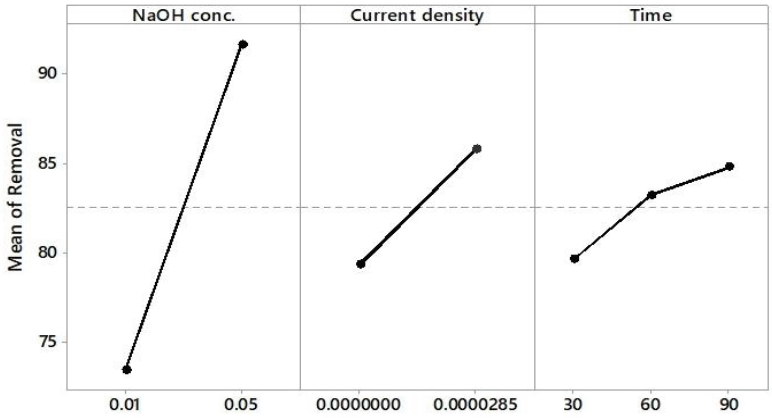

Figure 10.5. Main effects for DBU removal

If a reaction parameter is a major impact over response, the mean value of response alters between the levels of this reaction parameter and its sign indicates that this parameter has a positive or negative effect on the response. Based on Figure 10. 5, among the reaction parameters, NaOH concentration has a greater degree of departure from the overall mean so that it could be deduced that it has a positive effect over the removal efficiency of DBU. In addition, current density has a similar impact on DBU removal. Yet, the effect of current density is lower compared to NaOH concentration. Furthermore, the impact of reaction duration has slightly diminished for 90 minutes of reaction duration.

10.1.1. Effect of NaOH Concentration

According to ANOVA table, the most effective reaction parameter for the treatment of DBU via hydrothermal hydrolysis is determined as NaOH concentration. Therefore, the impact of NaOH concentration over the DBU removal was investigated at different NaOH concentrations (0, 0.001, 0.01 and 0.05 M). These experiments were carried out using 6 mM of DBU solution applying current density (0.0027 mA/cm^2) at

the reaction temperature of 240 °C for various reaction durations (30, 60 and 90 minutes) and the results are given in Figure 10.6.

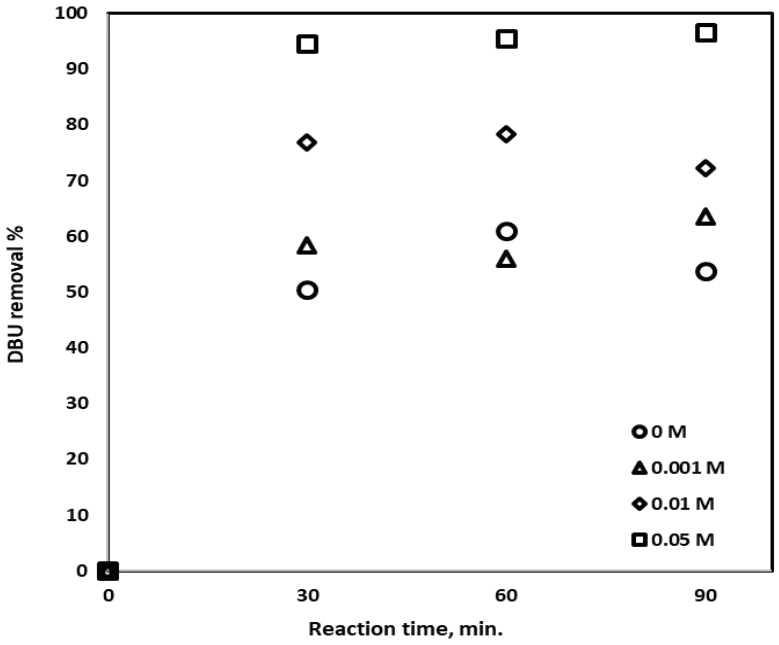

Figure 10.6. Effect of NaOH concentration on DBU removal (Reaction conditions: C_{DBU}= 6 mM, current density=0.0027 mA/cm^2, T=240 °C)

According to Figure 10.6, the highest DBU removal was achieved as almost 97% using 0.05 M of NaOH concentration. The DBU removal efficiency enhanced with respect to the increased concentration of NaOH for all reaction durations. In literature, similar results are reported in many studies. For instance, Yuksel et al. carried out a study over the decomposition of glycerol via hydrothermal electrolysis and they were reported that higher glycerol conversions were observed as the NaOH concentrations increase (Yuksel et al., 2011a). Consequently, this result implies that ionic conductivity boosts due to the increasing concentration of electrolyte concentration and the removal efficiency of compounds enhances. Even though DBU removal can be achieved without using NaOH applying 0.0027 mA/cm^2 of current density at 240 °C, the highest TOC conversion (29.6%) was obtained for 90 minutes of reaction duration. On the other hand, using 0.05 M of NaOH as an electrolyte, TOC conversions were obtained as 29.6% and 41.0% for 60 and 90 minutes of reaction duration, respectively. Therefore, only HCW usage is not enough for higher TOC conversions and DBU removal efficiencies in a shorter reaction duration so that an electrolyte should be used.

10.1.2. Effect of Current Density

Whereas hydrogen and oxygen form via the electrolysis of water at normal conditions, oxygen formation can be controlled if the electrolysis of water is performed under subcritical conditions. The illustration of electrolysis at normal and subcritical conditions is given in Figure 10. 7 (Serikawa, 2007).

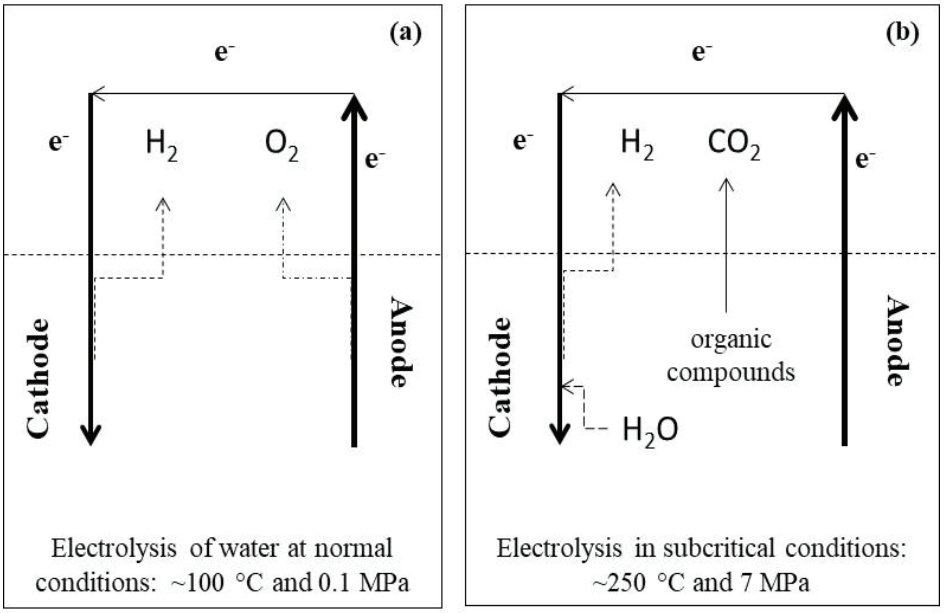

Figure 10.7. Electrolysis at normal **(a)** and subcritical **(b)** conditions

Consequently, in hydrothermal electrolysis, HCW behaves as a catalyst so that an oxidizer or/and catalyst are not required (Yuksel et al., 2011b). Furthermore, any organic solvent does not utilize in hydrothermal electrolysis and hence, it becomes a greener and environmentally friendly approach for wastewater treatment. In this process, many oxidants ($H^{\bullet}$, $OH^{\bullet}$ etc.) as well as free hydroxyl radicals, ions and sometimes hydrogen atoms form. Furthermore, hydrogen, oxygen and hydrogen peroxide form by the decomposition of water molecules in liquid region and the possible reactions are given in Eq. 26-30 (Yuksel et al. 2011b; Miller and Hawthorne, 1998; Savage 1999). Tough $OH^{\bullet}$ is the strongest oxidant among the formed oxidants, it has a very short life span. Hence, the secondary oxidants are generated via the destruction of $OH^{\bullet}$ to maintain the decomposition of organic compounds.

$$H^{\bullet} + H^{\bullet} \rightarrow H_2 \qquad \textbf{Eq. 26}$$

$$H^{\bullet} + OH^{\bullet} \rightarrow H_2O \qquad \textbf{Eq. 27}$$

$$OH^{\bullet} + OH^{\bullet} \rightarrow H_2O_2 \qquad \textbf{Eq. 28}$$

$$OH^{\bullet} + H_2O_2 \rightarrow HO_2^{\bullet} + H_2O \qquad \textbf{Eq. 29}$$

$$OH^{\bullet} + HO_2^{\bullet} \rightarrow H_2O + O_2 \qquad \textbf{Eq. 30}$$

Based on the statistical analysis results, current density has considerable effect on DBU removal in hydrothermal electrolysis so that the impact of current density on DBU removal are searched at various current densities which are 0 mA/cm^2 (0 A), 0.0007 mA/cm^2 (0.25 A) and 0.0027 mA/cm^2 (1A). The experiments were performed 6 mM DBU solution at 240 °C applying the current for different reaction times (30, 60 and 90 min.) and obtained results are represented in Figure 10. 8. As the current density rise, DBU removal enhanced for 30 and 60 minutes of reaction duration but almost the same DBU removal was achieved for 90 minutes of reaction duration. TOC conversion was not achieved without applying 0 mA/cm^2 of current density for 30 and 60 minutes of reaction duration whereas 11.5% and 31.1% of TOC conversions were obtained applying 0.0027 mA/cm^2 of current density for 30 and 60 minutes of reaction duration, respectively. In addition, 11.1 % and 31.1 % TOC conversions were obtained for 90 minutes of reaction duration applying 0 and 0.0027 mA/cm^2 of current density, respectively. Therefore, almost same TOC conversions were obtained applying current in a short reaction duration (30 min.) and in the absence of current for 90 minutes of reaction duration. Hence, TOC conversion could not accomplish in the absence of current. Moreover, based on the GC-MS results, toxic by-products formed during hydrothermal treatment of DBU, namely, without applying current whereas toxic by-products did not form in hydrothermal electrolysis of DBU. Therefore, the formation of toxic by-products could be prevented by applying current. TOC conversions enhanced due to the increased current density. Dai et al. studied the degradation p-nitrophenol in wastewater via a novel wet electrocatalytic oxidation and reported that he conversion of TOC and removal of p-nitrophenol enhanced due to the increased current density (Dai et al., 2008). Sasaki et al. studied about hydrothermal electrolysis of glucose and based on the results, as the current density

increases the TOC and glucose conversion (Sasaki et al., 2007). Additionally, amidines (i.e. DBU) could degrade by pyrolysis under subcritical conditions without using any oxidant. Yet, lower TOC conversions could be accomplished without applying current (Shriner and Neumann, 1944).

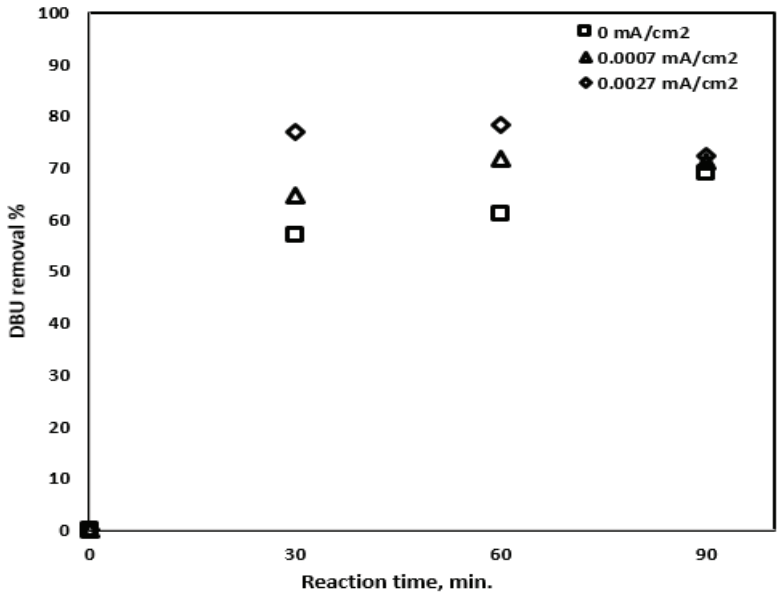

Figure 10.8. Effect of current density on DBU removal (Reaction conditions: C_{DBU}= 6 mM, T=240 °C, C_{NaOH}= 0.01 M)

Therefore, DBU removal and TOC conversion could rise by applying current. Additionally, there is no requirement for an oxidant in hydrothermal electrolysis and it is a benefit to remove hazardous end or by-products during the wastewater treatment. Therefore, this hybrid hydrothermal electrolysis system (HES) can be considered as an environmentally benign and greener solution for the degradation of organic contaminants in wastewater.

10.1.3. Initial DBU Concentration Effect

DBU removal and TOC conversions were investigated depending on the initial concentration of DBU (3, 6 and 12 mM) and the results are represented in Figure 10. 9.

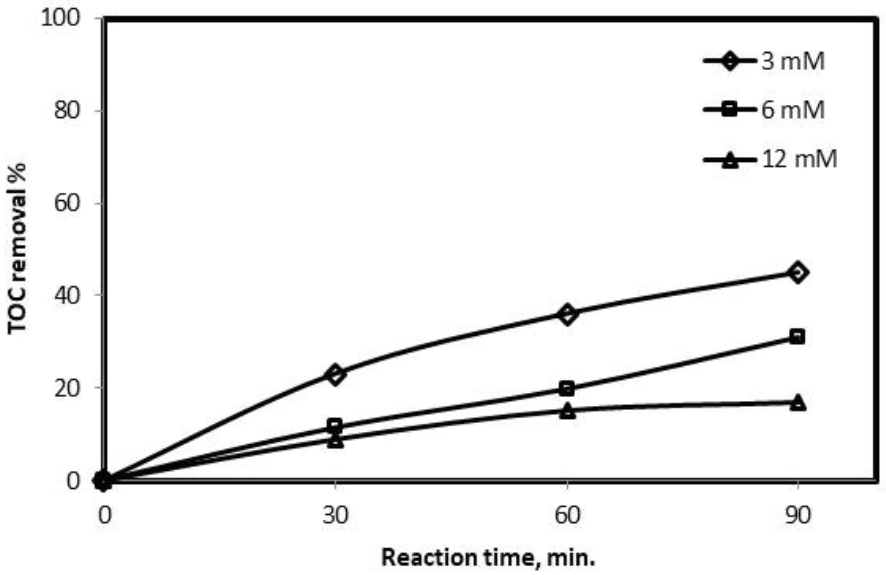

Figure 10.9. Initial DBU concentration effect on TOC conversion (Reaction conditions: C_{NaOH}= 0.01 mM, current density=0.0027 mA/cm^2, T=240 °C)

The highest DBU removal and TOC conversion were obtained as 91.2% and 45% at the lowest initial DBU concentration during the all reaction durations. At 90 minutes of reaction duration, approximately same DBU removal was achieved for 6 and 12 mM of initial DBU concentration.

10.1.4. GC-MS Analysis

The major compounds that form throughout the hydrothermal and hydrothermal electrolysis of DBU under subcritical conditions at the following reaction conditions: 240 °C of reaction temperature, 0.1 and 0.5 M of NaOH concentration, 0 mA/cm^2 and 0.0027 mA/cm^2 of current density and 30, 60 and 90 minutes of reaction duration were defined via GC-MS analysis. Whereas the main products of hydrothermal treatment of DBU were identified as methylcaprolactam, 1-methyl-2 phenyl indole, caprolactam, 4-amino-3-methylphenol, nitrobenzene and toluene, main compounds of hydrothermal electrolysis of DBU were identified as 1-methyl-2 phenyl indole, caprolactam, 4-amino-3-methylphenol, N-methylcaprolactam. The main compounds of hydrothermal and hydrothermal electrolysis of DBU under subcritical conditions were listed with their retention times in Table 10. 8.

Table 10.8. GC–MS results for main compounds of hydrothermal electrolysis of DBU (current density: 0.0027 mA/cm^2, T: 240 °C, C_{DBU}: 6 mM, C_{NaOH}: 0.01 M, t: 60 min)

Retention time, min.	Compounds
4.04	1-methyl-2-phenylindole
15.71	Caprolactam
20.62	4-amino-3-methylphenol
24.72	N-Methylcaprolactam

Nitrobenzene (2.27 min. of retention time) and toluene (3.17 min. of retention time), which are the products of hydrothermal treatment of DBU, have severe hazards on aquatic life and human health (Holder 1999; Kim et al., 2019). Yet, they were eliminated by applying current. Additionally, the main products of hydrothermal electrolysis of DBU do not have any hazardous impact on human and environmental health. As a result, the hazardous end products can be eliminated by hydrothermal electrolysis so that it is a greener approach for wastewater treatment and stable and hazardous compounds in various wastewaters could be degraded by this method.

10.1.5. Reaction Temperature Effect

Reaction temperature is another important parameter for DBU removal and TOC conversion and thus, the experiments were carried out different reaction temperatures (200, 240 and 280 °C) to investigate the impact of this parameter and the results are given in Figure 10. 10.

TOC conversion enhanced with respect to the increase in reaction temperature and duration. Although DBU removal was approximately same for all reaction conditions at 200 °C, a slight increase in DBU removal was observed at 240 and 280 °C of reaction temperature applying current density (0.027 mA/cm^2).

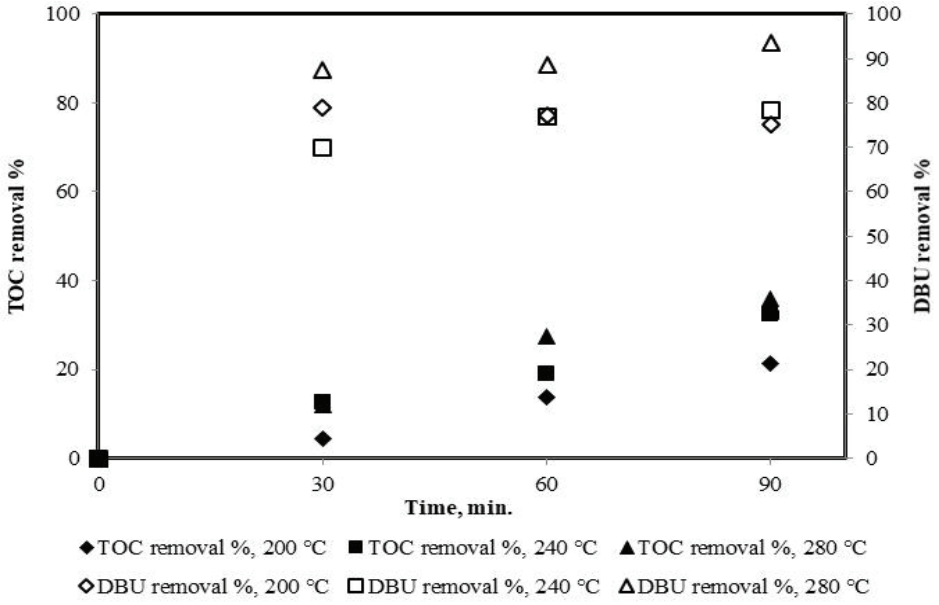

Figure 10.10. Temperature effect on TOC and DBU removal % (Reaction conditions: C_{DBU}= 6 mM, C_{NaOH}= 0.01 M, current density = 0.0027 mA/cm^2)

In order to define the reaction kinetic model and rate constants for TOC conversion, 1st and 2nd order reaction kinetic models were applied and it follows observed 1st order reaction kinetic model. The R^2 values and reaction rate constants at different reaction temperatures for the 1st order model for TOC conversion is listed in Table 10. 9. The linearized first order kinetic data is given in Figure 10. 11.

Table 10.9. Calculated values of R^2 and rate constants for the first order reaction model

Temperature, °C	R^2, First Order	First order kinetic rate constant, min^{-1}
200	0.97	0.0025
240	0.98	0.0041
280	0.99	0.005

The1st order reaction rate constants for TOC conversion at 200, 240 and 280 °C of reaction temperature was found as 0.0025, 0.0041 and 0.005 min^{-1}, respectively. As expected, as the reaction temperature rise, the reaction rate constants increased. The

Arrhenius plot of lnk versus 1/T was given in Figure 10.12. The activation energy for this observed reaction was calculated by Arrhenius equation and it was found as 79.86 kJ/mol.

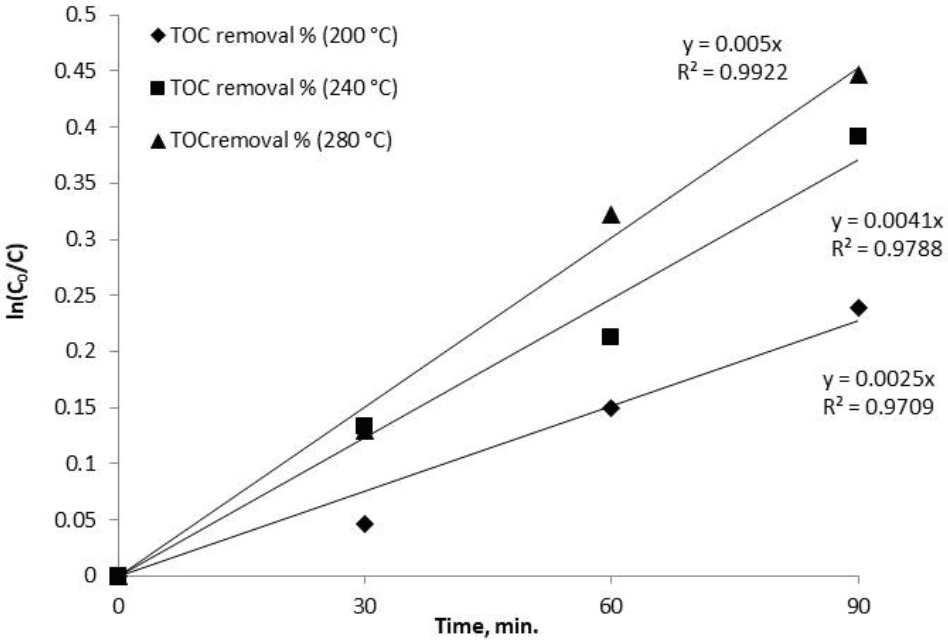

Figure 10.11. Linearized first order kinetic plot

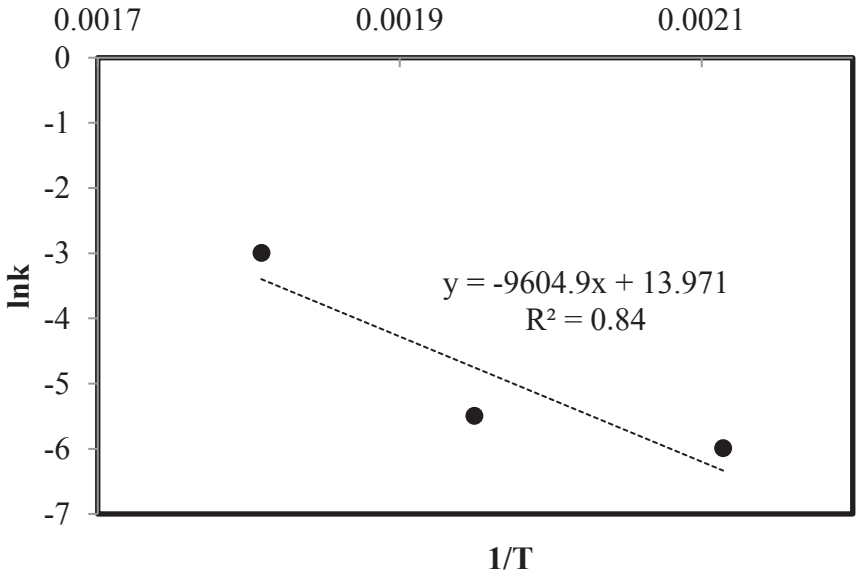

Figure 10.12. lnk vs 1/T

CHAPTER 11

CONCLUSION

In this thesis, perovskite (LFO, BFO and LRO) and hybrid (GLFO, GBFO and GLRO) were synthesized and their characterization study comprises SEM-EDX, BET, XRD, FT-IR, PL, TEM and XPS analyzes was carried out. SEM-EDX analysis showed that all of them had porous structure and incorporation of graphene did not cause any change in perovskite structure. BET analysis results show that GLRO had the highest BET area while BFO had the lowest. Incorporation of graphene cause an enhancement in the BET areas of hybrid catalysts compared to perovskite catalysts. Additionally, they were mesoporous. XRD results prove that all synthesized catalysts had orthorhombic structure. FT-IR analysis showed that Fe-O and O-Fe-O bonds that are characteristic bonds of FeO_6 structure in perovskite catalysts formed. PL analysis showed that incorporation of graphene caused a decrease in the intensities of peaks and thus hybrid catalysts could show better photocatalytic activity than perovskite catalysts. Besides, addition of graphene caused a small shift in peaks compared to perovskite catalysts and it implies that the hybrid catalysts needed lower photon energy for photocatalytic hydrogen production. Based on PL results, it could be concluded that the most promising solar-driven photocatalyst is GLFO. Incorporation of graphene brought about a shift in binding energies of La3d5, Fe2p and O1s based on XPS results and hence, it pointed out that there was an electronic interaction between LFO crystals and graphene. Therefore, it could be concluded that graphene supported LFO was successfully synthesized. TEM image of GLFO showed that LFO was covered with a graphene layer. The incorporation of graphene did not occur any change in perovskite structure. Moreover, XRD results supported the TEM results. Therefore, the introduction of graphene was successfully accomplished. SAED patterns prove their poly-crystallinity characteristics. Besides, these patterns confirmed that the orthorhombic structure of LFO was successfully accomplished. Consequently, the result of analyses showed that all of them were successfully synthesized.

Firstly, the synthesized catalyst were used to produce hydrogen from distilled water at various reaction conditions and obtained hydrogen amounts were varied between

371 and 912 μmol/g_{cat}. Then, they were used for photocatalytic hydrogen production from SMS, real sugar beet wastewater and DBU model solution under stimulated solar light irradiation.

Then, all synthesized catalyst were used to produce hydrogen from SMS. In this context, firstly, effects of light, pH and catalyst loading over produced hydrogen amount from SMS were investigated. According to results of light effect experiments, usage of solar light caused considerable increase in the produced hydrogen amount. Hybrid catalysts showed higher catalytic efficiency than perovskite catalysts. Slightly higher hydrogen production amounts were obtained in the presence of LFO and GLFO with respect to other catalysts and PL results of these catalysts support the experimental results. Based on the results of catalyst loading effect experiments, increasing amount of catalyst loading for all catalysts caused a decrease in the produced hydrogen amounts. However, in all cases, hybrid catalysts showed higher photocatalytic activities in terms of produced hydrogen amounts than perovskite catalysts. It could be deduced that the supporting with graphene enhanced their photocatalytic activities. Additionally, it implies that introduction of graphene causes a decrease in the probability of recombination of electrons and holes while it enhances the efficiency of separation. According to results of pH effect experiments, all catalysts showed higher photocatalytic activity in acidic reaction media compared to pH of 7.5 since pH of 3 is lower than their pHzpc and hence their surfaces can charge below their pHzpc so that the evolved hydrogen amounts enhanced. Among them, LFO and GLFO showed a significant increase in the produced amount of hydrogen. As a result, LFO and GLFO were chosen as the most promising catalysts to produce hydrogen from SMS based on the experimental results as well as PL results.

Full Factorial Design (FFD) was used to build an experimental design via Minitab 2018 statistical analysis program to comprehend the effects of reaction parameters that are initial pH of SMS, catalyst loading, graphene content and $[H_2O_2]_0$ over the hydrogen evolution via photocatalytic oxidation using most promising catalysts (LFO and GLFO). Based on the results of FFD for SMS, addition of hydrogen peroxide led to an increase over produced hydrogen amount. Higher hydrogen amounts were observed in the presence of GLFO. The value of R^2 for this model is determined as 86.53 %. Based on ANOVA table, graphene had a major impact and among 2-way interactions, pH*$[H_2O_2]_0$

had an impact over the produced amount of hydrogen and hence they show a synergetic effect for hydrogen evolution via photocatalytic oxidation.

The calcination temperature is another important factor for photocatalytic hydrogen evolution so that the effect of it was investigated. The highest hydrogen evolution was achieved for 700 °C of calcination temperature. It could be attributed that the GLFO (calcined at 700 °C) has more crystalline structure and results of XRD analysis support this finding. Reusability of this catalyst was also investigated and based on results it conserved its ~94 of photocataltic activity for five cycles.

Then, the experiments for optimization of reaction conditions for SMS was performed using the hybrid catlaysts. In this context, a Box Behnken design was created by Minitab 18 software with six repeats at centre to optimize the reaction parameters which are pH, catalyst loading, and $[H_2O_2]_0$ for the photocatalytic hydrogen evolution from SMS using each of them. Based on the results of Box Behnken design for SMS, GLFO showed better photocatalytic activity. The obtained highest H_2 amount was 3520.35 $\mu mol/g_{cat}$ using this catalyst at the following reaction conditions: pH of 5.25, 7.5 mM of $[H_2O_2]_0$ and 0.15 g/L of catalyst loading.

After that, a kinetic study was performed for photocatalytic hydrogen evolution from SMS and it was described with observed second order kinetic model based on TOC removal %. Additionally, activation energy for this observed reaction was calculated as 27.25 kJ/mol.

After completing SMS experiments, the hydrogen production from real sugar beet wastewater was investigated. Firstly, the characterization of wastewater was performed via ICP-MS and HPLC analysis. The results show that each sugar beet wastewater has their own characteristic. In addition, this wastewater contains 22 ppm sucrose. Then, the same experimental matrix was used to search the effects of pH, catalyst loading and $[H_2O_2]_0$ over the produced hydrogen amounts from real sugar beet wastewater in the presence of all hybrid catalysts and the highest hydrogen production (7035 $\mu mol/g_{cat}$) was observed in the presence of GLFO. Methane production from SMS was not observed whereas methane production was observed in a few experiments which were carried out using real sugar beet wastewater. In all experiments, the production of CO and CO_2 from SMS and real sugar beet wastewater were observed. The produced amounts of these gases from real sugar beet wastewater was higher than the produced amounts of them from SMS since the real sugar beet wastewater contains different organic compounds as well as sucrose. After that, a kinetic study was performed and the hydrogen production from real

sugar beet wastewater were described with observed first order reaction based on TOC removal %. Additionally, activation energy for this observed reaction was calculated as 32 kJ/mol. Consequently, the organic compounds in wastewater can be used for the hydrogen production. Hence, the wastewater treatment and production of hydrogen can be achieved as concomitant.

Same experimental matrix was also used for photocatalytic hydrogen evolution from DBU model solution using all hybrid catalysts. The obtained hydrogen amounts from DBU solution were relatively lower compared to SMS and the highest produced hydrogen amount (3119 $\mu mol/g_{cat}$) was obtained using GBFO. The highest DBU removal % was found as 90.3 in the presence of GLFO. Based on the number of produced gases it could be said that the degradation DBU was lower and thus, it was also treated in HCW reactor system. In this context, FFD was built to search main and interaction impacts of NaOH concentration, current density and reaction duration. According to the results, NaOH concentration and current density have impact over DBU removal % via hydrothermal electrolysis. The experimental study for the effect of NaOH concentration show that only HCW usage is not enough for higher TOC conversions and DBU removal efficiencies in a shorter reaction duration so an electrolyte should be used. Based on the experiemental results of current density experiments, almost same TOC conversions were obtained applying current in a short reaction duration (30 min.) and in the absence of current for 90 minutes of reaction duration. Hence, TOC conversion could not accomplish in the absence of current.

The reaction was described by observed first order reaction kinetic model based on TOC removal %. The activation energy for this observed reaction was calculated as 79.86 kJ/mol. Based on GC-MS results, main products of hydrothermal electrolysis of DBU do not have any hazardous impact on human and environmental health. As a result, the hazardous end products can be eliminated by hydrothermal electrolysis so that it is a greener approach for wastewater treatment and stable and hazardous compounds in various wastewaters could be degraded by this method. Consequently, according to the results of GC-MS analysis, applying current could prevent the formation of hazardous intermediates.

REFERENCES

Acar, C.; Dincer, I.; Zamfirescu, C. A Review on Selected Heterogeneous Photocatalysts for Hydrogen Production. *Int. J. Hydrogen Energy*. 2014, 38, 1903–1920.

Acar, C.; Dincer, I. Impact Assessment and Efficiency Evaluation of Hydrogen Production Methods. *Int. J. Energy Res.* 2015, 39, 1757–1768.

Acar, C.; Dincer, I.; Naterer, G. F. Review of Photocatalytic Water-Splitting Methods for Sustainable Hydrogen Production. *Int. J. Hydrogen Energy.* 2016, 40, 1449–1473.

Acharya S.; Padhi D. K.; Parida K. M. Visible Light Driven $LaFeO_3$ Nano Sphere/RGO Composite Photocatalysts for Efficient Water Decomposition Reaction. *Catal. Today.* 2017, 353, 220-231.

Afifah, N.; Saleh, Effect of Crystallite Structure and Graphene Incorporation on Photocatalytic Performance of $LaFeO_3$. R. *IOP Conf Ser: Mater. Sci. Eng.* 2017, 202, 012063.

Ahmad, H.; Kamarudin, S. K.; Minggu, L. J.; Kassim, M. Hydrogen from Photo-catalytic Water Splitting Process: A Review. *Renew. Sustain. Energy Rev.* 2015, 43, 599-610.

Akal, D.; Öztuna, S.; Büyükakın, M. K. A Review of Hydrogen Usage in Internal Combustion Engines (gasoline-Lpg-diesel) from Combustion Performance Aspect. *Int. J. Hydrog. Energy.* 2020, 45, 35257-35268.

Akın, O.; Yuksel, A. Novel Hybrid Process for the Conversion of Microcrystalline Cellulose to Value-added Chemicals: Part 1: Process Optimization. *Cellulose.* 2016, 23, 3475–3493.

Akkerman, I.; Janssen, M.; Rocha, J.; Wijffels, R. H. Photobiological Hydrogen Production: Photochemical Efficiency and Bioreactor Design. *Int. J. Hydrogen Energy.* 2002, 27, 1195–1208.

Al-Azri, Z. H. N.; Chen, W. T.; Chan, A.; Jovic, V.; Ina, T.; Idriss, H.; Waterhouse, G. I. N. The Roles of Metal Co-catalysts and Reaction Media in Photocatalytic Hydrogen Production: Performance Evaluation of M/TiO_2 Photocatalysts (M=Pd, Pt, Au) in Different Alcohol–Water Mixtures. *J. Catal.* 2015, 329, 355–367.

Al-Duri, B.; Alsoqyiani, F. Supercritical Water Oxidation (SCWO) for the Removal Of Nitrogen Containing Heterocyclic Waste Hydrocarbons. Part II: System Kinetics. *J. Supercrit. Fluid*s. 2017, 128, 412–418.

Al-Duri, B.; Alsoqyiani, F.; Kings, I. Supercritical Water Oxidation (SCWO) for the Removal of N-containing Heterocyclic Hydrocarbon Wastes. Part I: Process

Enhancement by Addition of Isopropyl Alcohol. *J. Supercrit. Fluids*. 2016, 116, 155–163.

Al-Duri, B.; Pinto, L.; Ashraf-Ball, N. H.; Santos, R. C. D. Thermal Abatement of Nitrogen-containing Hydrocarbons by Non-catalytic Supercritical Water Oxidation (SCWO). *J. Mater. Sci.* 2008, 43, 1421–1428.

Alkaya, E.; Demirer, G. N. Anaerobic Acidification of Sugar-beet Processing Wastes: Effect of Operational Parameters. *Biomass Bioenerg.* 2011a, 35, 32-39.

Alkaya, E.; Demirer, G. N. Anaerobic Mesophilic Co-Digestion of Sugar-beet Processing Wastewater and Beet-pulp in Batch Reactors. *Renew. Energy.* 2011b, 36, 971-975.

Almohammed, F.; Mhemdi, H.; Vorobiev, E. Pulsed Electric Field Treatment of Sugar Beet Tails as a Sustainable Feedstock for Bioethanol Production. *Appl. Energy.* 2016, 162, 49–57.

Ameta, R.; Ameta, S. C. Photocatalysis. Photocatalysis Principles and Applications; *CRC Press, Taylor & Francis Group*. 2017, 9-12.

Babu, G; Aparna, P; Satishkumar, G; Ashokkumar, M; Neppolian, B. Ultrasound-assisted Mineralization of Organic Contaminants using a Recyclable $LaFeO_3$ and Fe^{3+}/persulfate Fenton-like System. *Ultrason. Sonochem.* 2017, 34, 924-930.

Badawy, M. I.; Ali, M. E. M.; Ghaly, M. Y.; El-Missiry, M. A. Mesoporous Simonkolleite-TiO_2 Nanostructured Composite for Simultaneous Photocatalytic Hydrogen Production and Dye Decontamination. *Process Saf. Environ. Prot.* 2015, 94, 11–17.

Badawy, M. I.; Ghaly, M. Y.; Ali, M. E. M. Photocatalytic Hydrogen Production over Nanostructured Mesoporous Titania from Olive Mill Wastewater. *Desalination.* 2011, 267, 250–255.

Bahari, N. A.; Isahak, W. N. R. W.; Masdar, M. S.; Yaakob, Z. Clean Hydrogen Generation and Storage Strategies via CO_2 Utilization into Chemicals and Fuels: A Review. *Int. J. Energy Res.* 2019, 43, 5128–5150.

Baniasadi, E.; Dincer, I.; Naterer, G. F. Performance Analysis of a Water Splitting Reactor with Hybrid Photochemical Conversion of Solar Energy. *Int. J. Hydrogen Energy.* 2012, 37, 7464–7472.

Bednarczyk, K.; Stelmachowski, M.; Gmurek, M. The Influence of Process Parameters on Photocatalytic Hydrogen Production. *Environ. Prog. Sustain.* 2019, 38, 680-687.

Bellido, C.; Infante, C.; Coca, M.; González-Benito, G.; García-Cubero, M. T. Efficient Acetone-Butanol-Ethanol Production by *Clostridium beijerinckii* from Sugar Beet Pulp. *Bioresour. Technol.* 2015, 190, 332-338.

Bouchareb, E. M.; Kerroum, D.; Arikan, E. B.; Isik, Z.; Dizge, N. Production of Bio-hydrogen from Bulgur Processing Industry Wastewater. *Energ. Source. Part A*. 2021, 0, 1-14.

Chang, C. J.; Chu, K. W.; Hsu, M. H.; Chen, C. Y. Ni-doped ZnS Decorated Graphene Composites with Enhanced Photocatalytic Hydrogen-production Performance. *Int. J. Hydrogen Energy.* 2015, 40, 14498-14506.

Chen X.; Mao, S. S. Titanium Dioxide Nanomaterials: Synthesis, Properties, Modifications, and Applications. *Chem. Rev.* 2007, 107, 2891-2959.

Chen, S.; Qi, Y.; Ding, Q.; Li, Z.; Cui, J.; Zhang, F.; Li, C. Magnesia Interface Nanolayer Modification of Pt/Ta_3N_5 for Promoted Photocatalytic Hydrogen Production under Visible Light Irradiation. *J. Catal.* 2016a, 339, 77–83.

Chen, W.; He, Z-C.; Huang, G-B.; Wu, C-L.; Chen, W-F.; Liu, X-H. Direct Z-scheme 2D/2D $MnIn_2S_4$/g-C_3N_4 Architectures with Highly Efficient Photocatalytic Activities Towards Treatment of Pharmaceutical Wastewater and Hydrogen Evolution. *Chem. Eng. J.* 2019, 359, 244-253.

Chen, W.; Jovic, V.; Sun-Waterhouse, D.; Idriss, H.; Waterhouse, G. I. N. The Role of CuO in Promoting Photocatalytic Hydrogen Production over TiO_2. *Int. J. Hydrogen Energy.* 2013, 38, 15036–15048.

Chen, X.; Shen, S.; Guo, L.; Mao, S. S. Semiconductor-based Photocatalytic Hydrogen Generation. *Chem. Rev.* 2010, 110, 6503–6570.

Chen, Y.; Zhao, S.; Wang, X.; Peng, Q.; Lin, R.; Wang, Y.; Shen, R.; Cao, X.; Zhang, L.; Zhou, G.; Li, J.; Xia, A.; Li, Y. Synergetic Integration of $Cu_{1.94}S$–$Zn_xCd_{1-x}S$ Heteronanorods for Enhanced Visible-light-driven Photocatalytic Hydrogen Production. *J. Am. Chem. Soc*. 2016b, 138, 4286–4289.

Cheng, P.; Yang, Z.; Wang, H.; Cheng, W.; Chen, M.; Shangguan, W.; Ding G. TiO_2-Graphene Nanocomposites for Photocatalytic Hydrogen Production from Splitting Water. *Int. J. Hydrogen Energy.* 2012, 37, 2224-2230.

Chiarello, G. L.; Dozzi, M. V.; Selli E. TiO_2-based Materials for Photocatalytic Hydrogen Production. *J. Energy Chem.* 2017, 26, 250–258.

Cho, Y-G.; Choi, K-Y.; Kim, Y-R.; Jung, J-S.; Lee, S-H. Characterization and Catalytic Properties of Surface La-rich $LaFeO_3$ Perovskite. *Bull. Korean Chem. Soc.* 2009, 30, 1368-1372.

Czernik, S.; Evans, R.; French, R. Hydrogen from Biomass-production by Steam Reforming of Biomass Pyrolysis Oil. *Catal. Today.* 2007, 129, 265–268.

Dai, Q.; Lei, L.; Zhang, X. Enhanced Degradation of Organic Wastewater Containing p-nitrophenol by a Novel Wet Electrocatalytic Oxidation Process: Parameter Optimization and Degradation Mechanism. *Sep. Purif. Technol.* 2008, 61, 123−129.

Das, D.; Veziroglu, T. N. Advances in Biological Hydrogen Production Processes. *Int. J. Hydrogen Energy.* 2008, 33, 6046–6057.

Demirel, B.; Scherer, P. Production of Methane from Sugar Beet Silage without Manure Addition by a Single-Stage Anaerobic Digestion Process. *Biomass Bioenerg.* 2008, 32, 203–209.

Dhar, B. R.; Elbeshbishy, E.; Hafez, H.; Lee, H-S. Hydrogen Production from Sugar Beet Juice using an Integrated Biohydrogen Process of Dark Fermentation and Microbial Electrolysis Cell. *Bioresour. Technol.* 2015, 198, 223-30.

Dincer, I.; Acar, C. Review and Evaluation of Hydrogen Production Methods for Better Sustainability. *Int. J. Hydrog. Energy.* 2015, 40, 11094-11111.

Dionysio, D. D.; Suidan, M. T.; Baudin, I.; Laîné, J.-M. Effect of Hydrogen Peroxide on the Destruction of Organic Contaminants-synergism and Inhibition in a Continuous-Mode Photocatalytic Reactor. *Appl. Catal. B.* 2004, 50, 259–269.

Dong, M.; Zhou, P.; Jiang, C.; Cheng, B.; Yu, J. First-principles Investigation of Cu-doped ZnS with Enhanced Photocatalytic Hydrogen Production Activity. *Chem. Phys. Lett.* 2017, 668, 1-6.

Dükkancı, M. Degradation of Bisphenol-A using a Sonophoto Fenton-like Hybrid Process over a $LaFeO_3$ Perovskite Catalyst and a Comparison of its Activity with that of a TiO_2 Photocatalyst. *Turk. J. Chem.* 2016, 40, 784-801.

El-Bery, H. M.; Matsushita, Y.; Abdel-moneim, A. Fabrication of Efficient TiO_2-RGO Heterojunction Composites for Hydrogen Generation via Water-splitting: Comparison between RGO, Au and Pt Reduction Sites. *Appl. Surf. Sci.* 2017, 423, 185–196.

Enzweiler, H.; Yassue-Cordeiro, P. H.; Schwaab, M.; Barbosa-Coutinho, E.; Scaliante, M. H. N. O.; Fernandes, N. R. C. Catalyst Concentration, Ethanol Content and Initial pH Effects on Hydrogen Production by Photocatalytic Water Splitting. *J. Photochem. Photobiol. A.* 2020, 388, 112051-112058.

Estahbanati, M. R. K.; Mahinpey, N.; Feilizadeh, M.; Attar, F.; Iliuta, M. C. Kinetic Study of the Effects of pH on the Photocatalytic Hydrogen Production from Alcohols. *Int. J. Hydrog. Energy.* 2019, 44, 32030-32041.

Fan, X.; Fan, J.; Hu, X.; Liu, E.; Kang, L.; Tang, C.; Ma, Y.; Wu, H.; Li, Y. Preparation and Characterization of Ag Deposited and Fe doped TiO_2 Nanotube Arrays for Photocatalytic Hydrogen Production by Water Splitting. *Ceram. Int.* 2014, 40, 15907–15917.

Feng, J.; Liu, T.; Xu, Y.; Zhao, J.; He, Y. Effects of PVA Content on the Synthesis of $LaFeO_3$ via Sol-gel Route. *Ceram. Int.* 2011, 37, 1203-1207.

Feng, Q; Zhou, J; Luo, W; Ding, L; Cai, W. Photo-Fenton Removal of Tetracycline Hydrochloride using $LaFeO_3$ as a Persulfate Activator under Visible Light. *Ecotoxicol. Environ. Saf.* 2020, 198, 110661.

Gao, H.; Zhang, P.; Zhao, J. Y.; Zhang, Y.; Zhang, Y.; Hu, J.; Shao, G. Plasmon Enhancement on Photocatalytic Hydrogen Production over the Z-scheme Photosynthetic Heterojunction System. *Appl. Catal. B.* 2017, 210, 297–305.

Gao, P.; Li, N.; Wang, A.; Wang, X.; Zhang, T. Perovskite $LaMnO_3$ Hollow Nanospheres: The Synthesis and the Application in Catalytic Wet Air Oxidation of Phenol. *Mater. Lett.* 2013, 92, 173–176.

Ghaly, M. Y.; Farah, J. Y.; Fathy, A. M. Enhancement of Decolorization Rate and COD Removal from Dyes Containing Wastewater by the Addition of Hydrogen Peroxide under Solar Photocatalytic Oxidation. *Desalination.* 2007, 217, 74-84.

Guan, Y. F.; Deng, M. C.; Yu, X. J.; Zhang, W. Two-stage Photo-biological Production of Hydrogen by Marine Green Alga Platymonas Subcordiformis. *Biochem. Eng. J.* 2004, 19, 69–73.

Guerra, M.; López, M. A.; Estéves, I.; Zubillaga, A. L.; Cróque, A. Fourier-Transformed Infrared Spectroscopy: A Tool to Identify Gross Chemical Changes from Healthy to Yellow Band Disease Tissues. Dis. *Aquat. Organ.* 2014, 107, 249-258.

Guo, S.; Zhang, G.; Guo, Y.; Yu, J. C. Graphene Oxide–Fe_2O_3 Hybrid Material as Highly Efficient Heterogeneous Catalyst for Degradation of Organic Contaminants. *Carbon.* 2013, 60, 437–44.

Güven, G.; Perendeci, A.; Tanyolac, A. Electrochemical Treatment of Simulated Beet Sugar Factory Wastewater. *Chem. Eng. J.* 2009, 151, 149–159.

Hao, P.; Lin, Z.; Song, P.; Yang, Z. Wang, Q. rGO-wrapped Porous $LaFeO_3$ Microspheres for High-performance Triethylamine Gas Sensors. *Ceram. Int.* 2020, 46, 9363–9369.

Hippargi, G.; Anjankar, S.; Krupadam, R. J.; Rayalu, S. S. Simultaneous Wastewater Treatment and Generation of blended Fuel Methane and Hydrogen using Au-Pt/TiO_2 Photo-reforming Catalytic Material. *Fuel.* 2021, 291, 120113-120124.

Hisatomi, T.; Kubota, J.; Domen, K. Recent Advances in Semiconductors for Photocatalytic and Photoelectrochemical Water Splitting. *Chem. Soc. Rev.* 2014, 43, 7520-7535.

Holder, J. W. Nitrobenzene Carcinogenicity in Animals and Human Hazard Evaluation. *Toxicol. Ind. Health.* 1999, 15, 445−457.

Holladay, J.D.; Hu, J.; King, D. L.; Wang Y. An Overview of Hydrogen Production Technologies. *Catal. Today.* 2009, 139, 244–260.

Hongfang, S. H.; Xue, T.; Wang, Y.; Cao, G.; Lu, Y.; Fang, G. Photocatalytic Property of Perovskite $LaFeO_3$ Synthesized by Sol-gel Process and Vacuum Microwave Calcination. *Mater. Res. Bull.* 2016. 84, 15-24.

Hosseini, S. E.; Wahid, M. A. Hydrogen from Solar Energy, a Clean Energy Carrier from a Sustainable Source of Energy. *Int. J. Energy Res.* 2020, 44, 4110–4131.

Hou, K. H.; Hughes, R. The Kinetics of Methane Steam Reforming over a Ni/alpha-Al_2O Catalyst. *Chem. Eng. J.* 2001, 82, 311–328.

Hu, J.; Men, J.; Ma, J.; Huang, H. Preparation of $LaMnO_3$/graphene Thin Films and their Photocatalytic Activity. *J. Rare Earths.* 2014, 32, 1126-1134.

Hussain, T.; Siddiqi, S. A.; Atiq, S.; Awan, M. S. Induced Modifications in the Properties of Sr Doped $BiFeO_3$ Multiferroics. *Prog. Nat. Sci.-Mater.* 2013, 23, 487–492.

Hussy, I.; Hawkes, F. R.; Dinsdale, R.; Hawkes, D. L. Continuous Fermentative Hydrogen Production from Sucrose and Sugarbeet. *Int. J. Hydrogen Energy.* 2005, 30, 471 – 483.

Iervolino, G.; Vaiano, V.; Sannino, D.; Rizzo, L.; Ciambelli, P. Production of Hydrogen from Glucose by $LaFeO_3$ Based Photocatalytic Process during Water Treatment. *Int. J. Hydrogen Energy.* 2016, 41, 959-966.

Iervolino, G.; Vaiano, V.; Sannino, D.; Rizzo, L.; Palma V. Enhanced Photocatalytic Hydrogen Production from Glucose Aqueous Matrices on Ru-doped $LaFeO_3$. *Appl. Catal. B.* 2017, 207, 182–194.

Jana, P.; Montero, C. M.; Pizarro P.; Coronado, J. M.; Serrano, D. P.; de la Peña O'Shea, V. A. Photocatalytic Hydrogen Production in the Water/Methanol System using Pt/RE:$NaTaO_3$ (RE = Y, La, Ce, Yb) Catalysts. *Int. J. Hydrogen Energy.* 2014, 39, 5283-5290.

Jang, J. S.; Borse, P. H.; Lee, J. S.; Lim, K. T.; Jung, O.-S.; Jeong, E. D.; Bae, J. S.; Kim, H. G. Photocatalytic Hydrogen Production in Water-Methanol Mixture over Iron-doped $CaTiO_3$. *Bull. Korean Chem. Soc.* 2011, 32, 95-99.

Jia, G.; Wang, Y.; Cui, X.; Zheng, W. Highly Carbon-doped TiO_2 Derived from MXene Boosting the Photocatalytic Hydrogen Evolution. *ACS Sustain. Chem. Eng.* 2018, 6, 13480–13486.

Jiang, D.; Sun, Z.; Jia, H.; Lu, D.; Du, P. A cocatalyst-free CdS nanorod/ZnS Nanoparticle Composite for High-performance Visible-light-driven Hydrogen Production from Water. *J. Mater. Chem. A.* 2016, 4, 675–683.

Kalyani, R.; Gurunathan, K. Metal Ions Doped and Polythiophene Coated Nanophotocatalysts: Synthesis and Spectroscopic Characterization for H_2 Production and Dye Degradation. *Optik.* 2016, 127, 4741-4745.

Kars, G.; Alparslan, Ü. Valorization of Sugar Beet Molasses for the Production of Biohydrogen and 5-aminolevulinic Acid by *Rhodobacter sphaeroides* O.U.001 in a Biorefinery Concept. *Int. J. Hydrogen Energy.* 2013, 38, 14488-14494.

Keskin, T.; Hallenbeck, P. C. Hydrogen Production from Sugar Industry Wastes using Single-stage Photofermentation. *Bioresour. Technol.* 2012, 112, 131–136.

Khan, R.; Mehran, M. T.; Naqvi, S. R.; Khoja, A. H.; Mahmood, K.; Shahzad, F.; Hussain, S. Role of Perovskites as a Bi-functional Catalyst for Electrochemical Water Splitting: A Review. *Int. J. Energy Res.* 2020, 44, 9714–9747.

Kiani, M.; Rizwan, S.; Irfan, S. Facile Synthesis of a $BiFeO_3$/Nitrogen-doped Graphene Nanocomposite System with Enhanced Photocatalytic Activity. *J. Phys. Chem. Solids.* 2018, 121, 8–16.

Kidambi, P. R.; Bayer, B. C.; Blume, R.; Wang, Z.; Baehtz, C.; Weatherup, R. S.; Willinger, M.; Schloeg, R.; Hofmann, S. Observing Graphene Grow: Catalyst-Graphene Interactions during Scalable Graphene Growth on Polycrystalline Copper. *Nano Lett.* 2013, 13, 4769-4778.

Kim, K.-H.; Szulejko, J. E.; Raza, N.; Kumar, V.; Vikrant, K.; Tsang, D. C. W.; Bolan, N. S.; Ok, Y. S.; Khan, A. Identifying the Best Materials for the Removal of Airborne Toluene Based on Performance Metrics - A Critical Review. *J. Clean. Prod.* 2019, 241, 118408.

Klare, M.; Scheen, J.; Vogelsang, K.; Jacobs, H.; Broekaert, J.A.C. Degradation of Short-Chain Alkyl- and Alkanolamines by TiO_2- and Pt/TiO_2-assisted Photocatalysis. *Chemosphere.* 2000, 41, 353-362.

Kuang, L.; Zhang, W. Enhanced Hydrogen Production by Carbon-doped TiO_2 Decorated with Reduced Graphene Oxide (rGO) under Visible Light Irradiation. *RSC Adv.* 2016, 3, 2479-2488.

Kucharczyk, B.; Okal, J.; Tylus, W.; Winiarski, J.; Szczygieł, B. The effect of the calcination temperature of $LaFeO_3$ precursors on the properties and catalytic activity of perovskite in methane oxidation. *Ceram. Int.* 2019, 45, 2779-2788.

Lee, H.; Park, Y.; Kang, M. Synthesis of characterization of Zn_xTi_yS and its photocatalytic activity for hydrogen production from methanol/water photo-splitting. *J. Ind. Eng. Chem.* 2013, 19, 1162–1168.

Lee, W-Y.; Yun, H. J.; Yoon, J-W. Characterization and Magnetic Properties of $LaFeO_3$ Nanofibers Synthesized by Electrospinning. *J. Alloys Compd.* 2014, 583, 320-324.

Levchuk, I.; Sillanpää, M. Titanium Dioxide-based Nanomaterials for Photocatalytic Water Treatment. Advanced Water Treatment Advanced Oxidation Processes; *Sillanpää, M., Eds.; Elsevier,* 2020, 8-14.

Li, J.; Pan, X.; Xu, Y.; Jia, L.; Yi, X.; Fang, W. Synergetic Effect of Copper Species as Cocatalyst on $LaFeO_3$ for Enhanced Visible-light Photocatalytic Hydrogen Evolution. *Int. J. Hydrogen Energy*. 2015, 40, 13918-13925.

Li, R.; Li, C. Photocatalytic Water Splitting on Semiconductor-Based Photocatalysts. *Adv. Catal.* 2017, 40, 1-57.

Li, X.; Yu, J.; Low, J.; Fang, Y.; Xiao, J.; Chen, X. Engineering Heterogeneous Semiconductors for Solar Water Splitting. *J. Mater. Chem. A.* 2015, 3, 2485–2534.

Li, Y.; Gu, G.; Zhao, J.; Yu, H. Anoxic Degradation of Nitrogenous Heterocyclic Compounds by Acclimated Activated Sludge. *Process Biochem.* 2001, 37, 81-86.

Liao, C-H.; Huang, C-W.; Wu, J. C. S. Hydrogen Production from Semiconductor-based Photocatalysis via Water Splitting. *Catalysts.* 2012, 2, 490-516.

Lin, K-H.; Wang, C-B.; Chien, S-H. Catalytic Performance of Steam Reforming of Ethanol at Low Temperature over $LaNiO_3$ Perovskite. *Int. J. Hydrogen Energy.* 2013, 38, 3226-3232.

Liu, Q.; Yang, C.; Dong, X.; Chen, F. Perovskite $Sr_2Fe_{1.5}Mo_{0.5}O_{6-\delta}$ as Electrode Materials for Symmetrical Solid Oxide Electrolysis Cells. *Int. J. Hydrogen Energy*. 2010, 35, 10039-10044.

Liu, S. Q.; Xiao, B.; Feng, L. R.; Zhou, S. S.; Chen, Z. G.; Liu, C. B.; Chen, F.; Wu, Z. Y.; Xu, N.; Oh, W. C.; Meng, Z. D. Graphene Oxide Enhances the Fenton-like Photocatalytic Activity of Nickel Ferrite for Degradation of Dyes under Visible Light Irradiation. *Carbon.* 2013, 64, 197–206.

Lu, X.; Wang, G.; Xie, S.; Shi, J.; Li, W.; Tong, Y.; Li, Y. Efficient Photocatalytic Hydrogen Evolution over Hydrogenated ZnO Nanorod Arrays. *Chem. Commun.* 2012, 48, 7717.

Marone, A.; Ayala-Campos, O. R.; Trably, E.; Carmona-Martínez, A. A.; Moscoviz, R.; Latrille, E.; Steyer, J-P.; Alcaraz-Gonzalez, V.; Bernet, N. Coupling Dark Fermentation and Microbial Electrolysis to Enhance Biohydrogen Production from Agro-industrial Wastewaters and By-Products in a Bio-Refinery Framework. *Int. J. Hydrogen Energy*. 2017, 42, 1609-1621.

Martha, S.; Parida, K., M. Fabrication of Nano N-doped $In_2Ga_2ZnO_7$ for Photocatalytic Hydrogen Production under Visible Light. *Int. J. Hydrogen Energy.* 2012, 37, 17936-17946.

Mazloomi, K.; Gomes, C. Hydrogen as an Energy Carrier: Prospects and Challenges. *Renew. Sustain. Energy Rev.* 2012, 16, 3024-3033.

Midilli, A.; Ay, M.; Dincer, I.; Rosen, M. A. On Hydrogen and Hydrogen Energy Strategies I: Current Status and Needs. *Renew. Sustain. Energy Rev*. 2005, 9, 255–271.

Moreau, E.; Ferrer, F. J.; Vignaud, D.; Godey, S.; Wallart, X. Graphene Growth by Molecular Beam Epitaxy using a Solid Carbon Source. *Phys. Status Solidi A.* 2010, 207(2), 300-303.

Navarro, R. M.; Sánchez-Sánchez, M. C.; Alvarez-Galvan, M. C.; del Valle, F.; Fierro, J. L. G. Hydrogen Production from Renewable Sources: Biomass and Photocatalytic Opportunities. *Energy Environ. Sci.* 2009, 2, 35–54.

Nguyen, V.; Do, H. H.; Nguyen, T. V.; Singh, P.; Raizada, P.; Sharma, A.; Sana, S. S.; Grace, A. N.; Shokouhimehr, M.; Ahn, S. H.; Xia, C.; Kim, S. Y.; Le, Q. V. Perovskite Oxide-based Photocatalysts for Solar-driven Hydrogen Production: Progress and Perspectives. *Sol. Energy.* 2020, 211, 584–599.

Ni, M.; Leung, D. Y. C.; Leung, M. K. H., Sumathy, K. An Overview of Hydrogen Production from Biomass. *Fuel Process. Technol.* 2006, 87, 461–472.

Ni, M.; Leung, M. K. H.; Leung, D. Y. C.; Sumathy, K. A Review and Recent Developments in Photocatalytic Water-splitting using TiO_2 for Hydrogen Production. *Renew. Sustain. Energy Rev.* 2007, 11, 401–425.

Nikolaidis, P.; Poullikkas, A. A Comparative Overview of Hydrogen Production Processes. *Renew. Sustain. Energy Rev.* 2017, 67, 597-611.

Nowotny, J.; Sorrell, C. C.; Sheppard, L. R.; Bak, T. Solar-hydrogen: Environmentally Safe Fuel for the Future. *Int. J. Hydrogen Energy.* 2005, 30, 521–544.

Ochuma, I. J.; Fishwick, R. P.; Wood, J.; Winterbottom, J. M. Optimisation of Degradation Conditions of 1,8-diazabicyclo[5.4.0]undec-7-ene in Water and Reaction Kinetics Analysis using a Cocurrent Downflow Contactor Photocatalytic Reactor. *Appl. Catal. B-Environ.* 2007b, 73, 259–268.

Ochuma, I. J.; Osibo, O. O.; Fishwick, R. P.; Pollington, S.; Wagland, A.; Wood, J.; Winterbottom, J. M. Three-phase Photocatalysis using Suspended Titania and Titania Supported on a Reticulated Foam Monolith for Water Purification. *Catal. Today.* 2007a, 128, 100–107.

Ozkan, L.; Erguder, T. H.; Demirer, G. N. Investigation of the Effect of Culture Type on Biological Hydrogen Production from Sugar Industry Wastes. *Waste Manag.* 2010, 30, 792–798.

Pan, K.; Yang, C.; Hu, J.; Yang, W.; Liu, B.; Yang, J.; Liang, S.; Xiao, K.; Hou, H. Oxygen Vacancy Mediated Surface Charge Redistribution of Cu-substituted $LaFeO_3$ for Degradation of Bisphenol A by Efficient Decomposition of H_2O_2. *J. Hazar. Mater.* 2020, 389, 122072-122085.

Parida, K. M.; Reddy, K. H.; Martha, S.; Das, D. P.; Biswal, N. Fabrication of Nanocrystalline $LaFeO_3$: An Efficient Sol-gel Auto-combustion Assisted Visible Light Responsive Photocatalyst for Water Decomposition. *Int. J. Hydrogen Energy.* 2010, 35, 12161-12168.

Perez-Larios, A.; Lopez, R.; Hernandez-Gordillo, A.; Tzompantzi, F.; Gomez, R.; Torres-Guerra, L. M. Improved hydrogen production from water splitting using TiO_2–ZnO mixed oxides photocatalysts. *Fuel.* 2012, 100, 139–143.

Pietri, E.; Barrios, A.; Gonzalez, O.; Goldwasser, M. R.; Pérez-Zurita, M. J.; Cubeiro, M. L.; Goldwasser, J.; Leclercq, L.; Leclercq, G.; Gingembre, L. Perovskites as Catalysts Precursors for Methane Reforming: Ru Based Catalysts. *Stud. Surf. Sci. Catal.* 2001, 136, 381-386.

Pinto, L. D. S.; Freitas dos Santos, L. M.; Al-Duri, B.; Santos, R. C. D. Supercritical water oxidation of quinoline in a continuous plug flow reactor-part 1: effect of key operating parameters. *J. Chem. Technol. Biotechnol.* 2006, 81, 912–918.

Puangpetch, T.; Sommakettarin, P.; Chavadej, S.; Sreethawong, T. Hydrogen Production from Water Splitting over Eosin Y-sensitized Mesoporous-assembled Perovskite Titanate Nanocrystal Photocatalysts under Visible Light Irradiation. *Int. J. Hydrogen Energy.* 2010, 35, 12428-12442.

Puangpetch, T.; Sreethawong, T.; Yoshikawa, S.; Chavadej, S. Hydrogen Production from Photocatalytic Water Splitting over Mesoporous-assembled $SrTiO_3$ Nanocrystal-based Photocatalysts. *J. Mol. Catal. A Chem.* 2009, 312, 97–106.

Reddy, M. P.; Srinivas, B., Kumari, V. D.; Subrahmanyam, M.; Sharma, P. N. An Integrated Approach of Solar Photocatalytic and Biological Treatment of N-Containing Organic Compounds in Wastewater. *Toxicol. Environ. Chem.* 2004, 86, 127-140.

Ren, X.; Yang, H.; Gen, S.; Zhou, J.; Yang, T.; Zhang, X.; Cheng, Z.; Sun, S. Controlled Growth of $LaFeO_3$ Nanoparticles on Reduced Graphene Oxide for Highly Efficient Photocatalysis. *Nanoscale.* 2016, 8, 752-756.

Riaz, K. N.; Yousaf, N.; Tahir, M. B.; Israr, Z.; Iqbal, T. Facile Hydrothermal Synthesis of 3D Flower-like La-MoS_2 Nanostructure for Photocatalytic Hydrogen Energy Production. *Int. J. Energy Res.* 2019, 43, 491–499.

Rusevova, K.; Köferstein, R.; Rosell, M.; Richnow, H. H.; Kopinke. F. D.; Georgi, A. $LaFeO_3$ and $BiFeO_3$ Perovskites as Nanocatalysts for Contaminant Degradation in Heterogeneous Fenton-like Reactions. *Chem. Eng. J.* 2014, 239, 322-331.

Sadanandam, G.; Lalitha, K.; Kumari, V. D.; Shankar, M. V.; Subrahmanyam, M. Cobalt Doped TiO_2: a Stable and Efficient Photocatalyst for Continuous Hydrogen Production from Glycerol:Water Mixtures under Solar Light Irradiation. *Int. J. Hydrogen Energy.* 2013, 38, 9655–9664.

Safa, Y.; Bhatti, H. N. Kinetic and Thermodynamic Modeling for the Removal of Direct Red-31 and Direct Orange-26 Dyes from Aqueous Solutions by Rice Husk. *Desalination.* 2011, 272, 313-322.

Samran, B.; lunput, S.; Tonnonchiang, S.; Chaiwichian, S. $BiFeO_3/BiVO_4$ Nanocomposite Photocatalysts with Highly Enhanced Photocatalytic Activity for Rhodamine B Degradation under Visible Light Irradiation. *Physica B: Condens. Matter.* 2019, 561, 23–28.

Sanaeishoar, T.; Tavakkolia, H.; Mohave, F. A Facile and Eco-friendly Synthesis of Imidazo[1,2-a]pyridines using Nano-sized $LaMnO_3$ Perovskite-type Oxide as an Efficient Catalyst under Solvent-free Conditions. *Appl. Catal. Gen-A.* 2014, 470, 56-62.

Saravanan, R.; Gracia, F.; Stephen, A. Basic Principles, Mechanism, and Challenges of Photocatalysis. Springer Series on Polymer and Composite Materials; Khan, M. M., Pradhan, D., Sohn, Y., Eds.; *Springer International Publishing AG.* 2017, 22-29.

Sasaki, M.; Wahyudiono, Yuksel, A.; Goto, M. Applications of Hydrothermal Electrolysis for Conversion of 1-butanol in Wastewater Treatment. *Fuel Process. Technol.* 2010, 19, 1125-1132.

Sasaki, M.; Yamamoto, K.; Goto, M. Reaction Mechanism and Pathway for the Hydrothermal Electrolysis of Organic Compounds. *J. Mater. Cycles Waste.* 2007, 9, 40−46.

Sekar, K.; Kassam, A.; Bai, Y.; Coulson, B.; Li, W.; Douthwaite, R. E.; Sasaki, K.; Lee, A. F. Hierarchical Bismuth Vanadate/Reduced Graphene Oxide Composite Photocatalyst for Hydrogen Evolution and Bisphenol A Degradation. *Appl. Mater. Today.* 2021, 22, 100963- 100973.

Serikawa, R. M. Wet Electrolytic Oxidation of Organic Sludge. *J. Hazard. Mater.* 2007, 146, 646−651.

Shariq, M.; Kaur, D.; Chandel, V. S.; Siddiqui, M. S. Investigation on Multiferroic Properties of $BiFeO_3$ Ceramics. *Mater. Sci.-Poland.* 2013, 31, 471-475.

Sharma, L.; Prabhakar, S.; Tiwari, V.; Dhar, A.; Halder, A. Optimization of EC Parameters using Fe and Al Electrodes for Hydrogen Production and Wastewater Treatment. *Environ. Adv.* 2021, 3, 100029-100037.

Shriner, R. L.; Neumann, F. W. The Chemistry of the Amidines. *Chem. Rev.* 1944, 35, 351−425.

Silva, C. G.; Faria, J. L.; Photocatalytic Oxidation of Phenolic Compounds by using a Carbon Nanotube-Titanium Dioxide Composite Catalyst. *Chem. Sus. Chem.* 2010, 3, 609–618.

Speltini, A.; Romani, L.; Dondi, D.; Malasavi, L.; Profumo, A. Carbon Nitride-Perovskite Composites: Evaluation and Optimization of Photocatalytic Hydrogen Evolution in Saccharides Aqueous Solution. *Catalysts.* 2020, 10, 1259-1270.

Sprick, R. S.; Bonillo, B.; Clowes, R.; Guiglion, P.; Brownbill, N. J.; Slater, B. J.; Blanc, F.; Zwijnenburg, M. A.; Adams, D. J.; Cooper, A. I. Visible-light-driven Hydrogen Evolution using Planarized Conjugated Polymer Photocatalysts. *Angew. Chem*. Int. *Ed.* 2015, 55(5), 1792–1796.

Stegbauer, L.; Schwinghammer, K.; Lotsch, B. V. A Hydrazone-based Covalent Organic Framework for Photocatalytic Hydrogen Production. *Chem. Sci.* 2014, 5, 2789–2793.

Steinfeld, A. Solar Hydrogen Production via a Two Step Water-Splitting Thermochemical Cycle Based on Zn/ZnO Redox Reactions. *Int. J. Hydrogen Energy.* 2002, 27, 611–619.

Suhartini, S.; Heaven, S.; Banks, C. J. Comparison of Mesophilic and Thermophilic Anaerobic Digestion of Sugar Beet Pulp: Performance, Dewaterability and Foam Control. *Bioresour. Technol.* 2014, 152, 202–211.

Sun, C.; Sheng, T.; Li, L.; Yang, L. Biohydrogen Production from Traditional Chinese Medicine Wastewater in Anaerobic Packed Bed Reactor System. *RSC Adv.* 2021, 11, 5601–5608.

Sürer, M. G.; Arat, H. T. State of Art of Hydrogen Usage as a Fuel on Aviation. *Eur. Mech. Sci.* 2018, 2, 20-30.

Taherian, S.; Entezari, M. H.; Ghows, N. Sono-catalytic Degradation and Fast Mineralization of p-chlorophenol: $La_{0.7}Sr_{0.3}MnO_3$ as a Nano-Magnetic Green Catalyst. *Ultrason. Sonochem.* 2013, 20, 1419-1427.

Tahir, M. B.; Iqbal, T.; Kiran, H.; Hasan, A. Insighting Role of Reduced Graphene Oxide in $BiVO_4$ Nanoparticles for Improved Photocatalytic Hydrogen Evolution and Dyes Degradation. *Int. J Energy. Res.* 2019a, 43, 2410–2417.

Tahir, M. B.; Rafique, M.; Khan, M. S.; Majid, A.; Nazar, F.; Sagir, M.; Gilani, S.; Farooq, M.; Ahmed, A. Enhanced Photocatalytic Hydrogen Energy Production of g-C_3N_4-WO_3 Composites under Visible Light Irradiation. *Int. J. Energy Res.* 2018, 42, 4667–4673.

Tahir, M. B.; Riaz, K. N.; Asiri, A. M. Boosting the Performance of Visible Light-driven WO_3/g-C_3N_4 Anchored with $BiVO_4$ Nanoparticles for Photocatalytic Hydrogen Evolution. *Int. J. Energy Res.* 2019b, 43, 5747–5758.

Tejuca, L. G.; Fierro, J. L. G. Structure and Reactivity of Perovskite-type Oxides. *Adv. Catal.* 1989, 36, 237-328.

Tentu, R. D.; Basu, S. Photocatalytic Water Splitting for Hydrogen Production. *Curr. Opin. Electrochem.* 2017, 5, 56–62.

Thirumalairajan, S.; Girija, K.; Hebalkar, N. Y.; Mangalaraj, D.; Viswanathan, C.; Ponpandian, N. Shape Evolution of Perovskite $LaFeO_3$ Nanostructures: A Systematic Investigation of Growth Mechanism, Properties and Morphology Dependent Photocatalytic Activities. *RSC Adv.* 2013, 3, 7549-7561.

Tijare, S. N.; Joshi, M. V.; Padole, P. S.; Mangrulkar, P. A.; Rayalu, S. S.; Labhsetwar, N. K. Photocatalytic Hydrogen Generation Through Water Splitting on Nano-Crystalline $LaFeO_3$ Perovskite. *Int. J. Hydrogen Energy.* 2012, 37, 10451-10456.

Vaiano V.; Iervolino, G. Photocatalytic Removal of Methyl Orange Azo Dye with Simultaneous Hydrogen Production Using Ru-Modified ZnO Photocatalyst. *Catalysts.* 2019, 9, 964-974.

Villar-Rodil, S.; Paredes, J. I.; Martínez-Alonso, A.; Tascón, J. M. D. Preparation of Graphene Dispersions and Graphene-polymer Composites in Organic Media. *J. Mater. Chem.* 2009, 19, 3591-3593.

Viswanathan, B. Photocatalytic Processes – Selection Criteria for the Choice of Materials. *Bull. Catal. Soc. India.* 2003, 2, 71-74.

Wang, C.; Hu, Q.; Huang, J.; Deng, Z.; Shi, H.; Wu, L.; Liu, Z.; Cao, Y. Effective Water Splitting using N-doped TiO_2 Films: Role of Preferred Orientation on Hydrogen Production. *Int. J. Hydrogen Energy.* 2014, 39, 1967–1971.

Wang, L.; Pang, Q.; Song, Q.; Pan, X.; Jia, L. Novel Microbial Synthesis of Cu Doped $LaCoO_3$ Photocatalyst and Its High Efficient Hydrogen Production from Formaldehyde Solution under Visible Light Irradiation. *Fuel.* 2015, 140, 267–274.

Wang, X.; Hu, C.; An, H.; Zhu, D.; Zhong, Y.; Wang, D.; Tang, C.; Sun, L.; Zhou, H. Photocatalytic Removal of MB and Hydrogen Evolution in Water by $(Sr_{0.6}Bi_{0.3}0_5)_2Bi_2O_7/TiO_2$ Heterostructures under Visible-Light Irradiation. *Appl. Surf. Sci.* 2021, 544, 148920-148933.

Wen, J.; Li, X.; Li, H.; Ma, S.; He, K.; Xu, Y.; Fang, Y.; Liu, W.; Gao, Q. Enhanced Visible-light H_2 Evolution of g-C_3N_4 Photocatalysts via the Synergetic Effect of Amorphous NiS and Cheap Metal-Free Carbon Black Nanoparticles as Co-Catalysts. *Appl. Surf. Sci.* 2015, 358, 204–212.

Wu, Y.; Li, Y.; Hu, H.; Zheng, G.; Li, C. Recovering Hydrogen Energy from Photocatalytic Treatment of Pharmaceutical-Contaminated Water Using Co_3O_4 Modified {001}/{101}-TiO_2 Nanosheets. *ACS ES&T Eng.* 2021, 1, 603-611.

Wu, Y.; Wang, H.; Tu, W.; Liu, Y.; Tan, Y. Z.; Yuan, X.; Chew, J. W. Quasi-polymeric Construction of Stable Perovskite-type $LaFeO_3$/g-C_3N_4 Heterostructured Photocatalyst for Improved Z-scheme Photocatalytic Activity via Solid p-n Heterojunction Interfacial Effect. *J. Hazard. Mater.* 2018, 347, 412-422.

Xiao, P.; Zhong, L.; Zhu, J.; Hong, J.; Li, J.; Li, H.; Zhu, Y.; CO and Soot Oxidation over Macroporous Perovskite $LaFeO_3$. *Catal. Today.* 2015, 258, 660-667.

Xie, Q.; Wang, Y.; Pan, B.; Wang, H.; Su, W.; Wang X. A Novel Photocatalyst LaOF: Facile Fabrication and Photocatalytic Hydrogen Production. *Catal. Commun.* 2012, 27, 21–25.

Xu, Y.; Kraft, M.; Xu, R. Metal-free Carbonaceous Electrocatalysts and Photocatalysts for Water Splitting. *Chem. Soc. Rev.* 2016, 45(11), 3039–3052.

Xu, Y.; Shen, M. Structure and Optical Properties of Nanocrystalline $BiFeO_3$ Films Prepared by Chemical Solution Deposition. *Mater. Lett.* 2008, 62, 3600–3602.

Yang, Z.; Huang, Y.; Dong, B.; Li, H-L. Controlled Synthesis of Highly Ordered $LaFeO_3$ Nanowires using a Citrate-based Sol-gel Route. *Mater Res Bull.* 2006, 41, 274-281.

Yılmaz, I.; İlbaş, M.; Taştan, M.; Tarhan, C. Investigation of Hydrogen Usage in Aviation Industry. *Energy Convers. Manag.* 2018, 63, 63-69.

Yotburut, B.; Thongbai, P.; Yamwong, T.; Maensiri, S. Synthesis and Characterization of Multiferroic Sm-doped $BiFeO_3$ Nanopowders and Their Bulk Dielectric Properties. *J. Magn. Magn. Mater.* 2017, 437, 51–61.

Yuksel, A.; Koga, H.; Sasaki, M.; Goto, M. Hydrothermal Electrolysis of Glycerol Using a Continuous Flow Reactor. *Ind. Eng. Chem. Res.* 2010, 49, 1520–1525.

Yuksel, A.; Sasaki, M.; Goto, M. A New Green Technology: Hydrothermal Electrolysis for the Treatment of Biodiesel Wastewater. *Res. Chem. Intermed.* 2011a, 37, 131−143.

Yuksel, A.; Sasaki, M.; Goto, M. Complete Degradation of Orange G by Electrolysis in Sub-critical Water. *J. Hazard. Mater.* 2011b, 190, 1058−1062.

Zamfirescu, C.; Dincer, I.; Naterer, G. F. Molecular Charge Transfer and Quantum Efficiency Analyses of a Photochemical Reactor for Hydrogen Production. *Int. J. Hydrogen Energy.* 2012, 37, 9537–9549.

Zhang, D.; Yang, M.; Dong S. Improving the Photocatalytic Activity of TiO_2 through Reduction. *RSC Adv.* 2015, 5, 35661–35666.

Zhang, G.; Zhang, W.; Crittenden, J. C.; Chen, Y.; Minakata, D.; Wang, P. Photocatalytic Hydrogen Production under Visible-light Irradiation on $(CuAg)_{0.15}In_{0.3}Zn_{1.4}S_2$ Synthesized by Precipitation and Calcination. *Chinese J. Catal.* 2013, 34, 1926–1935.

Zhang, J.; Qi, L.; Ran, J.; Yu, J.; Qiao, S. Z. Ternary NiS/$ZnCd_{1-X}$ S/Reduced Graphene Oxide Nanocomposites for Enhanced Solar Photocatalytic H_2-Production Activity. *Adv. Energy Mater.* 2014, 4, 1301925.

Zhang, X.; Sun, Y.; Cui, X.; Jiang, Z. A Green and Facile Synthesis of TiO_2/Graphene Nanocomposites and Their Photocatalytic Activity for Hydrogen Evolution. *Int. J. Hydrogen Energy*. 2012, 37, 811-815.

Zhao, Y.; Hoivik, N.; Wang, K. Recent Advance on Engineering Titanium Dioxide Nanotubes for Photochemical and Photoelectrochemical Water Splitting. *Nano Energy*. 2016, 30, 728–744.

Zheng, D.; Huang, C.; Wang, X. Post-annealing Reinforced Hollow Carbon Nitride Nanospheres for Hydrogen Photosynthesis. *Nanoscale.* 2015, 7, 465–470.

Zhu, W.; Han, D.; Niu, L.; Wu T.; Guan, H. Z-scheme Si/$MgTiO_3$ Porous Heterostructures: Noble Metal and Sacrificial Agent Free Photocatalytic Hydrogen Evolution. *Int. J. Hydrogen Energy.* 2016, 41, 14713-14720.

Zieliñska, B.; Borowiak-Palen, E.; Kalenczuk, R. J. Photocatalytic Hydrogen Generation over Alkaline-earth Titanates in the Presence of Electron Donors. *Int. J. Hydrogen Energy.* 2008, 33, 1797–1802.

Zou, Y.; Kang, S. Z.; Li, X.; Qin, L.; Mu, J. TiO_2 Nanosheets Loaded with Cu: A Low-cost Efficient Photocatalytic System for Hydrogen Evolution from Water. *Int. J. Hydrogen Energy.* 2014, 39, 15403–15410.

VITA

CEREN ORAK

EDUCATION:

2017-2021, Ph.D., İzmir Institute of Technology, Institute of Engineering and Science, Department of Chemical Engineering. (Izmir, Turkey).

2014-2017, Master, Ege University, Graduate School of Natural and Applied Sciences, Department of Chemical Engineering, (Izmir, Turkey).

2012-2013, and 2017, Erasmus Student Exchange Program and Erasmus Internship Program, Università degli Studi di Salerno (Salerno, Italy).

2008-2013, Bachelor, Ege University, Faculty of Engineering, Chemical Engineering Department, (Izmir, Turkey).

SCHOLARSHIPS:

YÖK, 100/2000 PhD Scholarship Program - Hydrogen and Fuel Cells, 2017-2021.

TÜBİTAK, 2211/C National PhD Scholarship Program in the Priority Fields in Science and Technology, 2019-2021.

TÜBİTAK, The valorization of wastewater of a factory for hydrogen production by photocatalytic oxidation in the presence of perovskite catalyst – Project No: 217M272.

TÜBİTAK, Treatment of personal care products based micropollutants over monolith structured perovskite catalysts by innovative methods – Project No: 114M080.

PUBLICATIONS:

Orak C., Atalay S., Ersöz G., 2016. Degradation of ethylparaben using photo-Fenton-like oxidation over $BiFeO_3$, Anadolu University Journal of Science and Technology A - Applied Sciences and Engineering, 17 (5), 915-925.

Orak C., Atalay S., Ersöz G., 2017. Photocatalytic and photo-Fenton-like degradation of methylparaben on monolith-supported perovskite-type catalysts, Separation Science and Technology, 52 (7), 1310-1320.

Orak C., Yüksel Özşen A., 2020. Electrolytic oxidation of 1,8-diazabicyclo[5.4.0]undec-7-ene in hot-compressed water on a titanium electrode, Industrial & Engineering Chemistry Research, 59 (43), 19153-19161.

Orak C., Yüksel Özşen A., 2021. Graphene-supported $LaFeO_3$ for photocatalytic hydrogen energy production. 1-17.

Orak C., Atalay S., Ersöz G., Metilparabenin $LaFeO_3$ varlığında Fenton-Benzeri Oksidasyon ile Giderimi, 12. Ulusal Kimya Mühendisleri Kongresi Ağustos 2016.

Orak C., Yüksel Özşen A., Hydrogen production from sugar beet wastewater in the presence of perovskite type catalysts by photocatalysis, ACS Spring 2019 National Meeting & Exposition, 31 Mart-04 Nisan 2019.